DOE/NASA/9235-75/2

100-kW METAL WIND TURBINE BLADE DYNAMICS ANALYSIS, WEIGHT/BALANCE, AND STRUCTURAL TEST RESULTS

By
W. D. Anderson

June 1975

Lockheed-California Company
Burbank, California

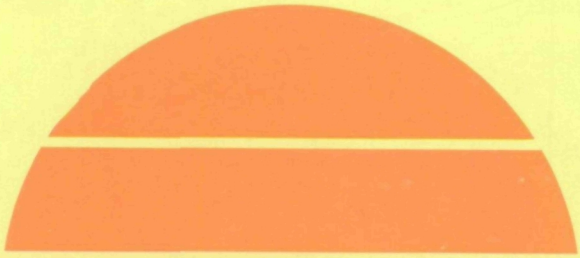

U.S. Department of Energy

Solar Energy

NOTICE

NASA CR-134957
Lockheed LR 27230

DOE/NASA/9235-75/2
Distribution Category UC-60

100-kW METAL WIND TURBINE BLADE DYNAMICS ANALYSIS, WEIGHT/BALANCE, AND STRUCTURAL TEST RESULTS

W. D. Anderson

Lockheed · California Company
Burbank, California

June 1975

Prepared for the
National Aeronautics and Space Administration
Lewis Research Center
Cleveland, Ohio 44135

Contract NAS 3-19235

and the
ENERGY RESEARCH AND DEVELOPMENT ADMINISTRATION
Division of Solar Energy
Federal Wind Energy Program

PREPARED BY _____
W. D. Anderson

APPROVED BY _____
R. H. Hopps
Division Manager
Advanced Design

APPROVED BY _____
W. A. Stauffer
Division Engineer
Structures & Materials

1 Report No	2 Government Accession No	3 Recipient's Catalog No
NASA CR-134957		

4 Title and Subtitle	5 Report Date
100-kW METAL WIND TURBINE BLADE DYNAMICS ANALYSIS, WEIGHT/BALANCE, AND STRUCTURAL TEST RESULTS	June 1975
	6 Performing Organization Code

7 Author(s)	8 Performing Organization Report No
W. D. Anderson	LR 27230
	10 Work Unit No
9 Performing Organization Name and Address	
Lockheed · California Company Burbank, CA	11 Contract or Grant No NAS 3-19235
	13 Type of Report and Period Covered
12 Sponsoring Agency Name and Address	Contractor Report
National Aeronautics and Space Administration Washington, D.C. 20546	14 Sponsoring Agency Code

15 Supplementary Notes

Final Report. Project Manager, Bradford S. Linscott, Power Systems Division, NASA Lewis Research Center, Cleveland, Ohio

16 Abstract

This report presents the results of dynamic analyses, weight and balance tests, static stiffness tests, and structural vibration tests on the 60-foot-long metal blades for the ERDA-NASA 100-kW wind turbine. The analytical results show the metal blades to be free from structural or dynamic resonance at the wind turbine design speed and show that aeroelastic instabilities are unlikely to occur within the normal operating range of the wind turbine.

17 Key Words (Suggested by Author(s))	18 Distribution Statement
	Unclassified - unlimited

19 Security Classif. (of this report)	20 Security Classif. (of this page)	21. No. of Pages	22 Price*
Unclassified	Unclassified	100	

* For sale by the National Technical Information Service, Springfield, Virginia 22161

TABLE OF CONTENTS

LIST OF FIGURES

LIST OF TABLES

1.0 INTRODUCTION

Recent shortages in the supply of clean energy, coupled with increasing costs of fuel, have forced the nation to reassess all forms of energy, including wind power, to determine their practicality. The national wind energy program, which originated at the National Science Foundation and is now directed by the Energy Research and Development Administration (ERDA), includes research and development on the many applications and concepts of wind-energy systems.

As part of this program, the NASA Lewis Research Center was assigned the project responsibility of designing and constructing a wind turbine generator large enough to assess the technological requirements and engineering problems of large wind turbine generators. The 100-kW wind turbine was assembled for this purpose at the NASA-Lewis Plum Brook Station in Sandusky, Ohio. While the design and assembly of the wind turbine was conducted by NASA-Lewis, the detail design, analyses, fabrication, and test of the 60-foot-long metal blades were performed by the Lockheed Aircraft Corporation under NASA contract NAS 3-19235.

This report presents the results of the dynamic analyses conducted on the metal wind turbine blades, of the weight and balance tests conducted on each of the three blades delivered to NASA, of the static stiffness tests, and of the structural vibration tests conducted on the first manufactured blade. The results of this report show the metal wind turbine blades to be free from structural or dynamic resonance at the wind turbine design speed. Also, the results indicate the blades to be free from aeroelastic instability within the normal operating range of the wind turbine.

100-kW WIND-TURBINE SYSTEM

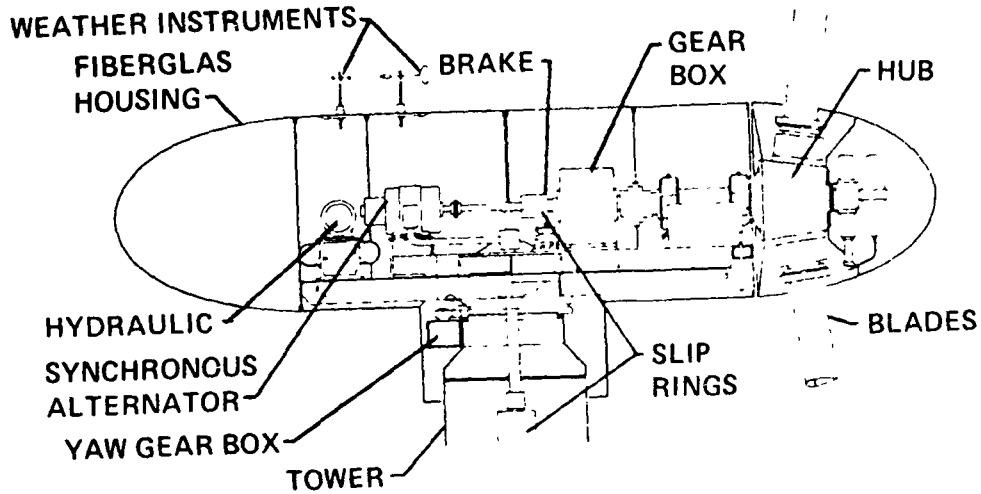

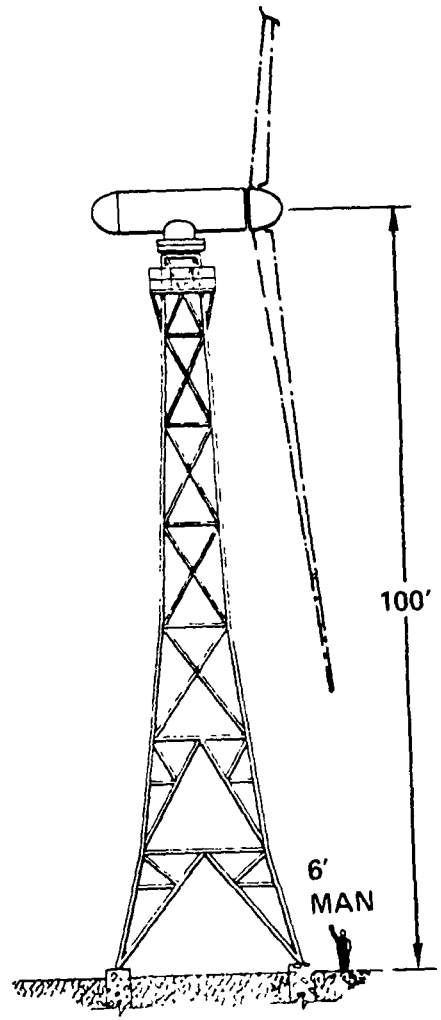

2.0 DYNAMIC ANALYSIS

Several dynamic analyses have been performed on the wind turbine blade and coupled wind turbine-tower system. The analyses include blade frequency determination, blade flutter and divergence, whirl mode stability and rotor blade transient response. The analytical results presented show the system to be free from any aeroelastic stability or dynamic response problem. Additionally, panel flutter has been precluded by the selection of the skin thicknesses and spar rib spacings. The results of the various dynamic studies conducted are now presented.

2.1 FLUTTER AND DIVERGENCE

Aeroelastic stability analyses have been performed and have shown the wind turbine system to be free from flutter and divergence throughout the entire range of operation of the system. These analyses have included examination of effect of rotor shaft and blade feathering constraint, rotor speed, collective blade angle, wind speed and direction, and control system flexibility.

Using the NASA furnished tower data and drawings to establish appropriate tower flexibility data, analyses were performed for the cantilever, antisymmetric or cyclic, and symmetric or collective boundary conditions. The collective feathering stiffness was based on data supplied by NASA however, no data was available on the cyclic or antisymmetric feathering stiffness so its nominal value was assumed to be twice the collective value.

The cantilever boundary condition is an artificial condition in that because of the two-bladed nature of the wind turbine, the relatively low drive system torsional impedance characteristics and the tower flexibility, the cantilever constraint cannot exist. Data is presented for this condition however just to provide a frame of reference for the effect of introducing the flexible tower and control system.

The cyclic or antisymmetric boundary condition is one where the rotor introduces shears into the tower normal to the rotor shaft axis and overturning

moments onto the shaft, or moment vectors perpendicular to the shaft axis. The rotor hub due to combined mast and tower flexibility is also allowed to move in these directions. The rotor hub is constrained not to move angularly in the direction of rotation nor translationally along the shaft axis.

For the collective or symmetric boundary condition, the rotor hub is allowed to have motion translationally along the shaft axis and angularly in the direction of rotation. Translation and angular motion perpendicular to the shaft axis is constrained not to occur. The collective blade feathering constraint is such that feathering loads are transmitted to the collective actuator and blade feathering is symmetric or in the same direction on both blades. For the cyclic case, the feathering moments are reacted across the feathering gear and no loads are transmitted to the collective actuator.

The basic rotor, hub and blade stiffness and inertial data used in the analyses presented herein are given in Reference 1. The tower and control flexibilities used are tabulated in Table 1.

Table 1. - TOWER AND CONTROL FLEXIBILITY DATA

Description	Flexibility
Tower Lateral Flexibility at Hub	38.2×10^{-6} in/lb.
Tower Vertical Flexibility at Hub	3.95×10^{-6} in/lb.
Tower Flexibility Along Shaft Axis	34.6×10^{-6} in/lb.
Tower Pitch Flexibility at Hub	3.66×10^{-9} rad/in-lb.
Tower Yaw Flexibility at Hub	9.12×10^{-9} rad/in-lb.
Tower Angular Flexibility About Shaft Axis	5.96×10^{-9} rad/in-lb.
Collective Control Flexibility (Total)	5.13×10^{-8} rad/in-lb.
Cyclic Control Flexibility (Total)	2.56×10^{-8} rad/in-lb.

The data presented in this table represent the combined flexibility of the tower, pylon and rotor shaft. The tower data was obtained from the tower NASTRAN data supplied by NASA-LeRC and the pylon and shaft flexibilities were

derived from NASA-LeRC furnished drawings. In the analyses presented herein rms values of the stiffnesses of the corresponding flexibilities in the table for the lateral-vertical axes and for the pitch-yaw axis were used.

The following table summarizes the conditions analyzed and for which data are presented. The table gives a definition of each condition and also indicates the figures presented in the following discussion in which the corresponding aeroelastic stability data are given.

Table 2. SUMMARY OF AEROELASTIC STABILITY CONDITIONS PRESENTED

rpm	$\theta_{3/4R}$	V_w-mph	Wind Direction	Control Stiffness	Rotor Brake On	Reference Figure (s)
0 - 80	0°	0.		Nominal	No	3 & 4
0 - 80	0°	18	(1)	Nominal	No	5, 6, & 7
0 - 80	0°	18	(1)	40% Nominal	No	8 & 9
0 - 80	-18°	50	(1)	Nominal	No	10, 11, & 12
0 - 80	-28°	80	(1)	Nominal	No	13, 14, & 15
0.0	-90°	0 - 140	(1)	Nominal	No	16, 17, & 18
0.0	-90°	140	(1)	Variable	No	19
0.0	-90°	0 - 140	(2)	Nominal	No	20 & 21
0.0	-90°	0 - 140	(2)	40% Nominal	No	22
0.0	-90°	0 - 200	(3)	Nominal	No	23, 24, & 25
0.0	-90°	0 - 200	(3)	Nominal	Yes	26
0.0	-90°	140	(3)	Variable	No	27 & 28
0.0	-90°	140	(3)	Variable	Yes	29

(1) Wind blowing along shaft axis

(2) Wind blowing over trailing edge of blade

(3) Wind blowing over trailing edge of blade at skewed angle of 45 degrees - worst case for static divergence

2.1.1 Blade Frequencies

Presented first are cantilever and cyclic blade frequency spectrums as a function of rotor speed. Referring to Figure 1 it is seen that for the cantilever blade the dirst flap frequency is located just below 3P or the third order crossing line and the first inplane mode is between 3P and 4P. The next higher frequency mode is the second flap mode with a frequency above 7P. The cantilever blade torsion frequency is at 34.6 cps or at approximately 52-P.

The effect of introducing the tower and control flexibilities on the blade natural frequencies for the cyclic boundary condition is seen in Figure 2. Note a reduction in the first flap and first inplane modes. Also note the torsion frequency is reduced to 22.6 cps or approximately 34-P. The other modes are similarly affected. These data have been presented to give a general overview of the dynamics of the wind turbine system prior to presentation of the aeroelastic stability results. Additional analytical frequency and mode shape data are given in Reference 1 and experimental data are given in Section 3.2 of this report.

2.1.2 Rotating Flutter and Divergence Results

Figures 3 through 15 present flutter solutions for the cantilever, cyclic, and collective boundary conditions for rotor speeds from zero to 80 rpm (40 in normal) and for wind speeds from 0 to 80 mph and collective blade angles for 0 to -28 degrees respectively. Figures 3 and 4 are for zero blade and zero wind speed, a powered condition, for the cyclic and collective boundary condition respectively. Note that all modes with the exception of mode 5 in each case increase in stability with increasing rotor speed. Mode 5 as indicated is the second inplane mode for the cyclic condition and the first inplane or pinwheel mode for the collective condition and therefore would be expected to be little influenced by the aerodynamic effects associated with rotor rotation.

Figures 5, 6, and 7 give results of the flutter analyses conducted at the nominal design wind speed of 18 mph for the cantilever, cyclic and collective boundary conditions respectively. The data shown in these and the figures to follow are presented for a constant tip speed ratio which is associated with

FIGURE 1
100 KW WIND MILL
CANTILEVER BLADE FREQUENCIES VS ROTOR SPEED

$\theta_{3/4R} = 0°$ VACUUM

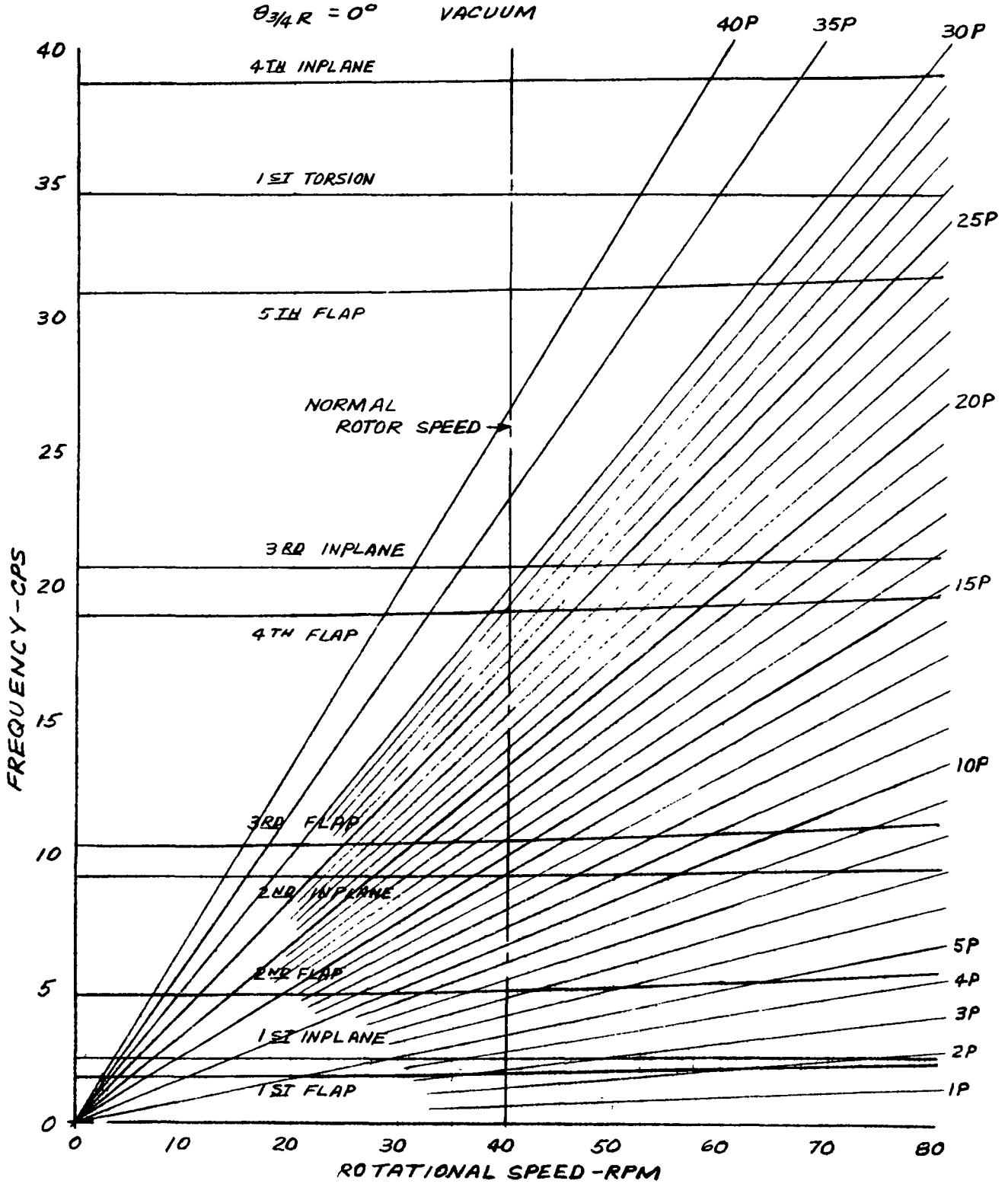

WM09

FIGURE 2
100 KW WINDMILL
CYCLIC BLADE FREQUENCIES VS ROTOR SPEED

$\theta_{3/4R} = 0°$ VACUUM

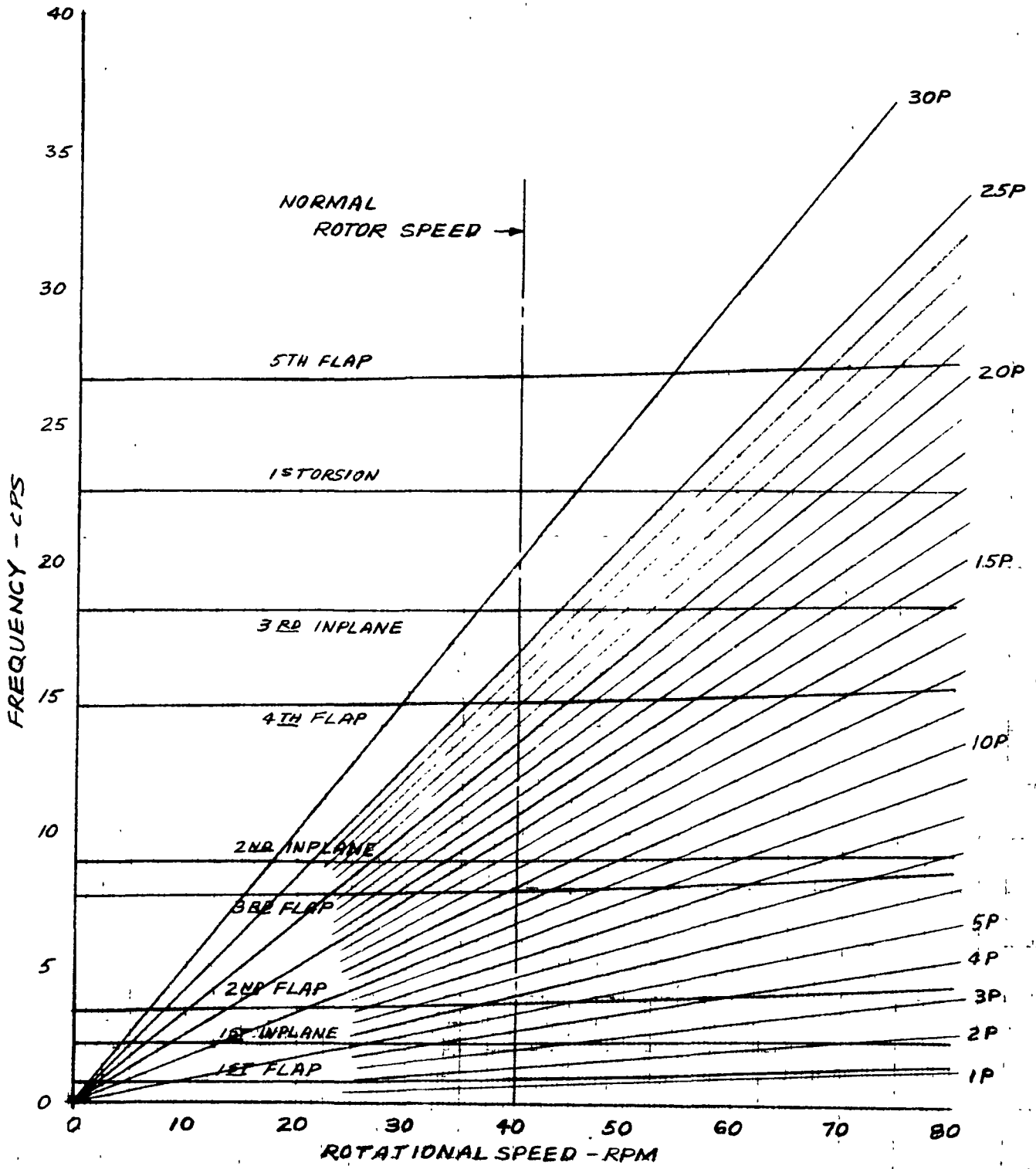

3-13-75

FIG 3

100 KW WINDMILL

CYCLIC BLADE STABILITY -

FREQUENCY AND DAMPING VS ROTOR SPEED

$\theta_{3/4R} = 0°$, $V_W = 0.0$

100 % $K_{CONTROL}$

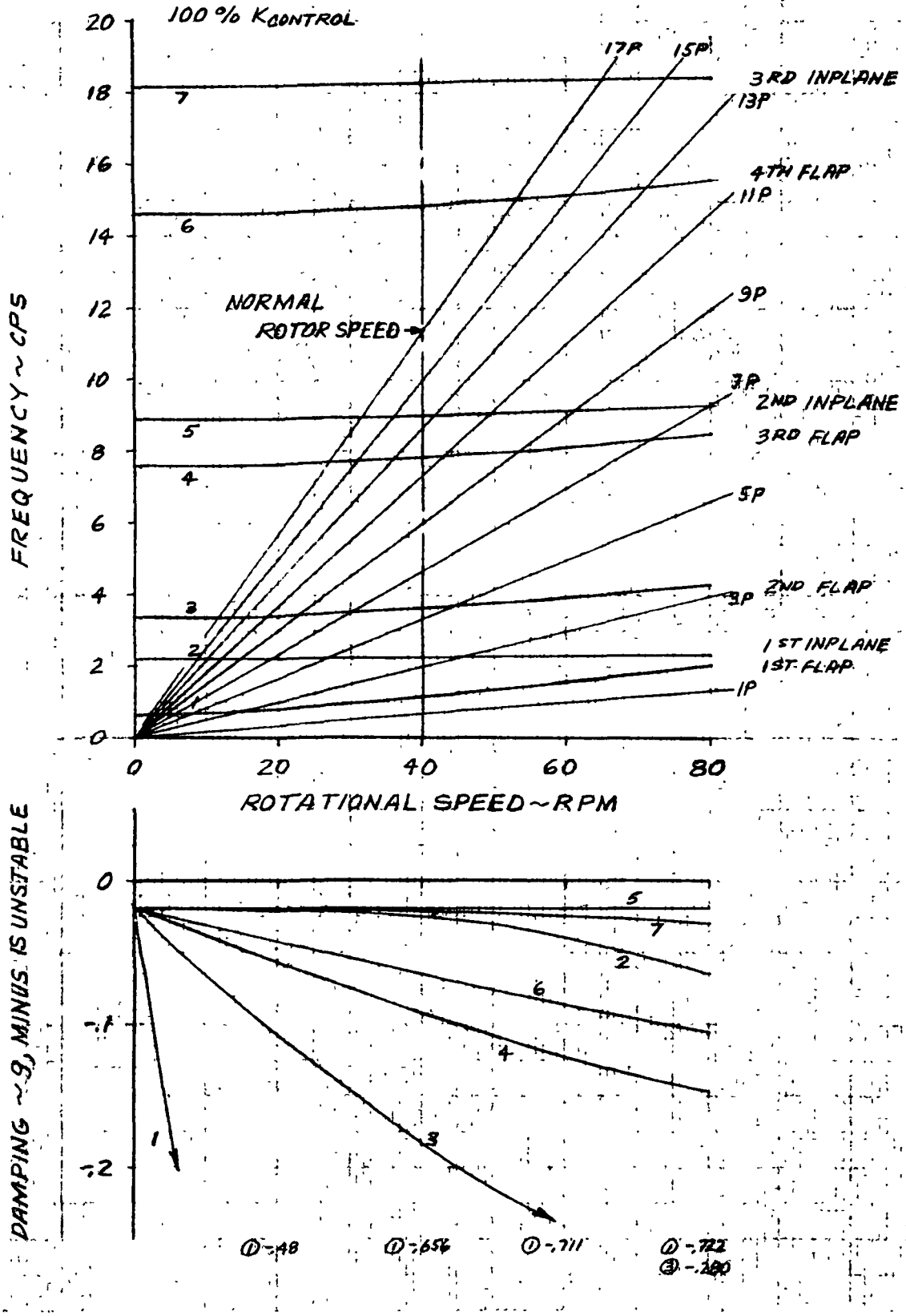

WM12

3-13-75

FIG. 4

100 KW WINDMILL
COLLECTIVE BLADE STABILITY - FREQUENCY AND DAMPING VS ROTOR SPEED

$\theta_{3/4R} = 0°$, $V_W = 0.0$

100% $K_{CONTROL}$

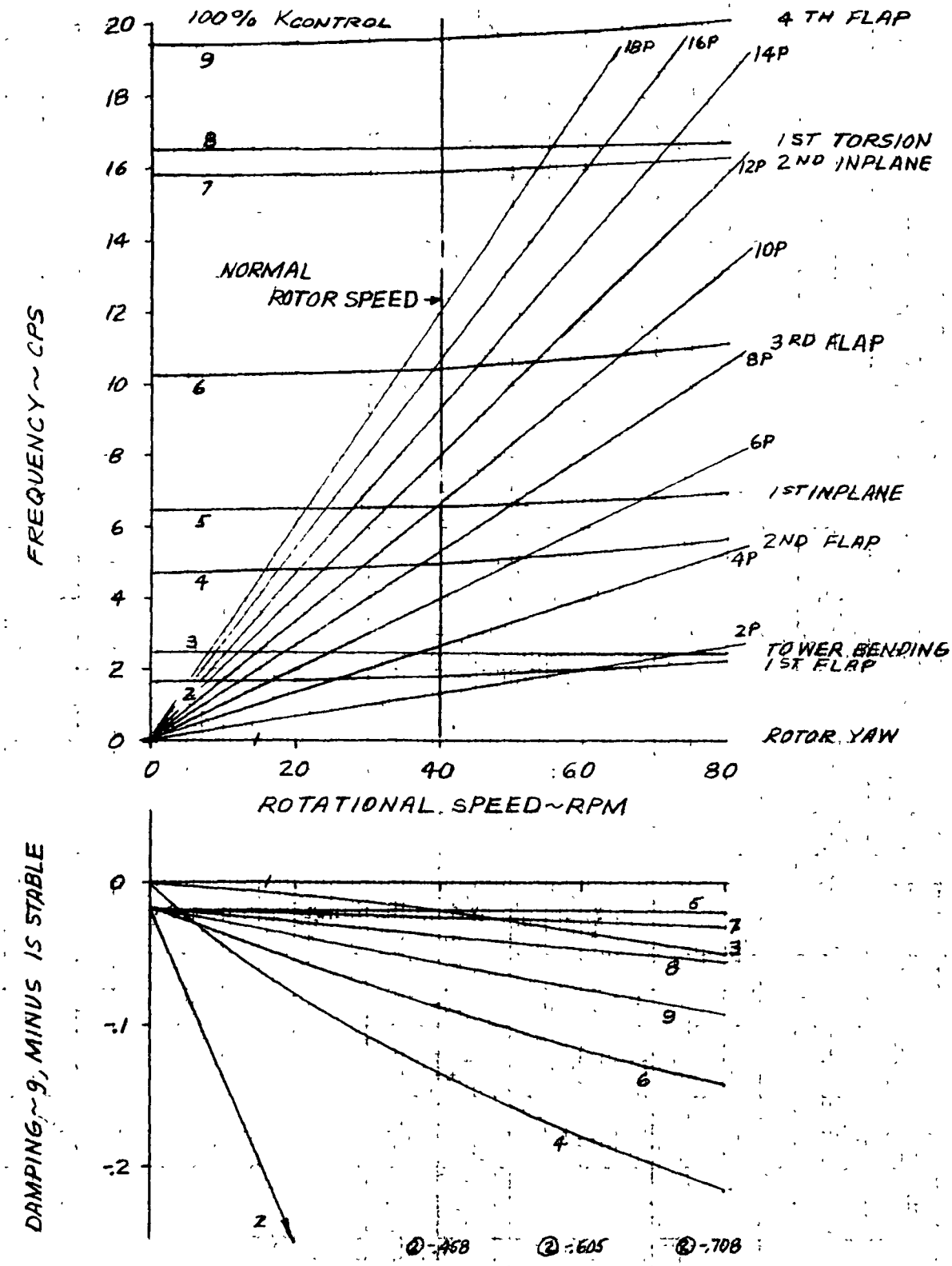

WM 12

2-28-75

FIG. 5

100 KW WINDMILL
CANTILEVER BLADE STABILITY-
FREQUENCY AND DAMPING VS ROTOR SPEED

$\theta_{3/4R} = 0°$ $V_W = 18$ mph @ 40 RPM

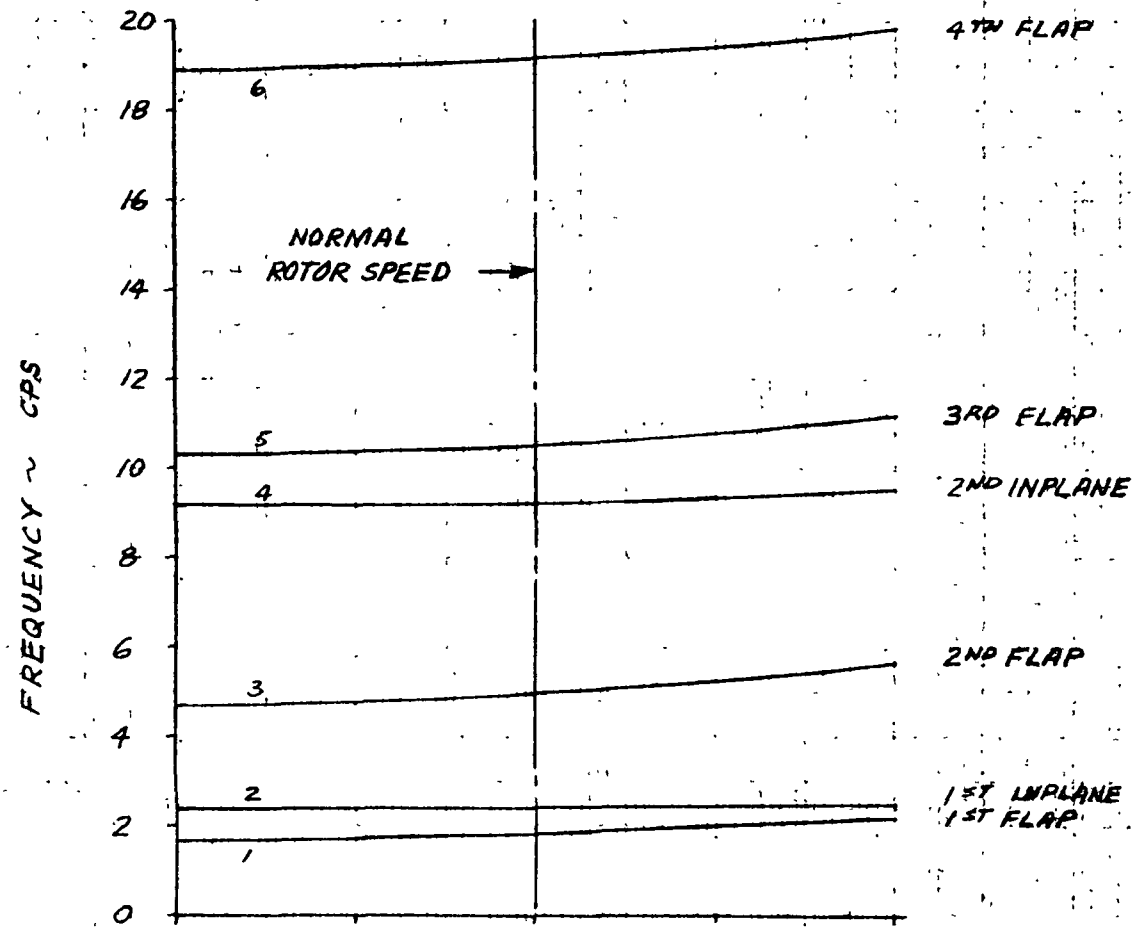

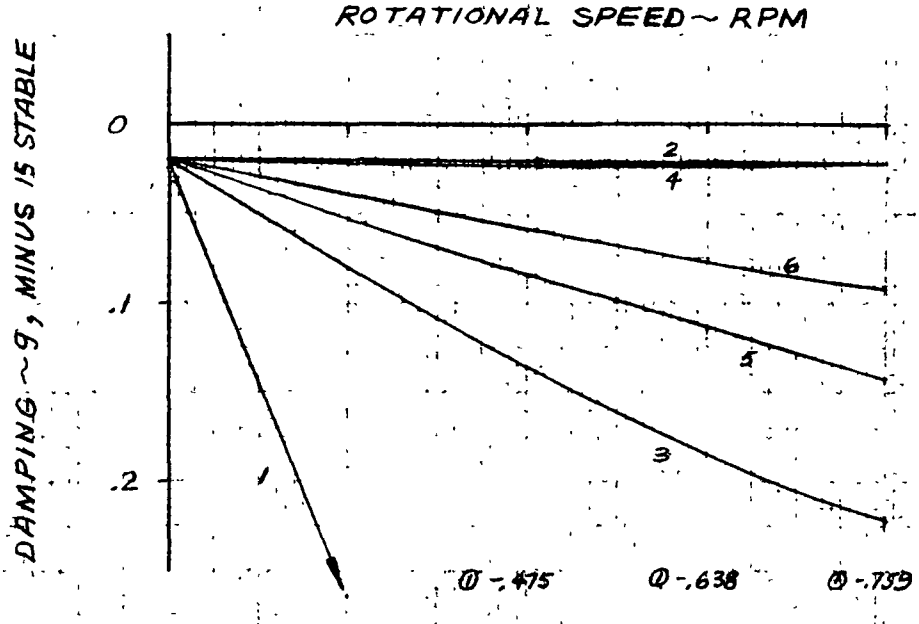

WM09

2-28-75

FIG. 5

100 KW WINDMILL
CYCLIC BLADE STABILITY - FREQUENCY AND DAMPING VS ROTOR SPEED

$\Theta_{3/4R} = 0°$, $V_W = 18$ mph @ 40 RPM
100% K CONTROL

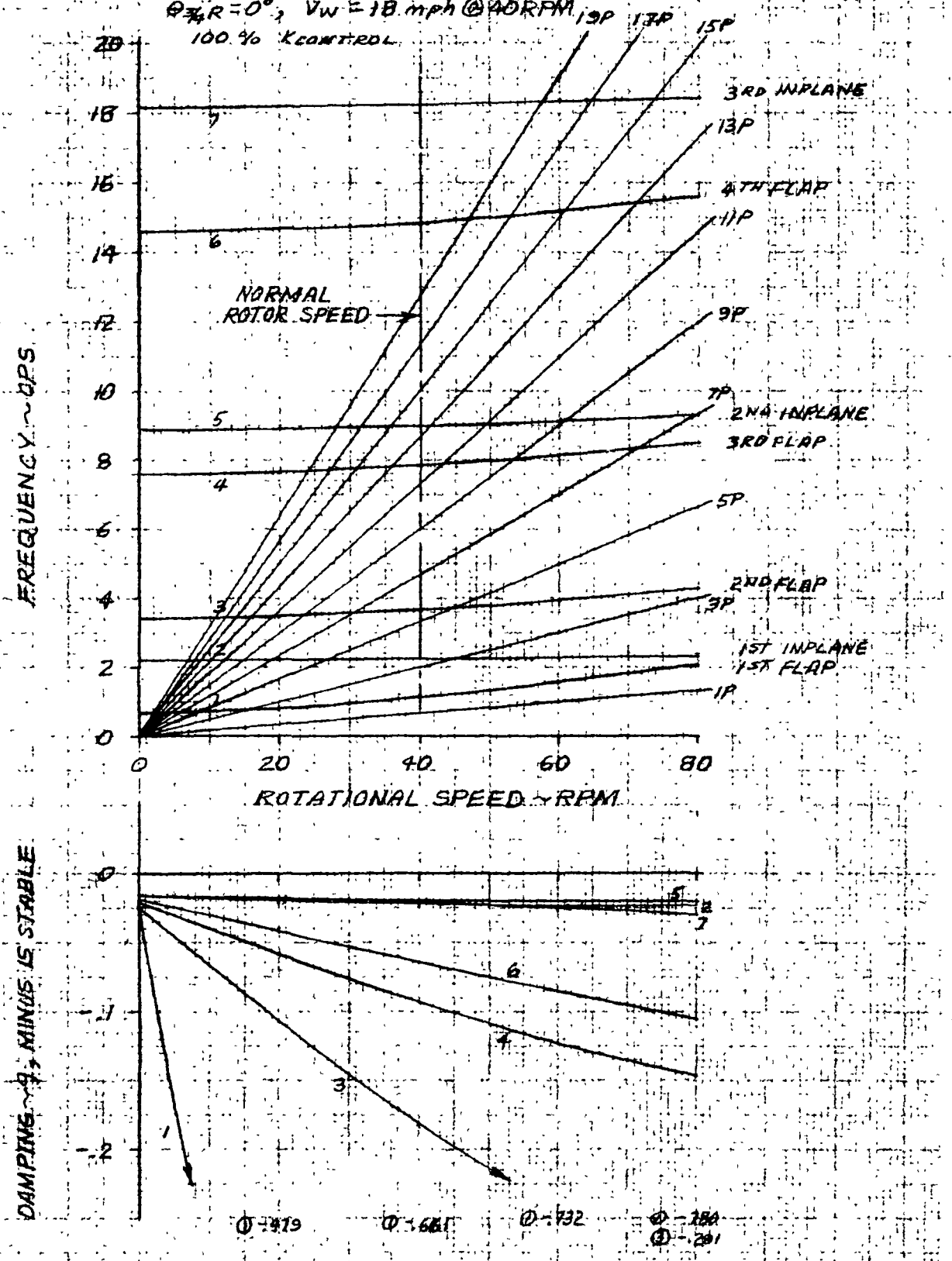

WM09

2-28-75

WM09

100 KW WINDMILL FIG 7
COLLECTIVE BLADE STABILITY
FREQUENCY AND DAMPING VS ROTOR SPEED

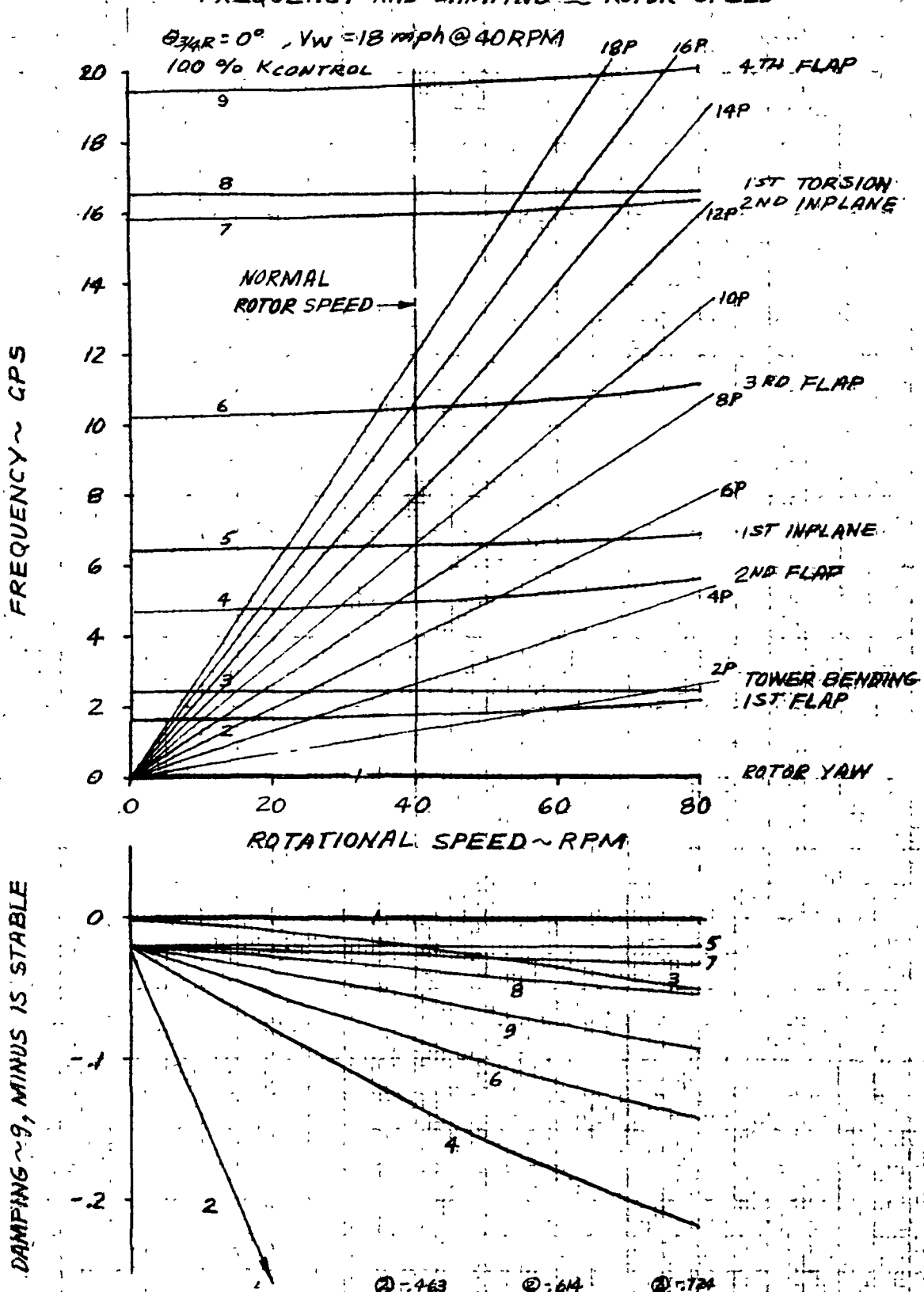

3-19-75

FIG. 8

100 KW WINDMILL
CYCLIC BLADE STABILITY
FREQUENCY AND DAMPING VS ROTOR SPEED

$\Omega_{3/4R} = 0°$ $V_W = 18$ mph @ 40 RPM
40% ($K_{CONTROL}$) ASSUMED

WM 15

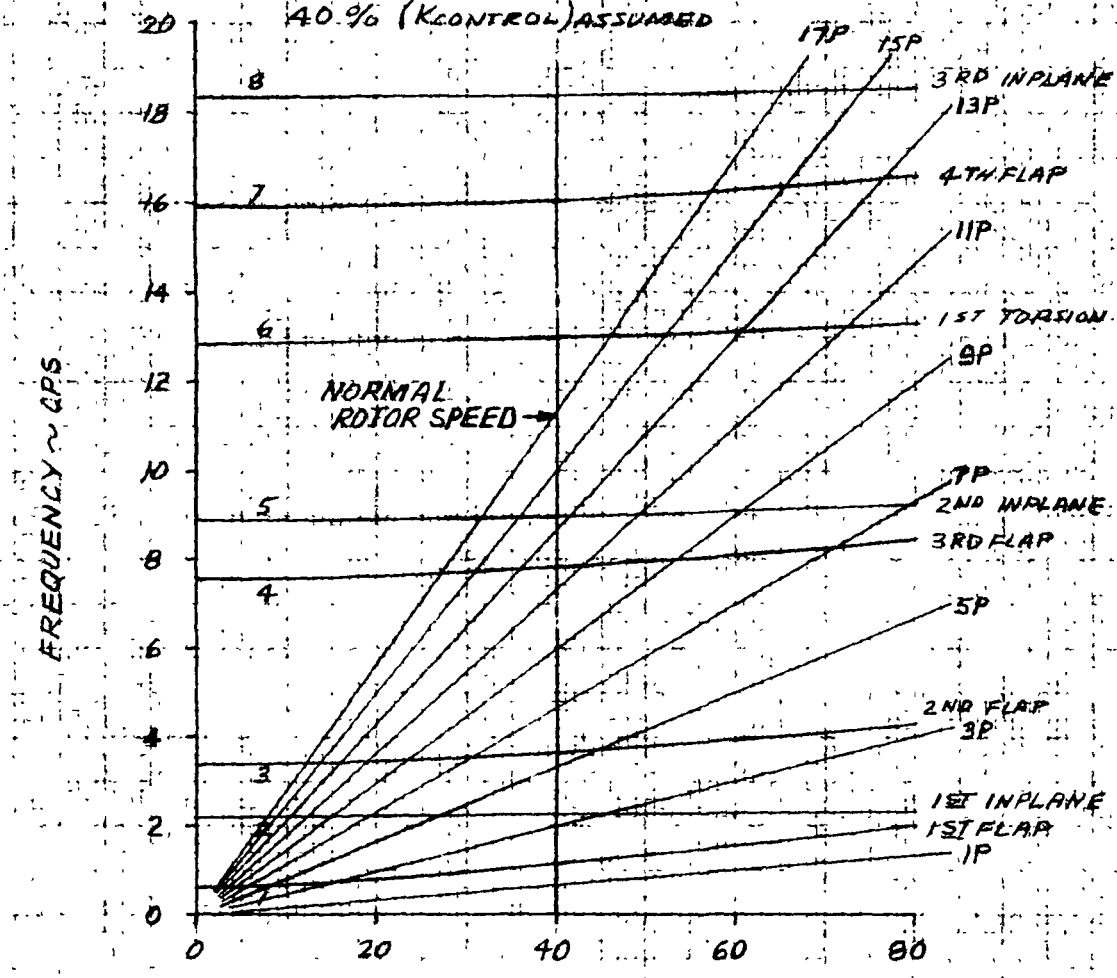

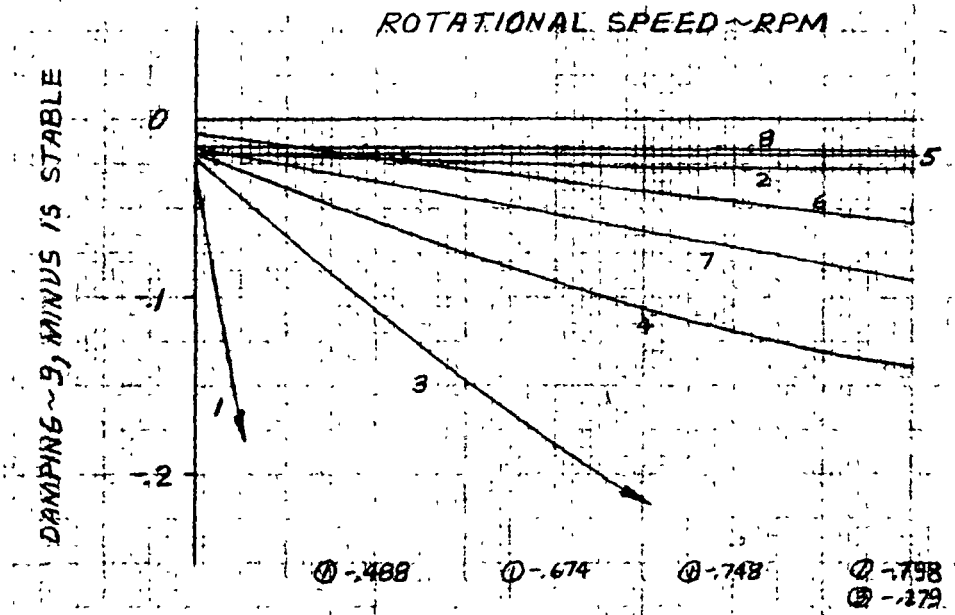

FIG c

100 KW WINDMILL
COLLECTIVE STABILITY
FREQUENCY AND DAMPING VS ROTOR SPEED
$\theta_{3/4R} = 0°$, $V_W = 18$ mph @40RPM
40% $K_{CONTROL}$

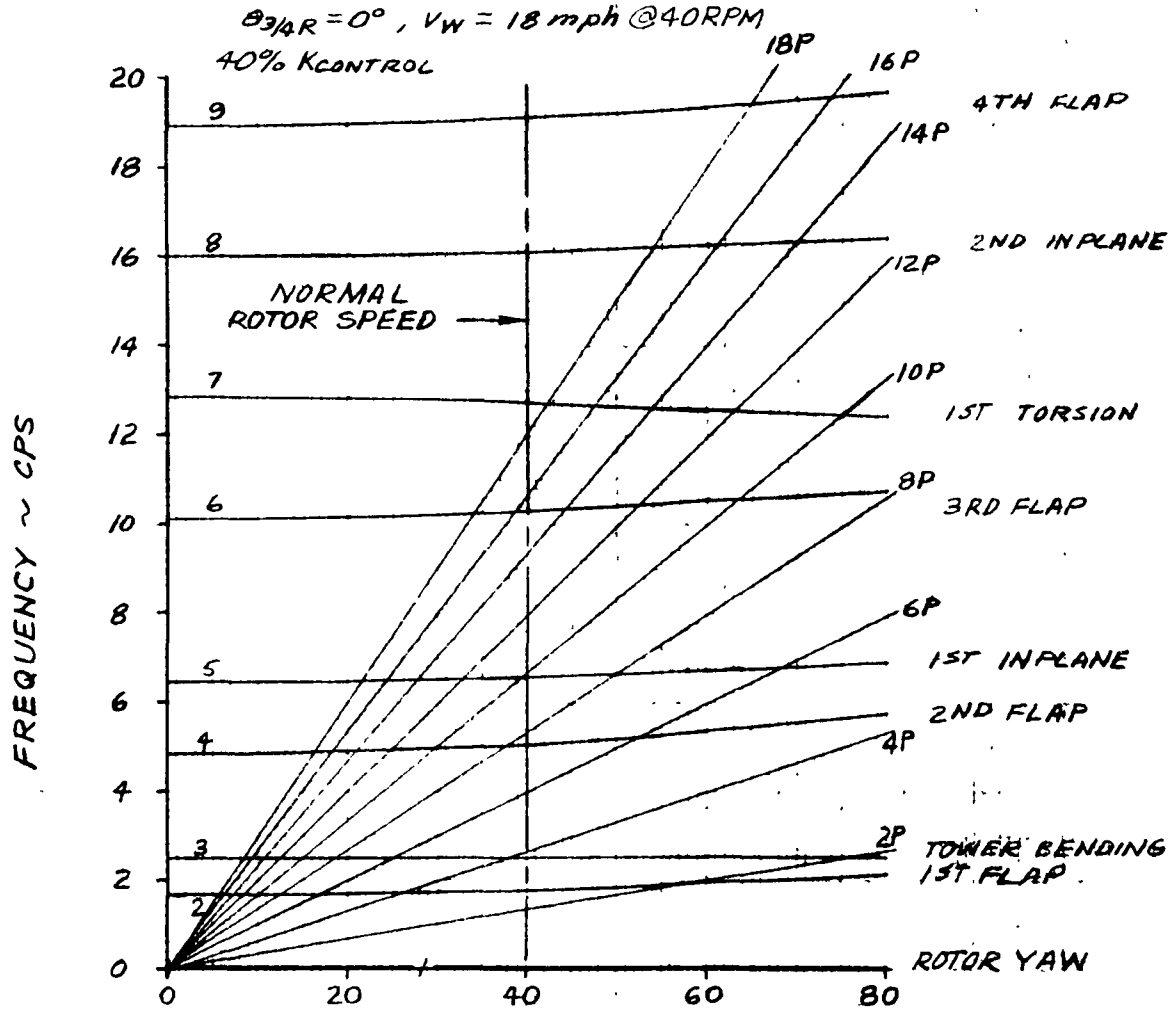

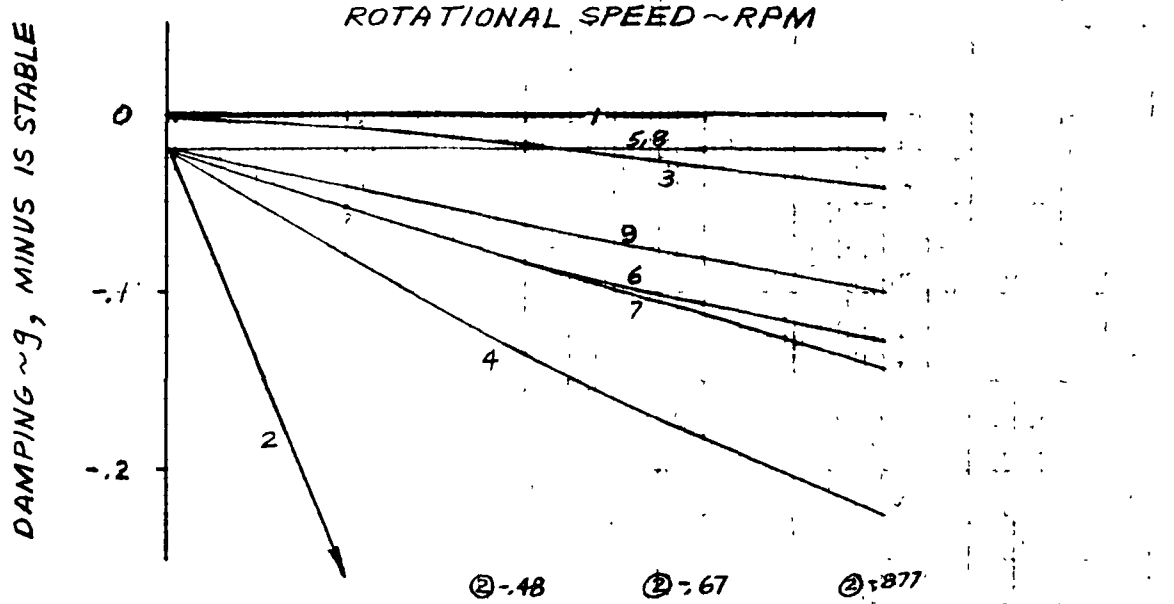

FIG. 10

100 KW WINDMILL
CANTILEVER BLADE STABILITY
FREQUENCY AND DAMPING VS ROTOR SPEED

$\theta_{3/4R}$ = -18 DEG , V_W = 50 mph @ 40 RPM

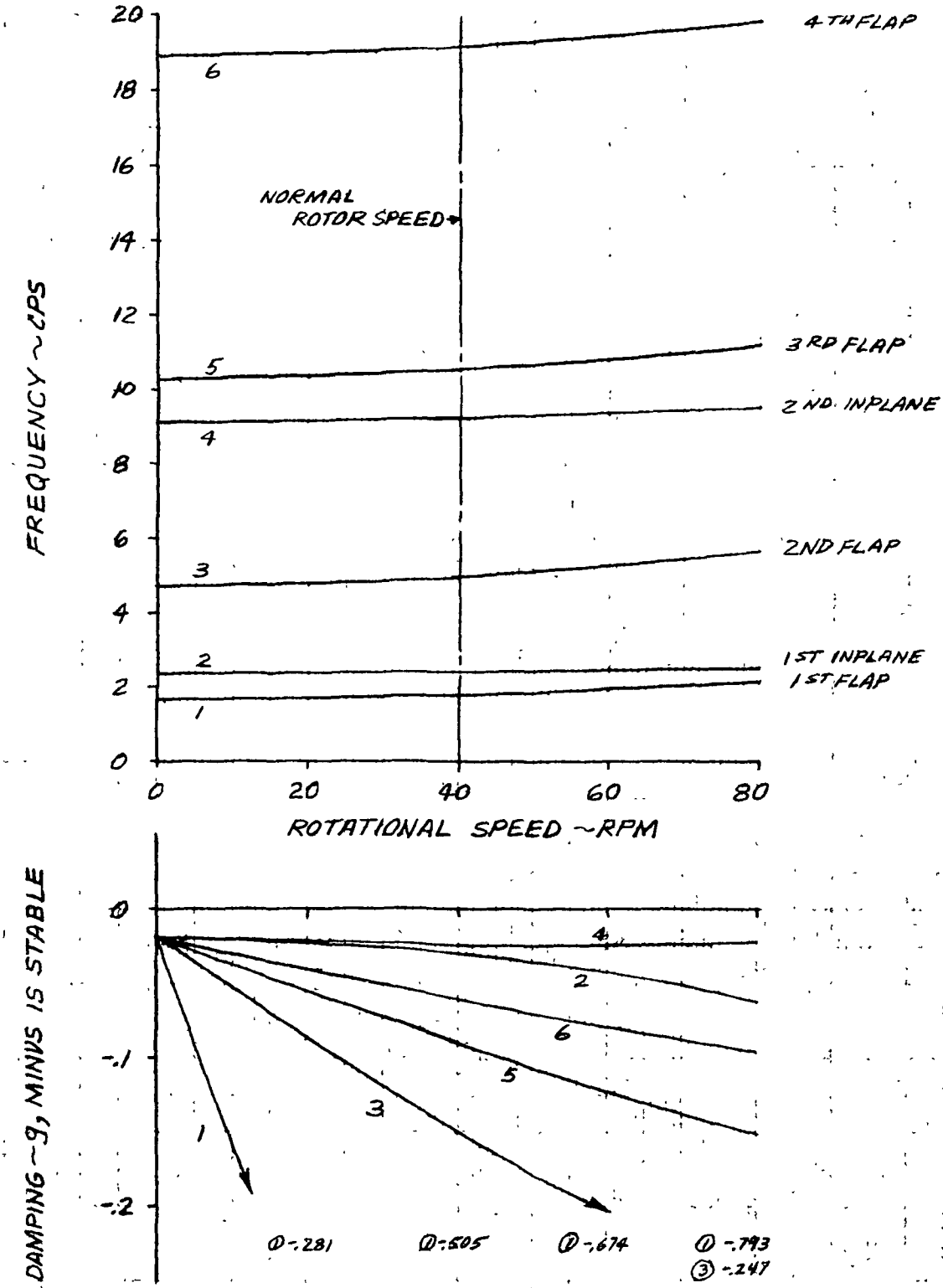

NIMOS

FIG. 11

100 KW WINDMILL
CYCLIC BLADE STABILITY
FREQUENCY AND DAMPING VS ROTOR SPEED

$\theta_{3/4R} = -18°$ $V_W = 50$ mph @ 40RPM

100% (K CONTRO) ASSUMED

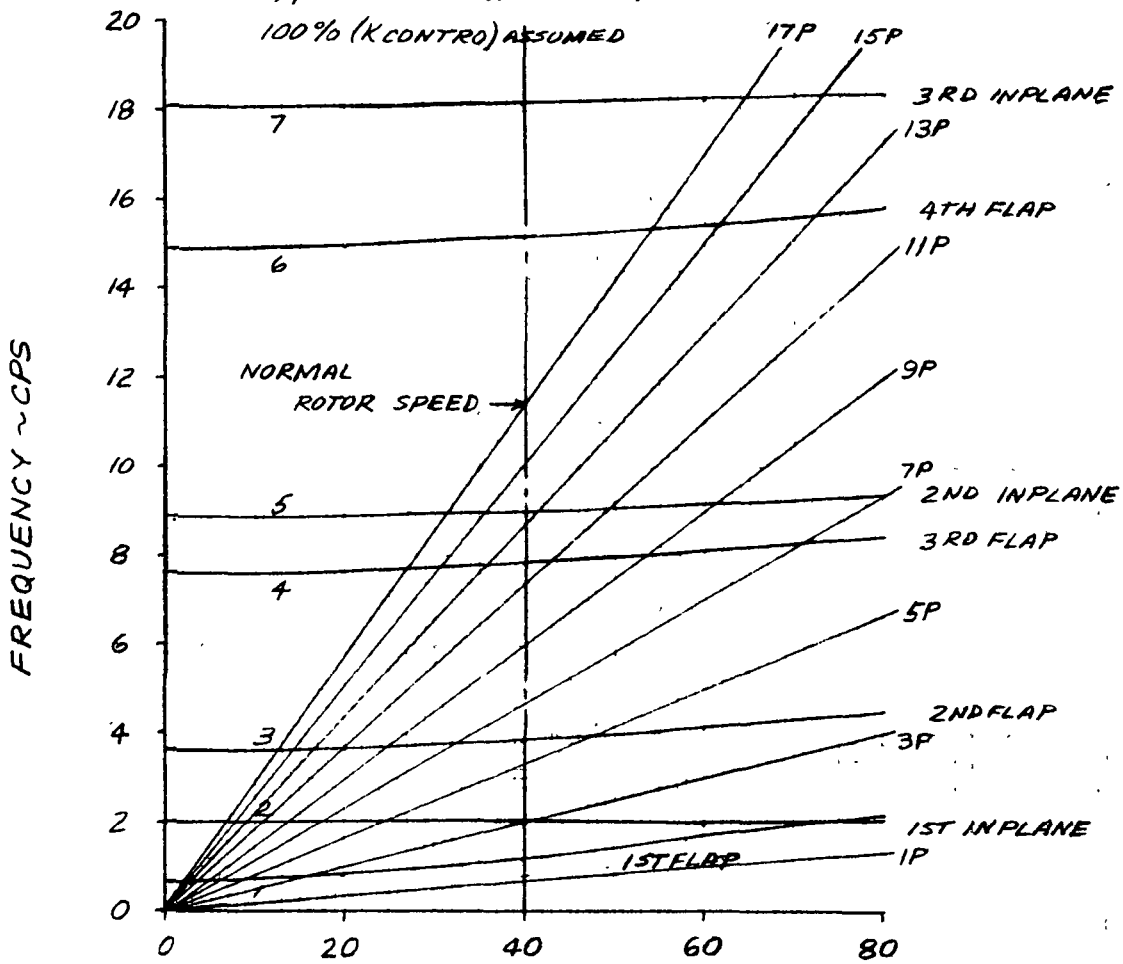

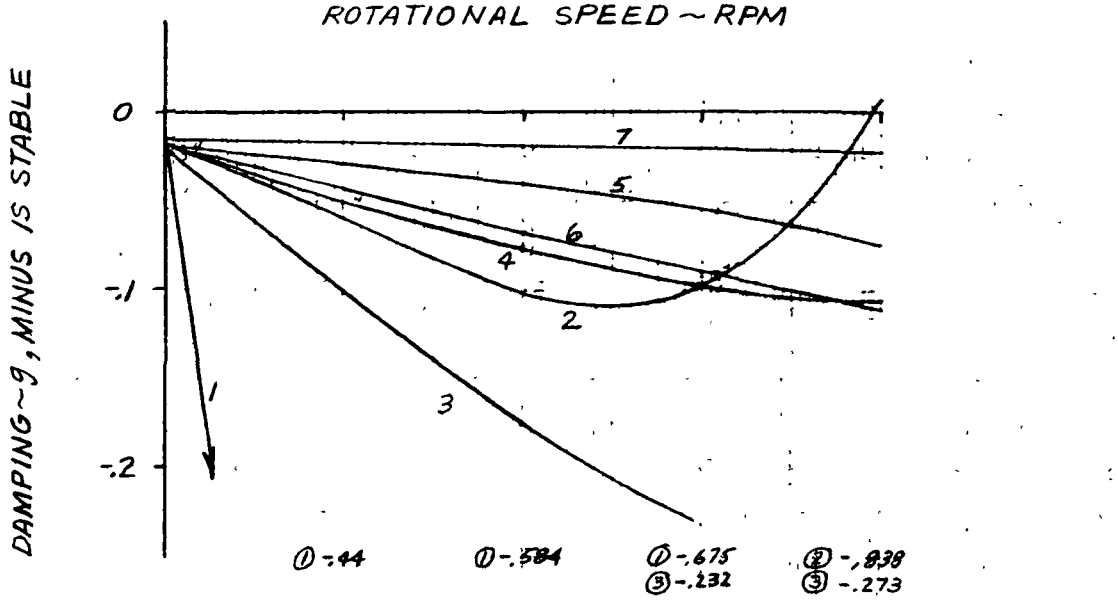

WM05

FIG. 12

100 KW WINDMILL
COLLECTIVE BLADE STABILITY
FREQUENCY AND DAMPING VS ROTOR SPEED

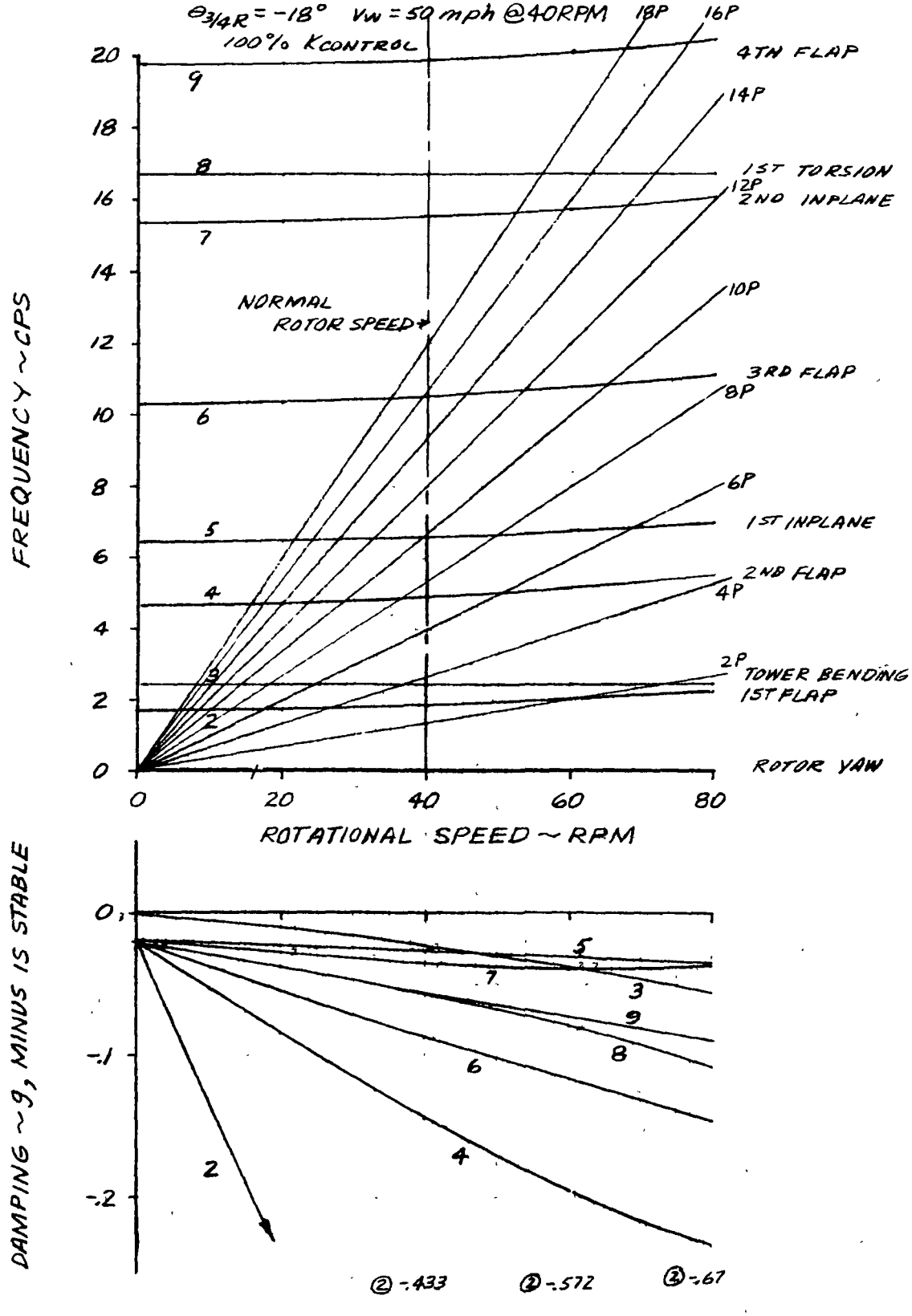

FIG 13

100 KW WINDMILL
CANTILEVER BLADE STABILITY
FREQUENCY AND DAMPING VS ROTOR SPEED

$\theta_{3/4R} = -28°$ $V_W = 80$ mph @ 40 RPM

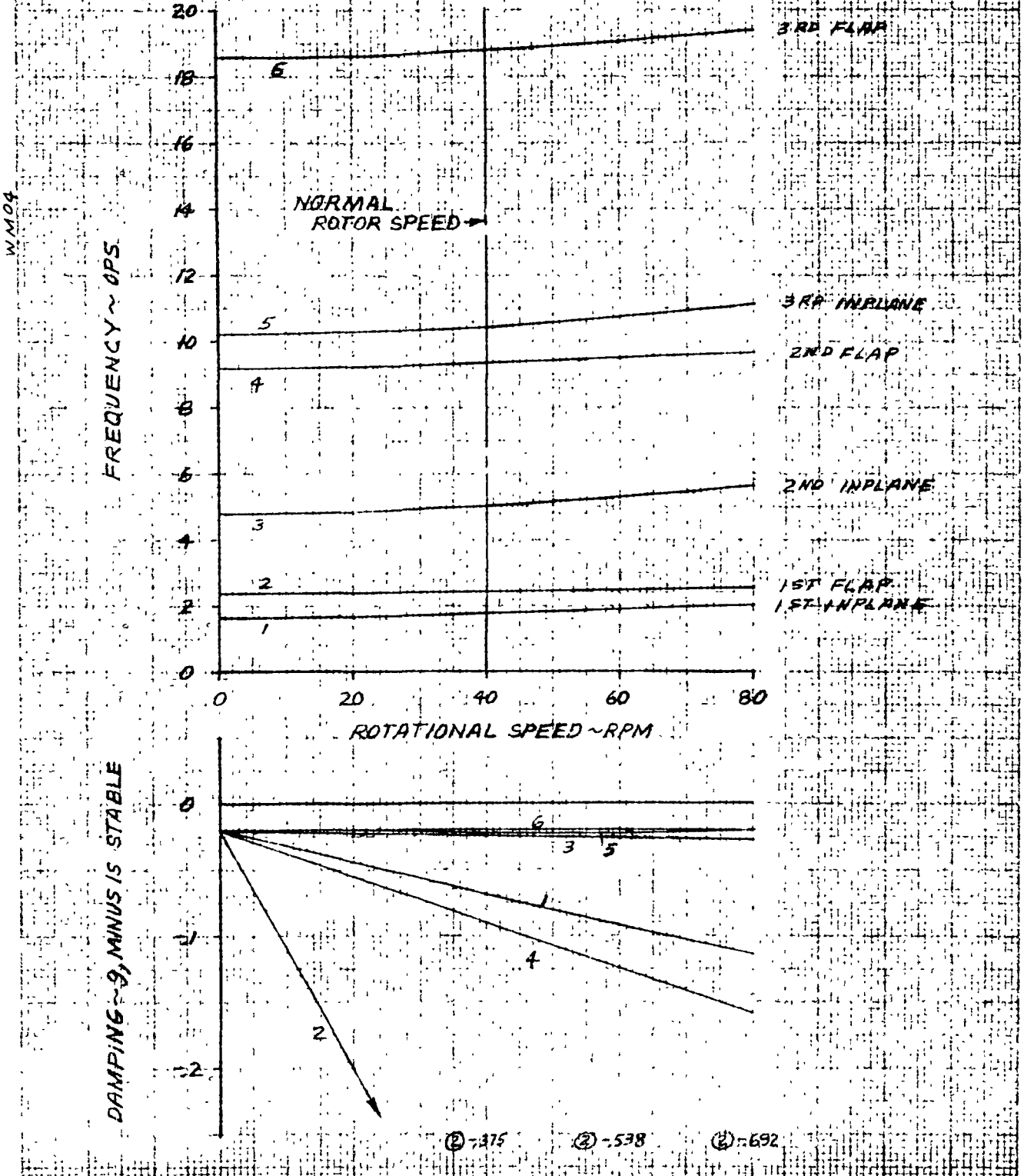

3-17-75

FIG. 14

100 KW WINDMILL

CYCLIC BLADE STABILITY

FREQUENCY AND DAMPING VS ROTOR SPEED

$\theta_{3/4R} = -2.8°$ $V_W = 80$ mph @ 40 PPM

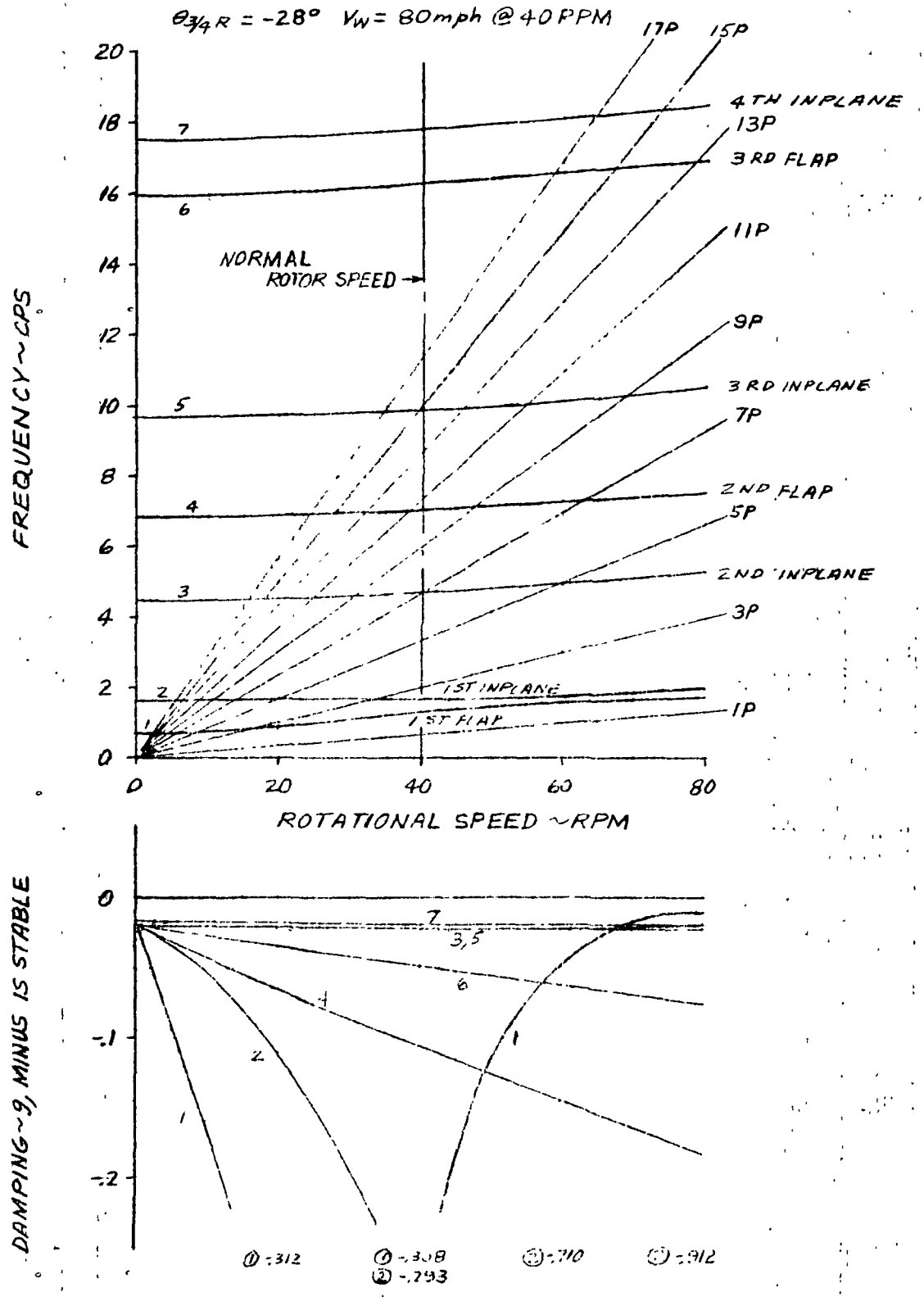

W1004

3-17-75

WM04

FIG. 15
100 KW WINDMILL
COLLECTIVE BLADE STABILITY
FREQUENCY AND DAMPING VS ROTOR SPEED

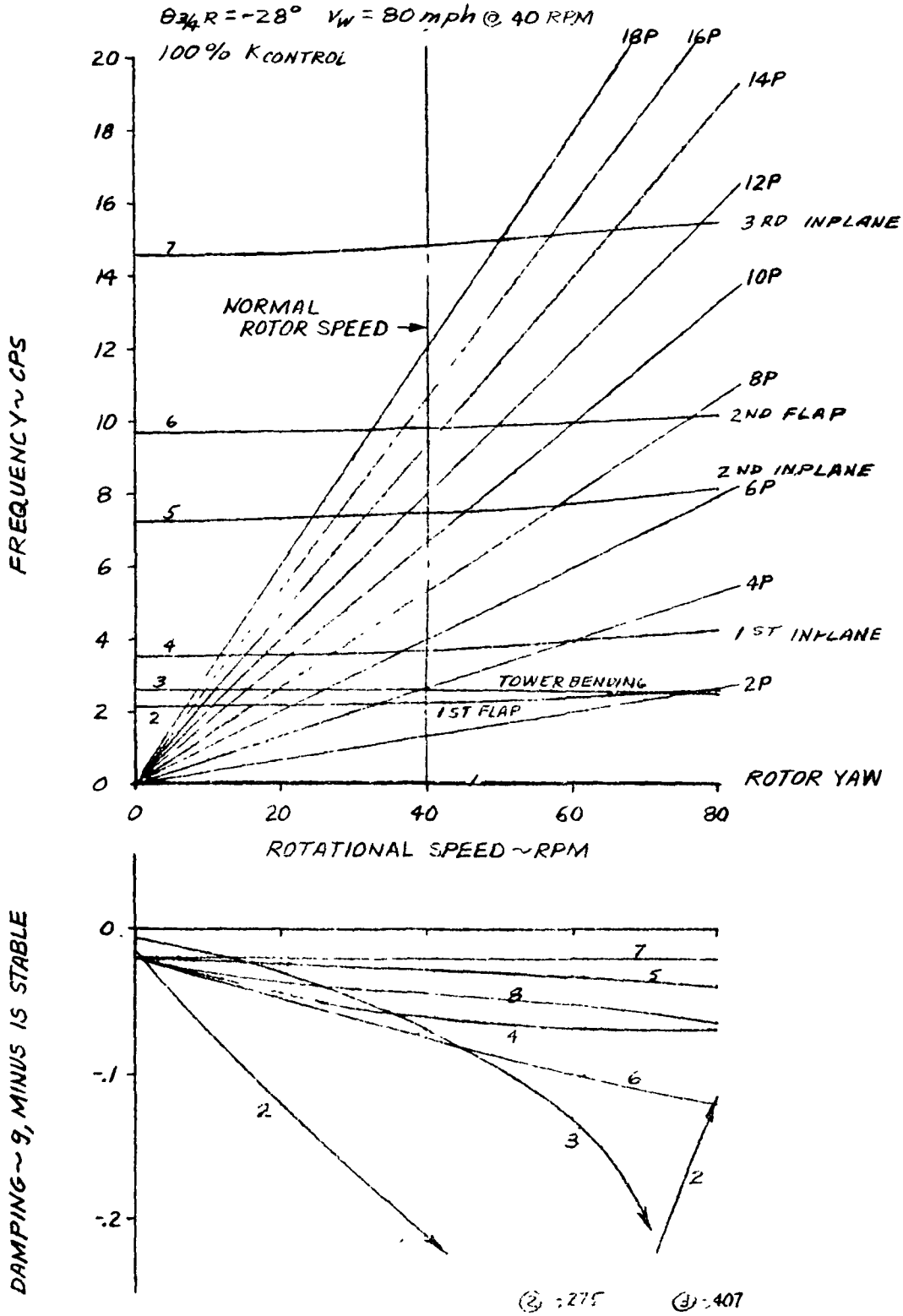

the indicated wind speed and the 40 rpm normal rotational speed. Again all modes are shown to be stable. Note however in Figure 6 that Mode 2, the first cyclic inplane mode damping is fairly independent of rotor speed in contrast to the effect of rotor speed on this mode at zero wind speed in Figure 3.

Figures 8 and 9 show the results at the same 18 mph wind speed blade angle condition for control system stiffnesses of 40% of the nominal values. Comparing these results with those on Figures 6 and 7 show a reduction in the first torsion mode frequencies but no real significant changes in stability characteristics. The damping of all the modes are still shown to be stable and with the exception of the inplane modes, shown an increase in damping with increasing rotational speed.

Figures 10 through 15 show the effect of increased windspeed and corresponding change in blade angle. For the cantilever, cyclic, and collective boundary conditions stability data are shown in Figures 10, 11, and 12 respectively for a 50 mph wind speed and -18 degree collective blade angle and in Figures 13, 14, and 15 for an 80 mph wind speed and a -28 degree collective blade angle. The collective blade angles were selected to maintain the angle of attack at the 3/4 radius at a value approximating that for the 18 mph speed condition.

In review of these figures and Figures 5, 6, and 7, it is seen that the most significantly affected modes again are the inplane modes. The change in blade angle has the effect of reorienting the principal axes of the blade so as to cause the flapping modes at the low blade angles to become the inplane modes at the higher blade angles and visa versa, for the cantilever blade case.

Referring to Figures 11 and 14 it is seen that the combined effect of the influence of the tower and the lowering of the inplane frequency has a significant effect on the stability of the first cyclic inplane mode as it couples with the first cyclic flapping mode. Also note that at -18 degrees of collective, the first cyclic inplane mode frequency is setting right on 3P, the third order crossing line. It is noted that many more combinations of blade angle and wind speed are possible than those analyzed and for which

data are presented. These conditions could be more or less critical than the stability data presented.

Therefore, even though the data presented does not show any instability within the operating range, it will be extremely important to proceed with due caution in expanding the rotor rpm, blade angle, wind speed envelope. Continuous monitoring of the measured loads and vibration levels must be maintained to assure no divergent oscillation occurs. It is also important to distinguish between powered and non-powered operation of the rotor system as far as inplane mode stability is concerned, since this also influences the sign of certain aerodynamic coupling terms which are important in establishing the stability of the inplane mode.

During the envelope expansion of the rotor every effort should also be made to locate the fundamental blade frequency crossings and to identify if any resonances occur in the normal operating rpm collective blade travel range.

It would be very desirable to supplement these analyses with additional points within the possible rpm, blade angle wind speed envelope, the wind turbine system might be subjected too. It would also be very desirable to actually excite the coupled tower-cyclic inplane mode during the envelope expansion of the wind turbine in order to obtain actual experimentally determined frequency and damping values of this mode.

Figures 13, 14, and 15 represent extreme conditions which in fact will never happen since it is planned to feather the rotor at wind speeds above 60 mph. As indicated before, for the cyclic case, the first inplane, tower-first flapwise bending mode couple and cause a reduction in the damping of the inplane mode at rotor overspeed. Also, in Figure 15 it is seen that the tower bending-first collective flapping modes couple with increase in rotor speed. There is no indication though of any potential stability problem as a result of this coupling. There merely appears to be an exchange of energy between the two modes.

One other thing should be noted. Since these analyses are performed at a constant tip speed ratio as a function of rpm, then 10 rpm corresponds to a

20 mph wind speed, 20 rpm corresponds to a 40 mph wind speed, and so on. The effect then of windspeed at zero rpm has been examined in an independent study, the results of which are presented in the following section.

2.1.3 Non-Rotating Flutter and Divergence Results

In Figures 16 through 29, data are presented as a function of wind speed and as a function of control flexibility at different wind conditions. Data are shown for the condition of the wind blowing directly at the leading edge of the blade, directly at the trailing edge of the blade and at the trailing edge but skewed at 45 degrees to give a most critical static divergence condition. For the wind blowing directly over the leading or trailing edge of the blade, wind velocities from zero to 140 mph have been examined. For the most critical static divergence case, wind velocities to 200 mph have been examined.

Figures 16, 17, and 18 present the results of these studies in terms of frequencies and damping of the various rotor blade/coupled rotor-tower modes as a function of wind speed with the wind blowing directly over the blade leading edge. Figure 16 is for the cantilever blade boundary condition and Figures 17 and 18 are for the cyclic and collective boundary conditions respectively. The data is shown with the rotor brake off and with the blades feathered into the wind.

As can be seen, all modes are shown to be stable and, with the exception of the chordwise mode, show increasing stability with wind speed. For the 140 mph wind speed condition, a variation in the collective control stiffness was made. The effects of this are shown in Figure 19. The stiffness is varied from its nominal value of 9.7×10^6 inch-pounds per radian to approximately one-quarter the nominal value of 2.4×10^6 inch-pounds per radian. No significant degradation is seen in damping of any of the modes due to the reduction in control system stiffness at the 140 mph wind speed, zero rotor speed condition.

Figures 20, 21, and 22 show the predicted frequency and damping as a function of windspeed for the condition of zero rotor speed and of the wind blowing

FIG. 16

100 KW WINDMILL
CANTILEVER BLADE STABILITY-
FREQUENCY AND DAMPING VS WIND SPEED

$\theta_{3/4R} = -90°$ $\Omega = 0.0$ WIND NORMAL TO L.E. AT 3/4R

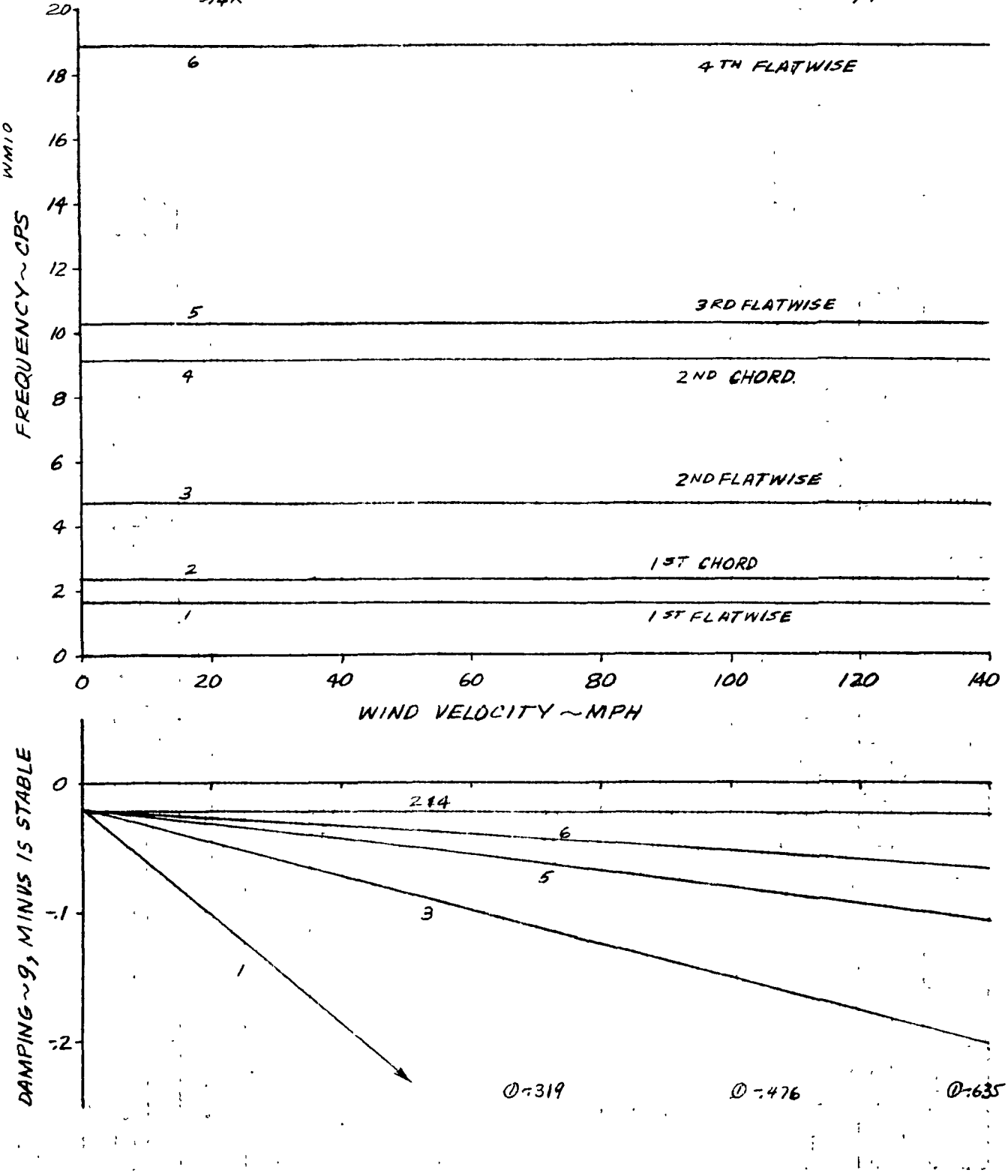

FIG. 17

100 KW WINDMILL
CYCLIC BLADE STABILITY
FREQUENCY AND DAMPING VS WIND SPEED

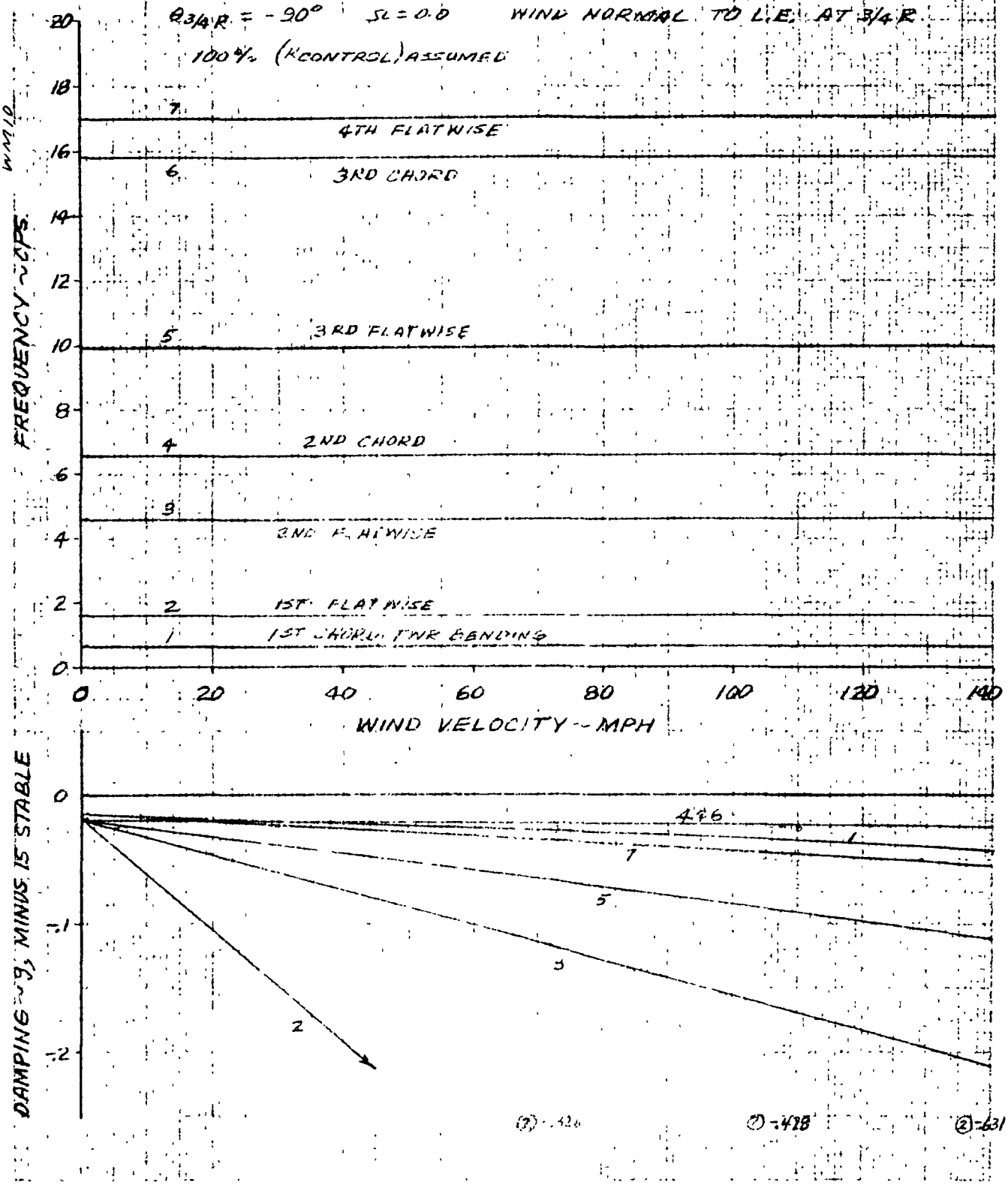

FIG. 19

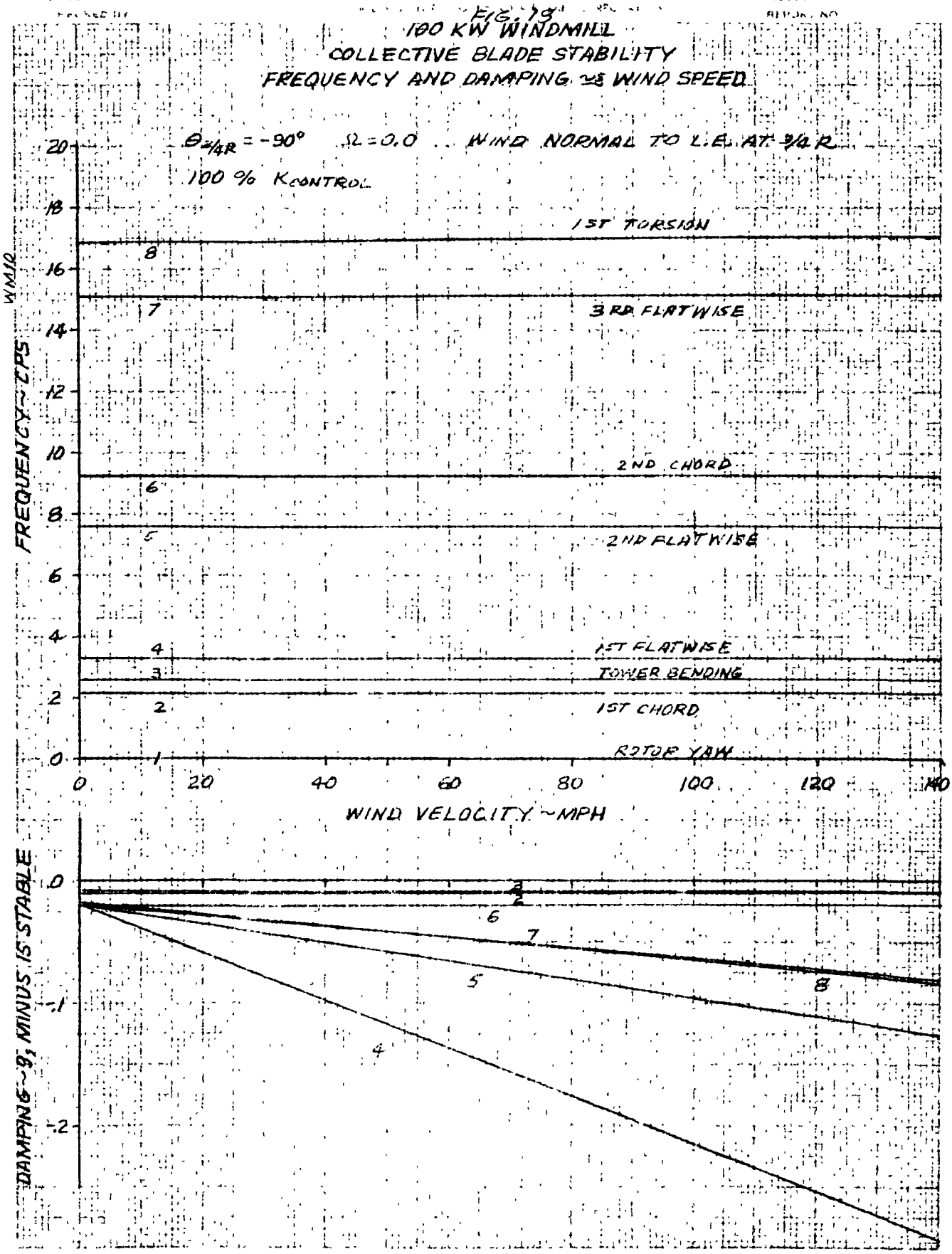
100 KW WINDMILL
COLLECTIVE BLADE STABILITY
FREQUENCY AND DAMPING VS WIND SPEED
θ3/4R = -90° Ω = 0.0 WIND NORMAL TO L.E. AT 3/4 R
100 % K CONTROL
1ST TORSION
3RD FLATWISE
2ND CHORD
2ND FLATWISE
1ST FLATWISE
TOWER BENDING
1ST CHORD
ROTOR YAW
WMIQ FREQUENCY ~ CPS
WIND VELOCITY ~ MPH
DAMPING ~ g's MINUS IS STABLE

FIG 19

100 KW WINDMILL

COLLECTIVE BLADE STABILITY

FREQUENCY AND DAMPING VS CONTROL SYSTEM STIFFNESS

$\theta_{3/4R} = -.30°$, $\Omega = 0.0$, $V_W = 140$ mph

WIND NORMAL TO L.E. AT 3/4 R

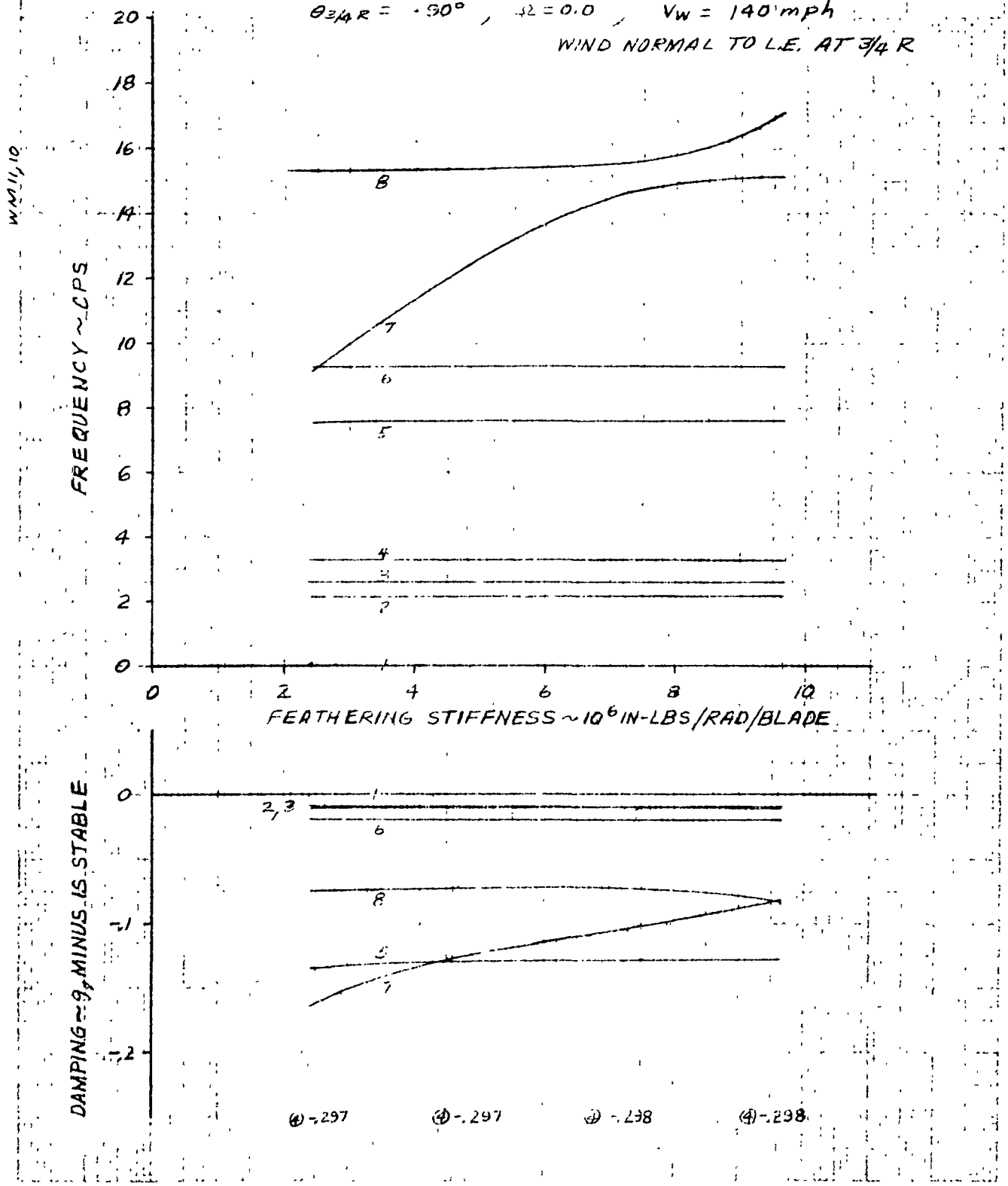

3-17-75

FIG. 20

100 KW WINDMILL
CANTILEVER BLADE STABILITY
FREQUENCY AND DAMPING VS WIND SPEED

$\theta_{3/4R} = -90°$ WIND BLOWING DIRECTLY OVER
$\Omega = 0.0$ RPM TRAILING EDGE OF BLADE

WM 13

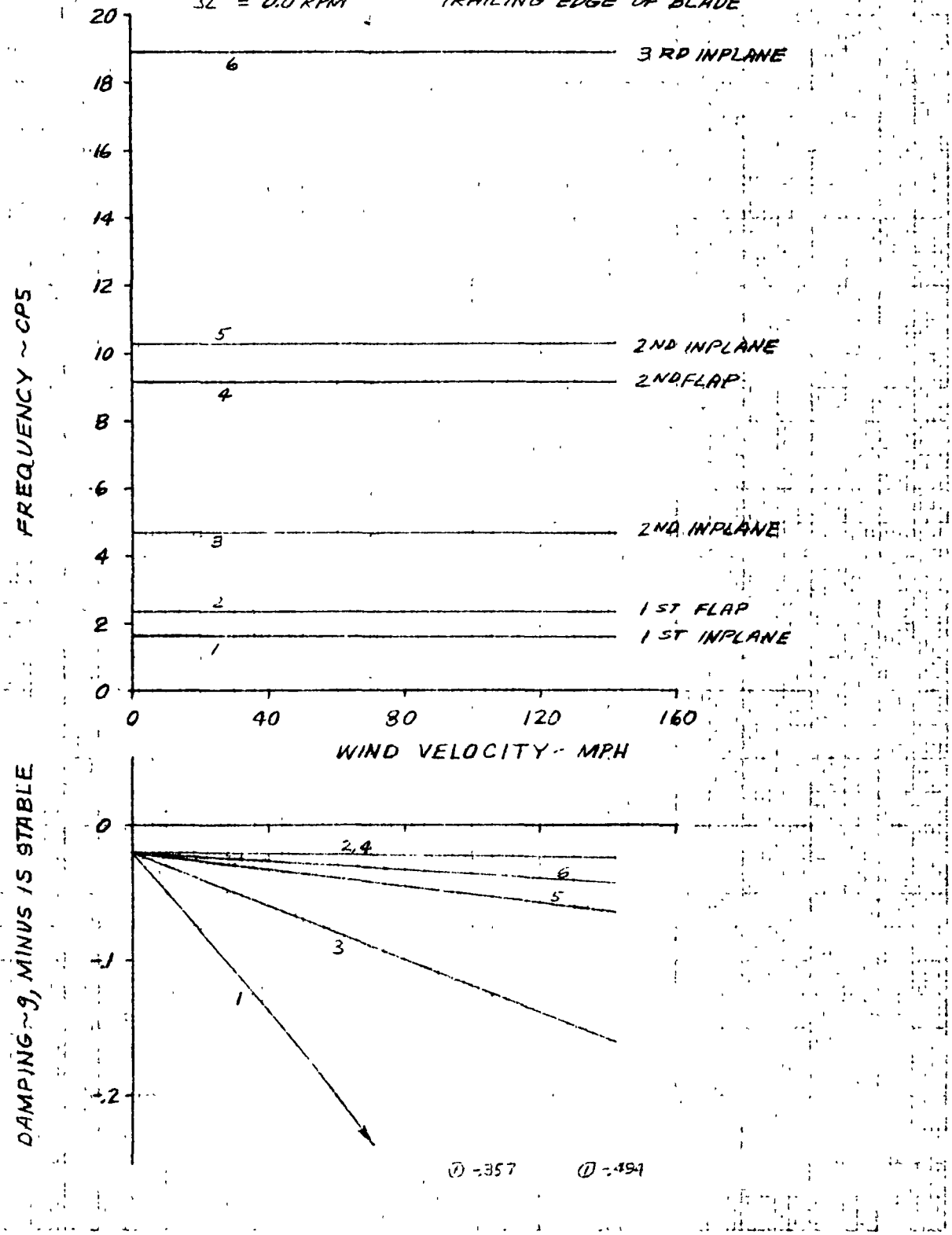

FIG. 21

100 KW WINDMILL

COLLECTIVE BLADE STABILITY

FREQUENCY AND DAMPING VS WIND SPEED

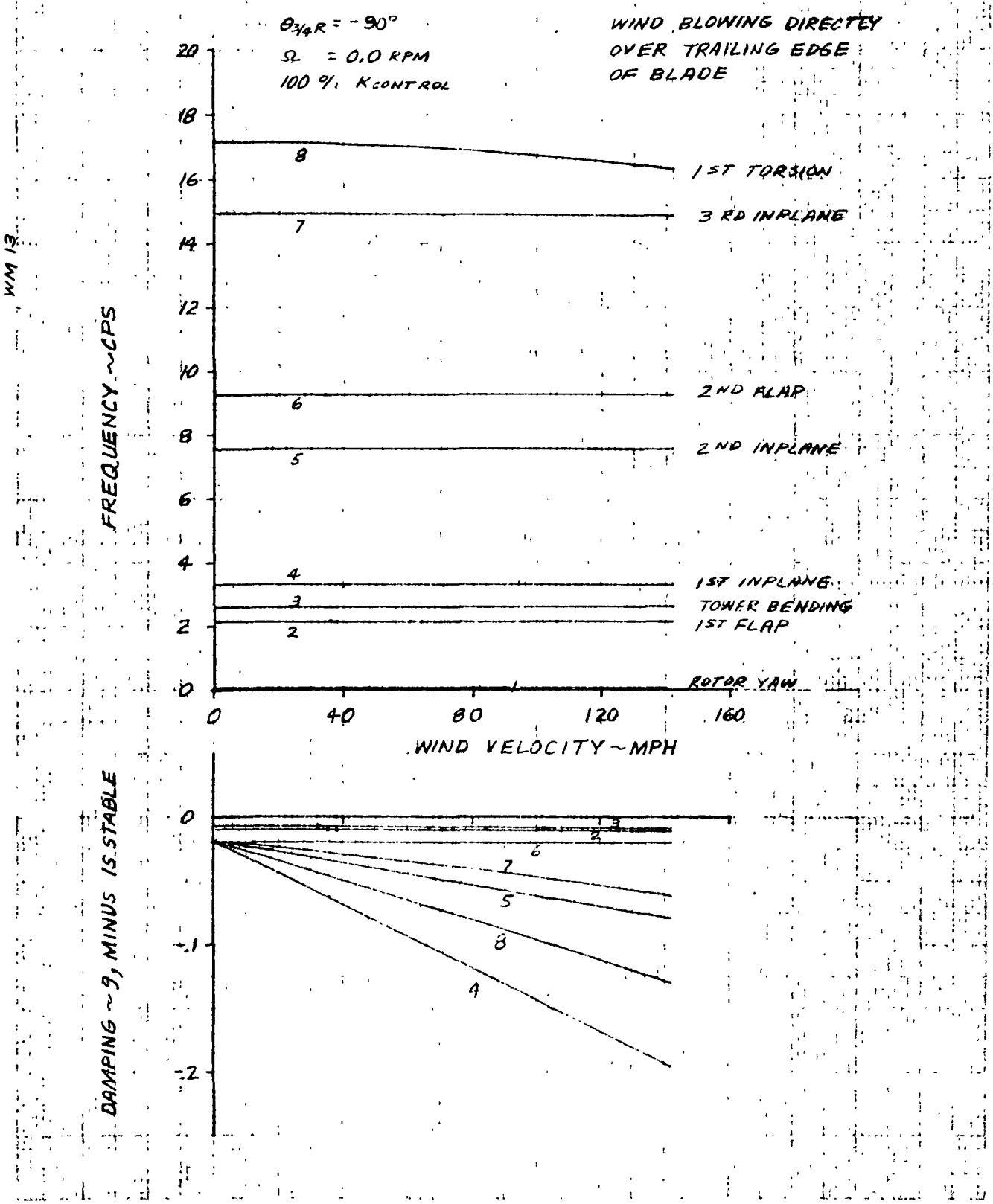

FIG 2.5

100 KW WINDMILL
CYCLIC BLADE STABILITY
FREQUENCY AND DAMPING VS WIND SPEED

$\theta_{3/4R} = -90°$
SL = 0.0 RPM
40 % ($k_{CONTROL}$) ASSUMED

WIND BLOWING DIRECTLY OVER TRAILING EDGE OF BLADE

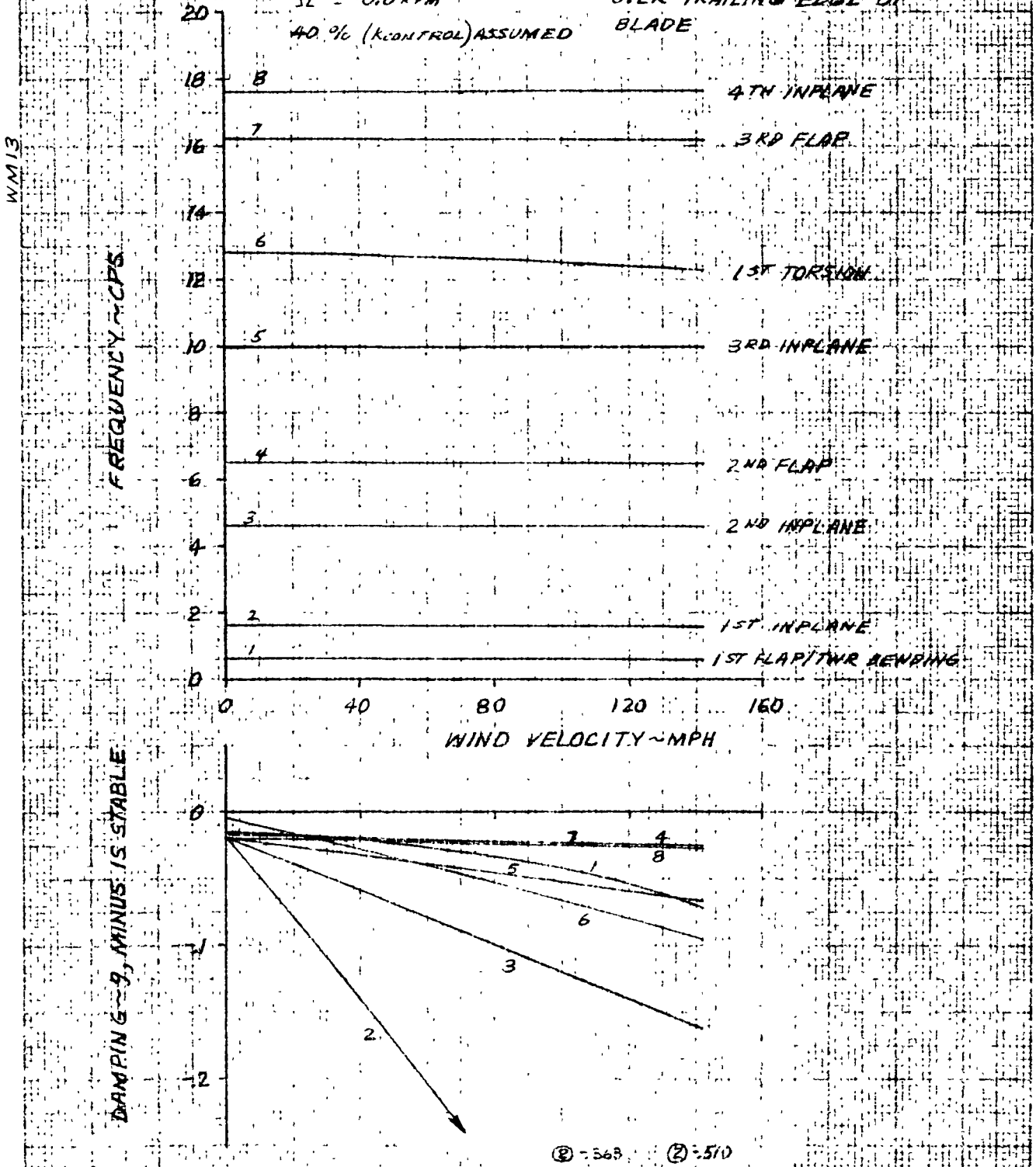

WM13

DATE 3-19-75

FIG. 23

100 KW WINDMILL
CANTILEVER BLADE STABILITY
FREQUENCY AND DAMPING VS ROTOR SPEED

$\theta_{3/4R} = -90°$
$\Omega = 0.0$ RPM

WIND BLOWING OVER TRAILING EDGE OF BLADE AT SKEWED ANGLE OF 45°

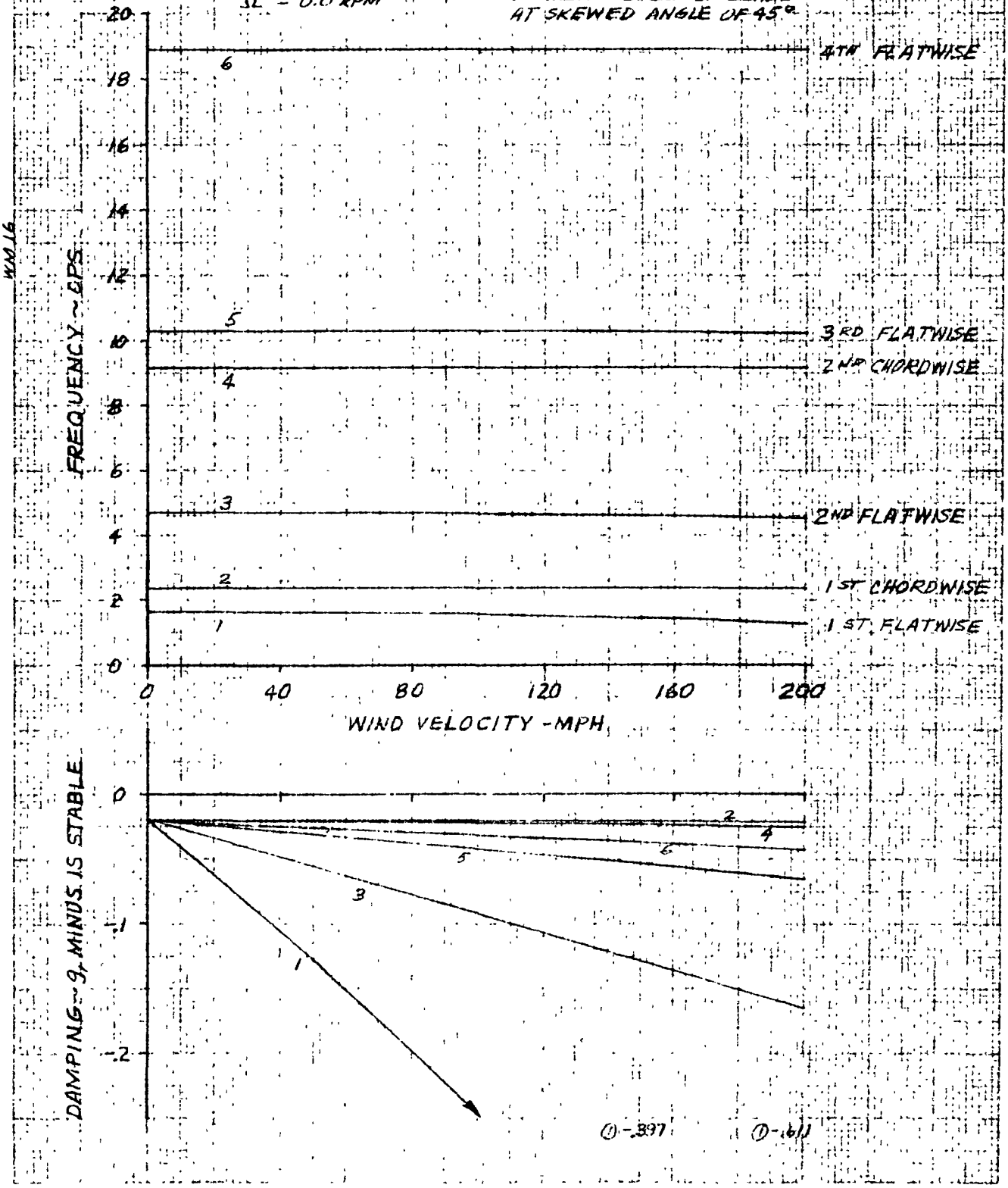

3-20-75

FIG. 24

100 KW WINDMILL
CYCLIC BLADE STABILITY
FREQUENCY AND DAMPING VS ROTOR SPEED

$\Theta_{3/4R} = -90°$
$\Delta L = 0.0$ RPM
100% ($K_{CONTROL}$) ASSUMED

WIND BLOWING OVER TRAILING EDGE OF BLADE AT SKEWED ANGLE OF 45°

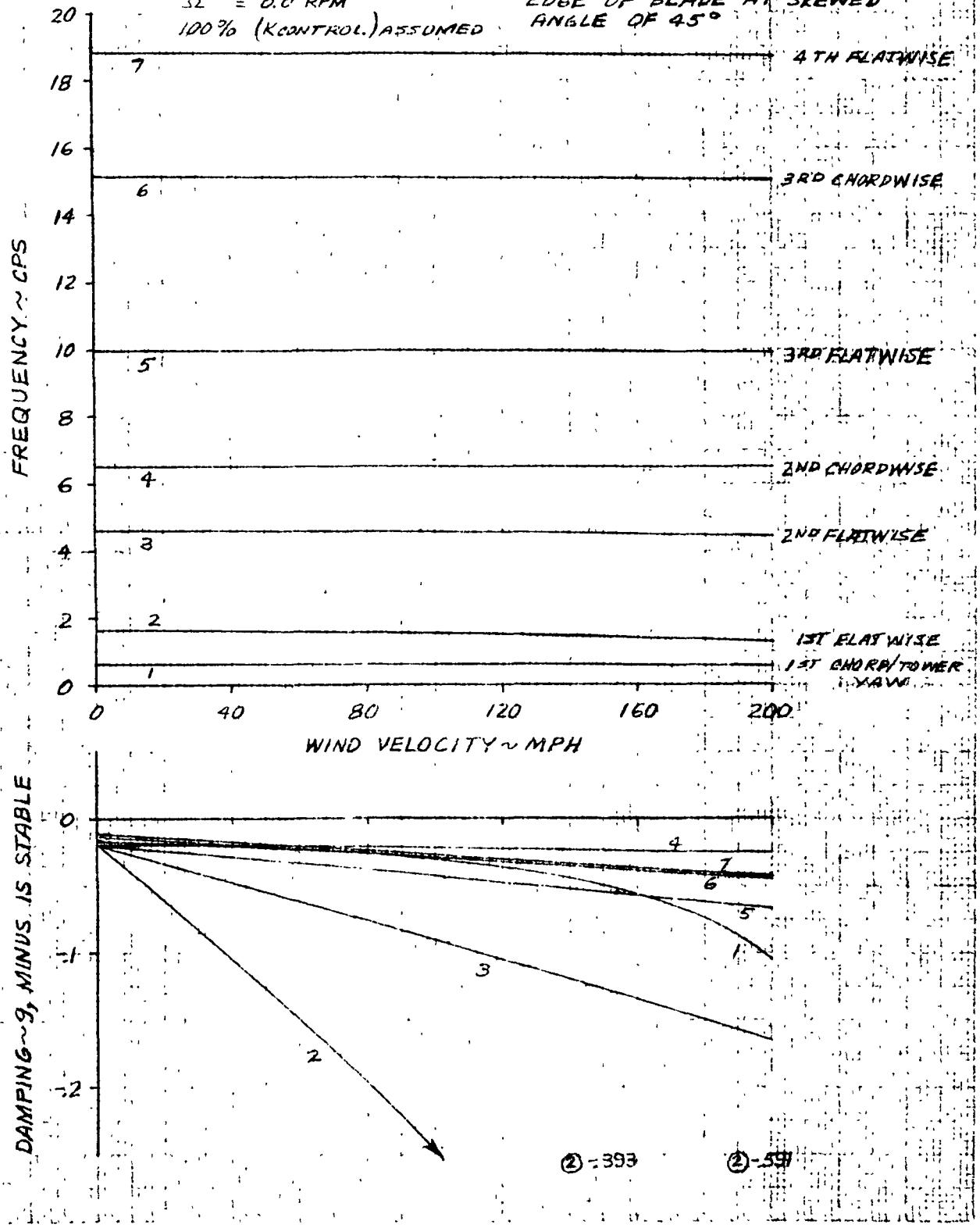

WM17

3-19-75

FIG 25

100 KW WINDMILL
COLLECTIVE BLADE STABILITY
FREQUENCY AND DAMPING VS WIND SPEED

$\theta_{3/4R} = -90°$
$\Omega = 0.0$ RPM
100 % K CONTROL

WIND BLOWING OVER TRAILING EDGE OF BLADE AT SKEWED ANGLE OF 45°

WM16

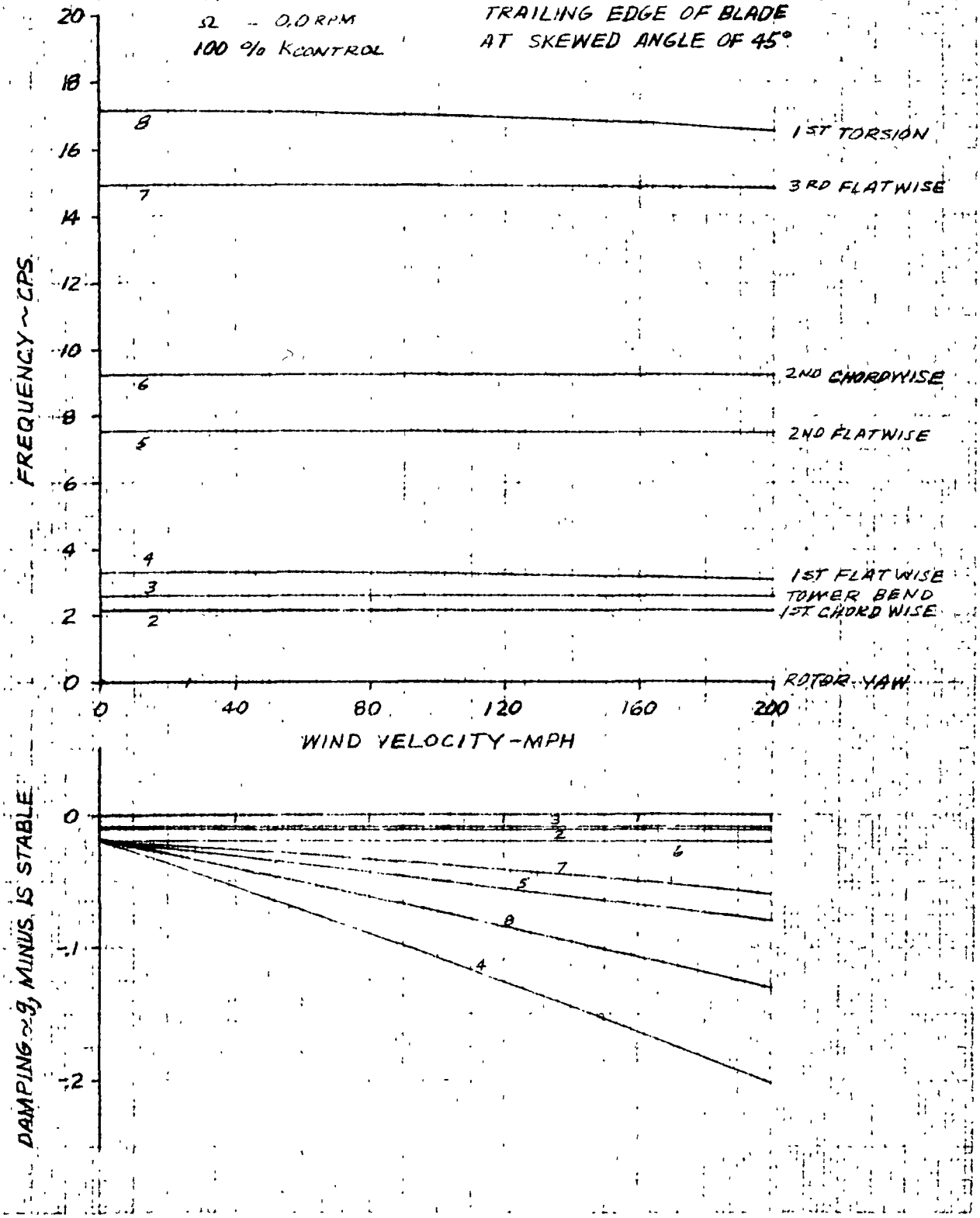

3-26-75

FIG 26

100 KW WINDMILL
COLLECTIVE BLADE STABILITY
FREQUENCY AND DAMPING VS WIND SPEED
ROTOR BRAKE ON

$\theta_{3/4R} = -90°$
$\Omega = 0.0$ RPM
100 % K CONTROL

WIND BLOWING OVER TRAILING EDGE OF BLADE AT SKEWED ANGLE OF 45°

KM 18

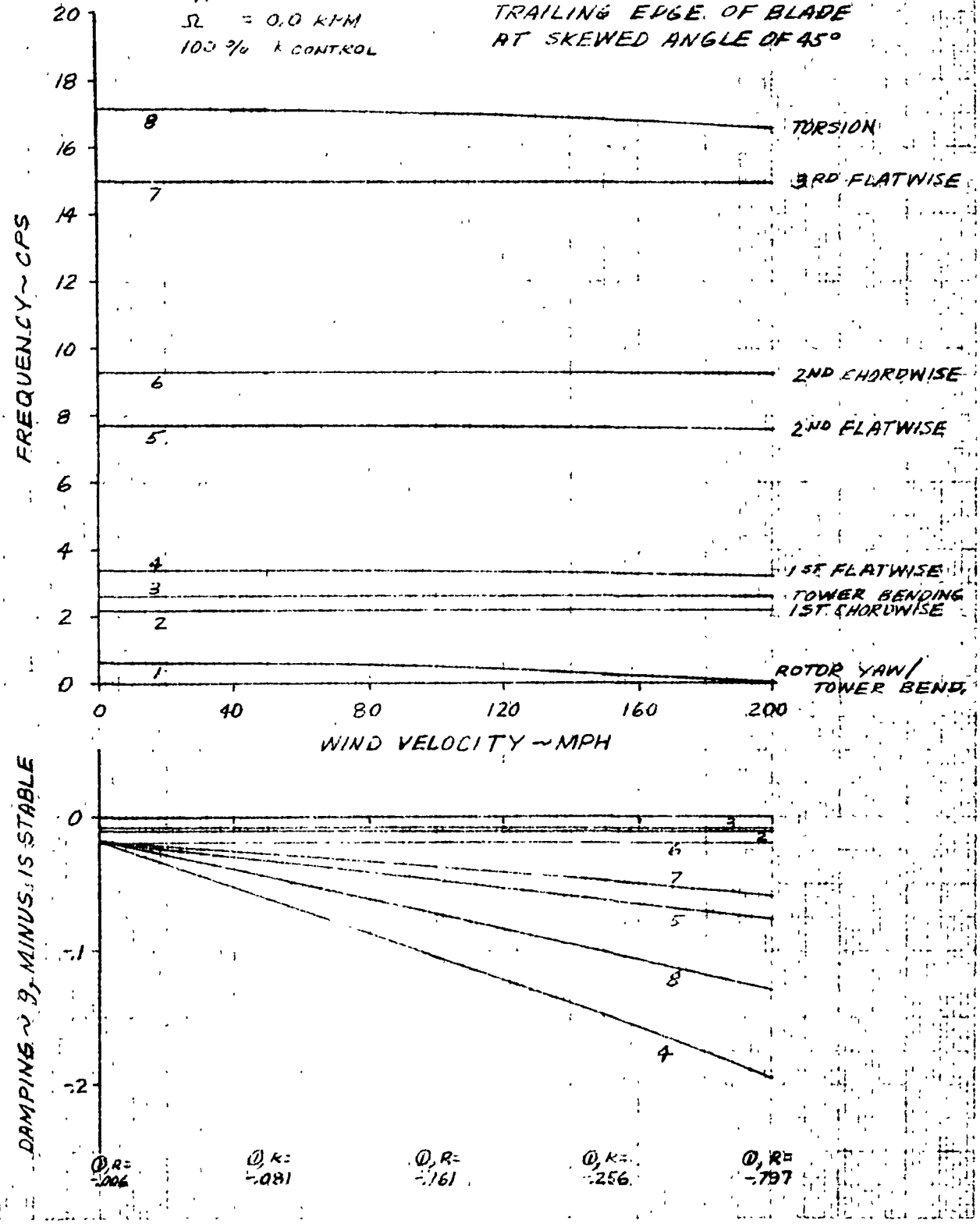

FIG 27

100 KW WINDMILL
CYCLIC BLADE STABILITY
FREQUENCY AND DAMPING VS CONTROL FLEXIBILITY

$\theta_{3/4R} = -90°$
$\Omega = 0.0$ RPM
$V_W = 140$ mph

WIND BLOWING OVER TRAILING EDGE OF BLADE AT SKEWED ANGLE OF 45°

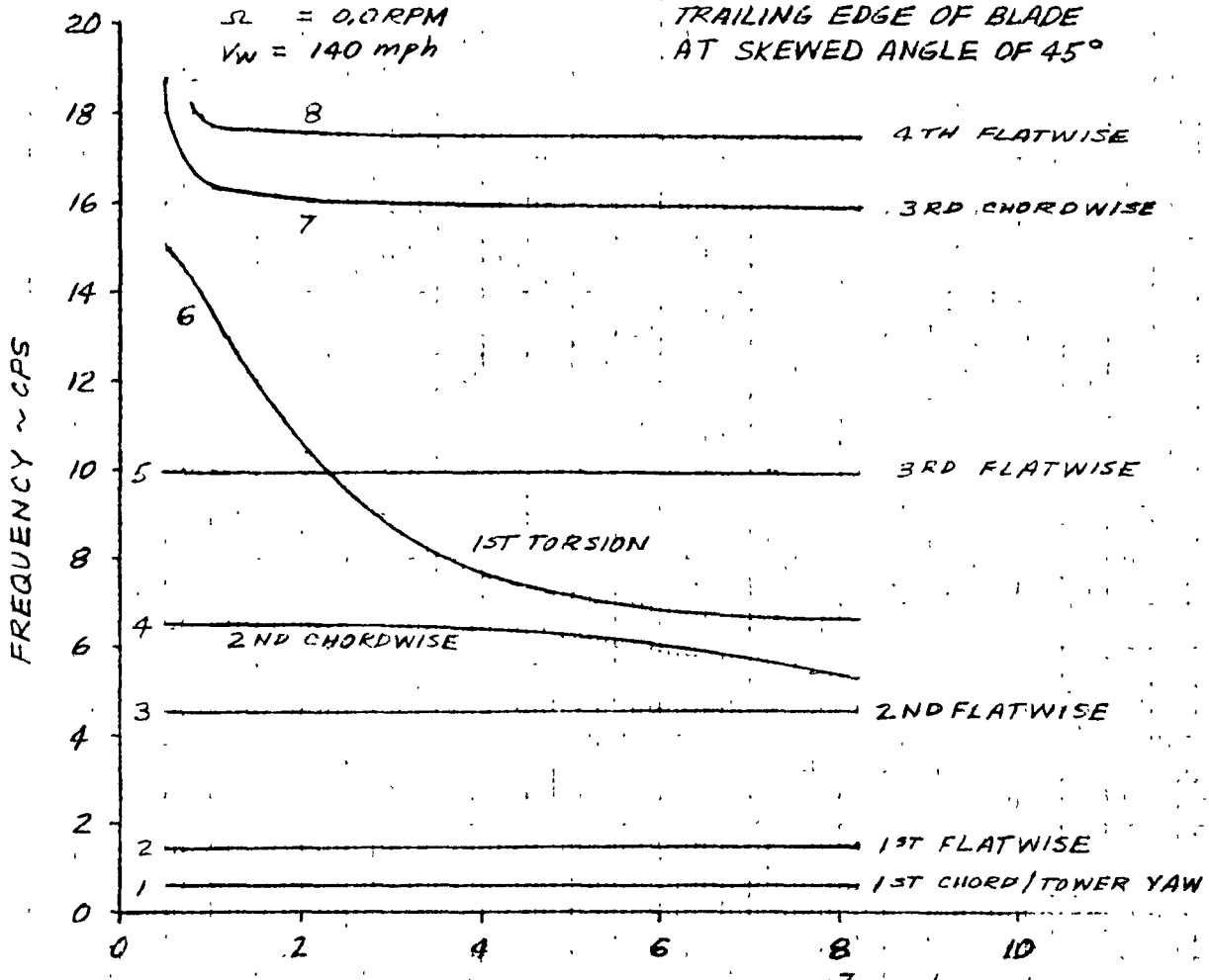

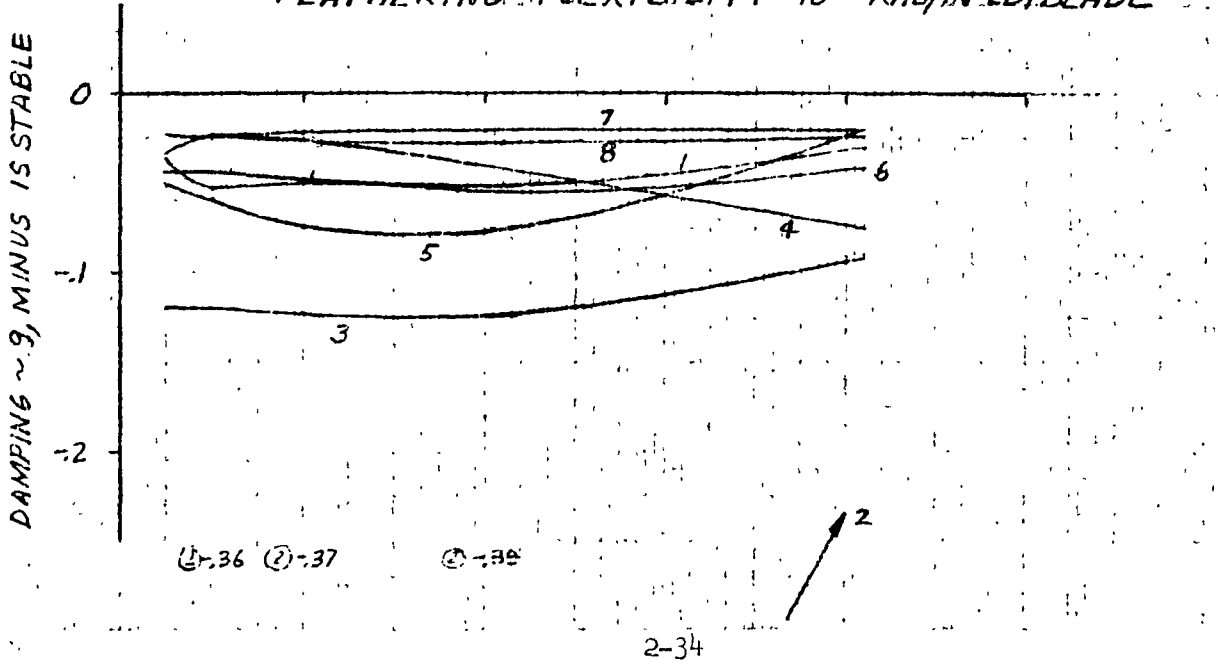

FIG 28

100 KW WINDMILL
COLLECTIVE BLADE STABILITY
FREQUENCY AND DAMPING VS CONTROL FLEXIBILITY

$\theta_{3/4R} = -90°$
$\Omega = 0.0$ RPM
$V_W = 140$ MPH

WIND BLOWING OVER TRAILING EDGE OF BLADE AT SKEWED ANGLE OF 45°

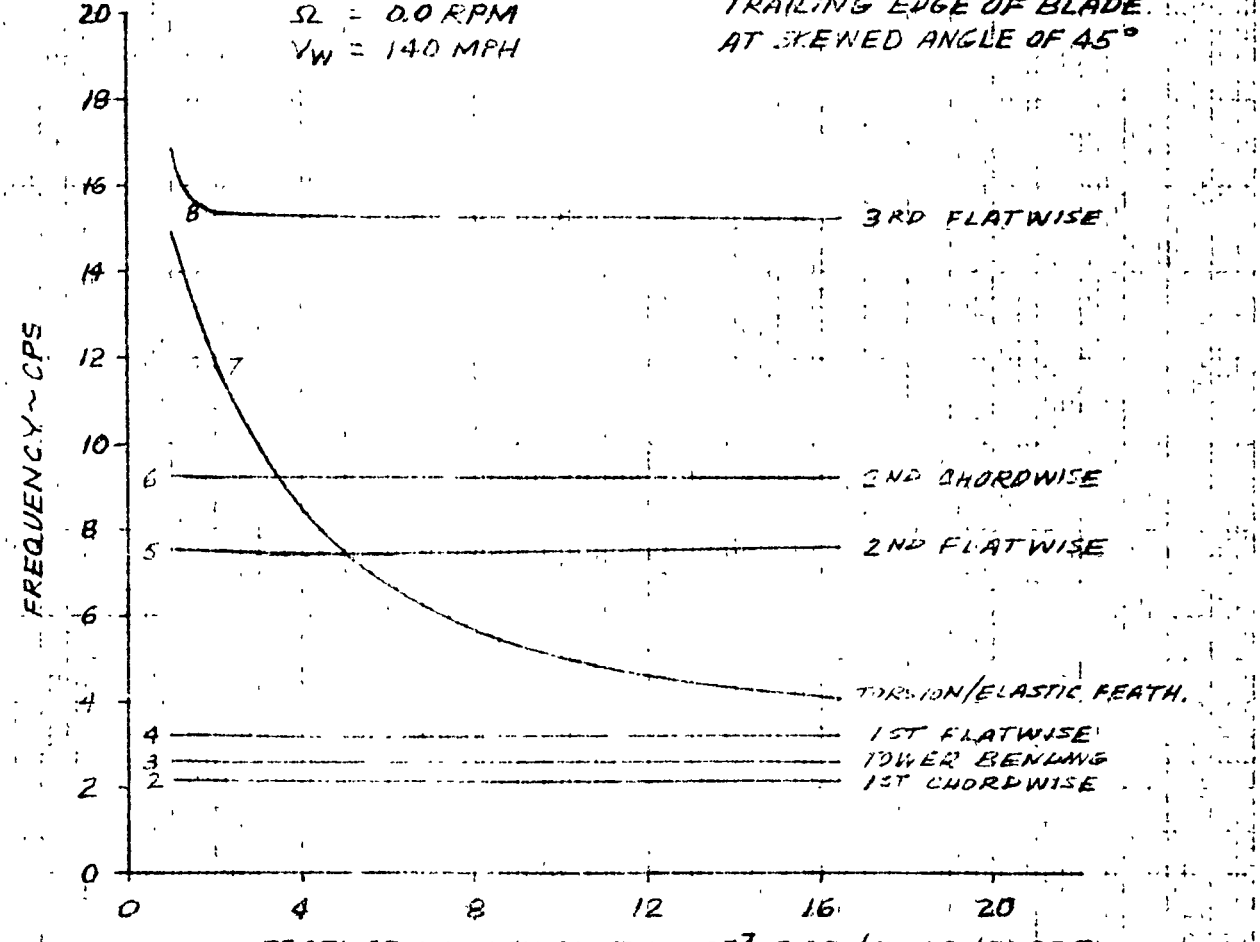

FEATHERING FLEXIBILITY ~ 10^{-7} RAD/IN-LB/BLADE

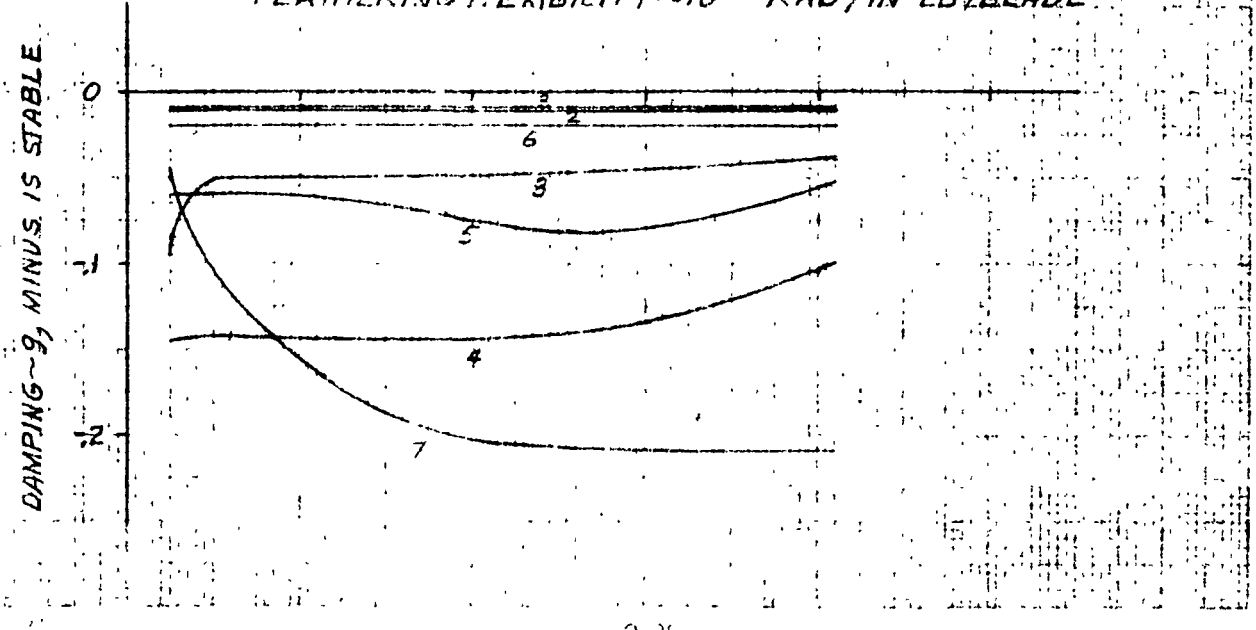

3-26-75

FIG 29

100 KW WINDMILL
COLLECTIVE BLADE STABILITY
FREQUENCY AND DAMPING VS CONTROL FLEXIBILITY

$\theta_{3/4R} = -90°$
$\Omega = 0.0$ RPM
$V_W = 140$ mph

WIND BLOWING OVER
TRAILING EDGE OF BLADE
AT SKEWED ANGLE OF 45°

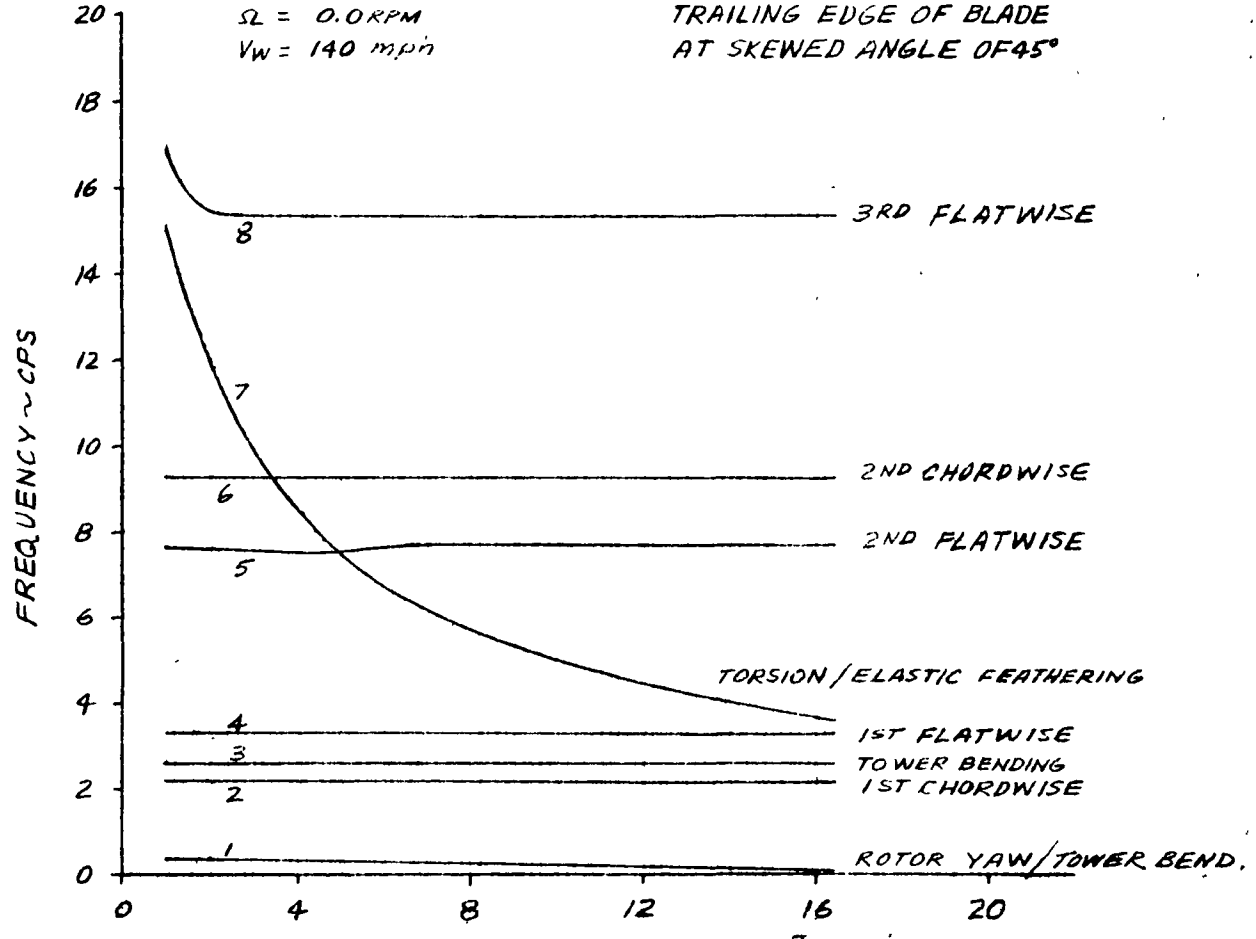

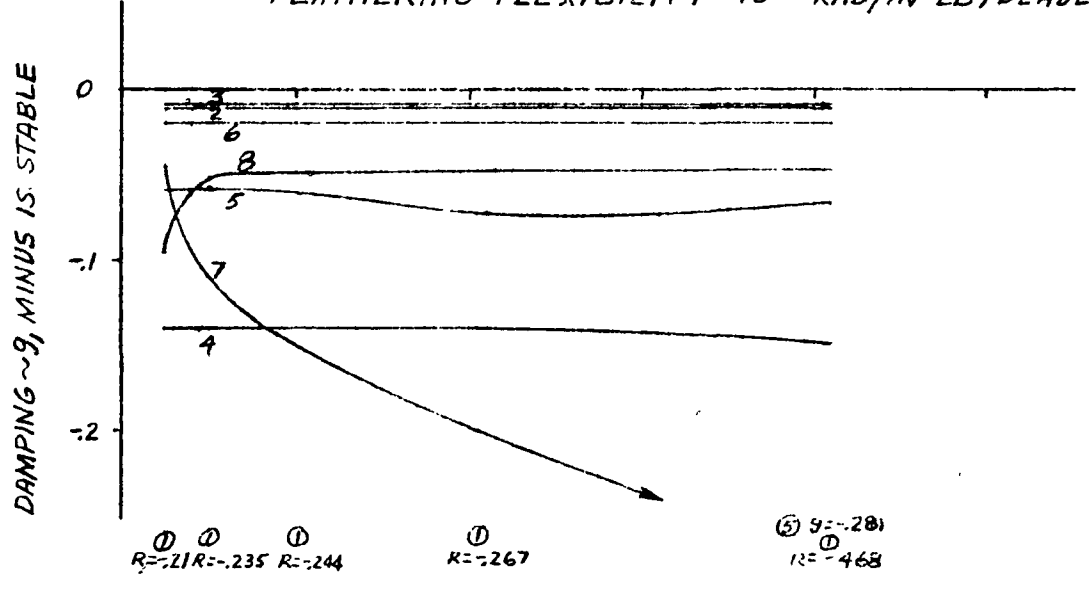

WM 18

directly over the trailing edge. These results are again shown for the cantilever, cyclic and collective boundary conditions. The cyclic case is shown with a control system stiffness of 40 percent of the assumed value. The data show some reduction in the torsion mode frequency with wind speed but the system if definitely predicted to be free from any static instability for this windspeed/rotor speed condition.

Figures 23 through 29 present data all for the condition of the wind blowing over the trailing edge but in a most critical static divergence direction of at 45 degrees towards the blade root as the wind progresses from the blade trailing edge to the blade leading edge.

Figure 23 shows the effect of windspeed on the frequency and damping for the cantilever blade boundary condition. Note that the first flatwise mode is dropping in frequency with increasing wind speed. However, even at 200 mph there is only a 25% drop in the frequency of this mode, indicating the basic blade is completely free from any potential static divergence problem.

Figure 24 is for the cyclic boundary condition and as can be seen, the chracteristic behavior of the first flatwise mode is the same as for the cantilever boundary condition.

Figure 25 and 26 are for the collective boundary condition. Figure 25 is with the rotor brake off and Figure 26 is with the rotor brake engaged. With the rotor brake disengaged there is no significant effect of windspeed except to increase the damping of all the flatwise and torsion modes and to lower the frequency of the torsion mode.

With the rotor brake locked however, the rotor yaw mode is predicted to statically diverge at approximately 200 mph. It is noted that the strength of the tower is well above the capacity of the rotor brake so even if a divergence tendency did occur the rotor brake would slip and act like a coulomb damper.

For this wind condition, the wind blowing over the trailing edge at a 45 degree skewed angle, the effect of control system flexibility on frequency and

damping of the coupled rotor blade-tower modes at a windspeed of 140 mph has been examined. The results of this study are shown in Figures 27, 28, and 29 for the cyclic and collective, with and without the rotor brake engaged, respectively.

These figures show that even for an approximate eight fold reduction in the control system stiffnesses from the nominal value the system is free from flutter and divergence. However, from Figure 29, it is seen that for a collective feather stiffness of approximately 1.1×10^6 inch-pounds per radian at 140 mph, the system would statically diverge in the rotor yaw/tower bending mode.

Again however, it is understood the capacity of the brake is below the load limit of the tower, so the brake would act as a coulomb damper in this mode.

2.2 TRANSIENT AND DYNAMIC RESPONSE ANALYSIS

A limited transient response and steady state time history analysis was performed on the windmill blades using the REXOR computer program the results of which are reported in Figures 30 and 31. Figure 30 is a plot of time histories of blade flapping, chordwise and torsion loads as a function of rotor azimuth at several spanwise stations along the rotor blade. The condition analyzed is at 40 rpm, zero blade angle at the three-quarter radius and 18 mph windspeed.

Figures 30a and 30b give the computed blade root moments and shears, the blade feathering moment and the blade tip twist. Figures 30c through 30e present the computed flapping moments at twelve stations along the span of the blade. Figures 30f through 30h present the computed flapping moments and the computed blade torsion moments are presented in Figures 30i through 30k.

Transient blade responses to a small step input in each mode are shown in Figures 31a through 31c. These data are shown to give a visual indication of the expected blade transient response due to a small disturbance while operating close to the design point condition.

FIG. 30a

WINDMILL - EXPANDED ONE REVOLUTION

PLOTS OF BLADE AND HUB LOADS AND RESPONSE

REXOR

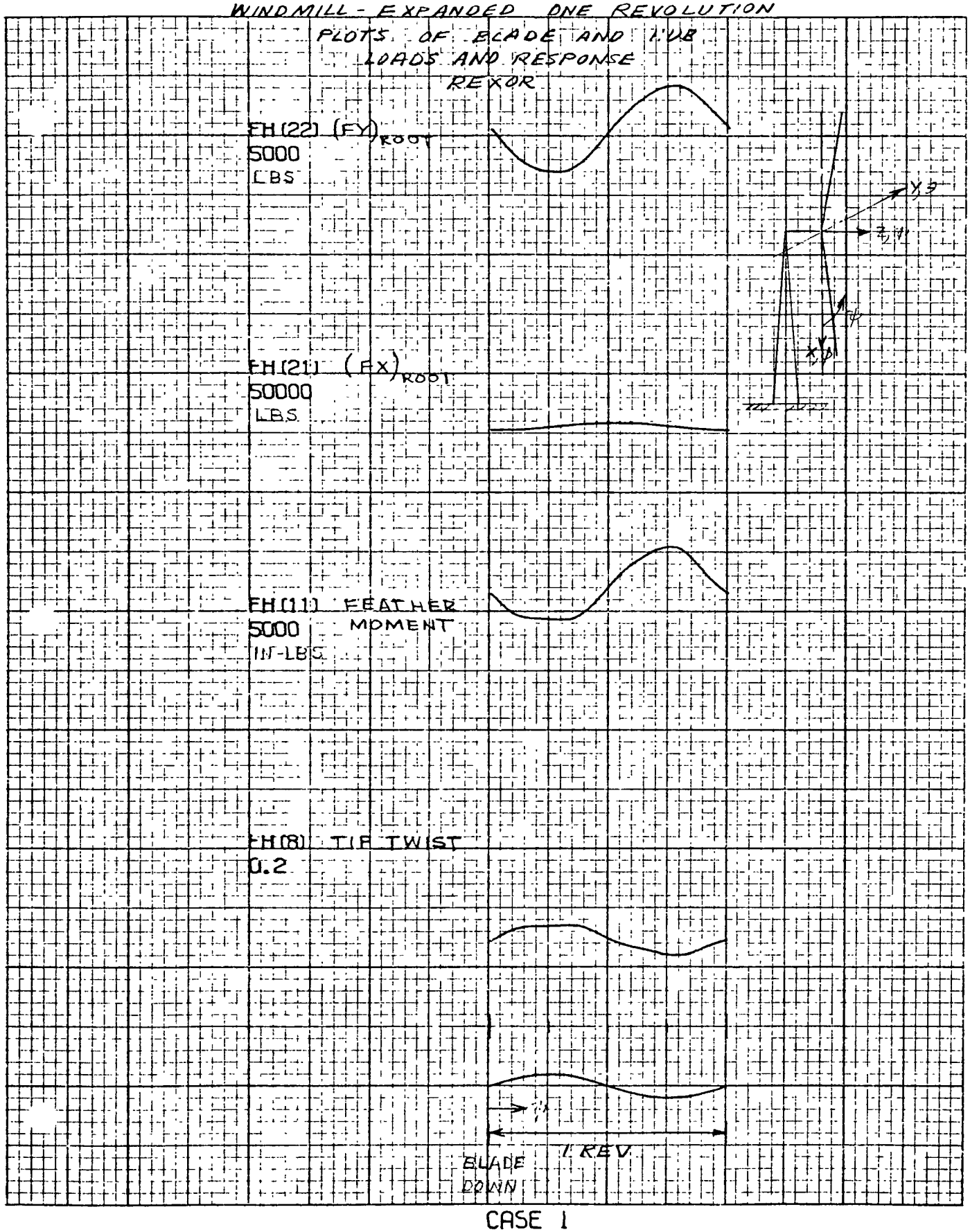

CASE 1
1-28-75

Fig. 30 b

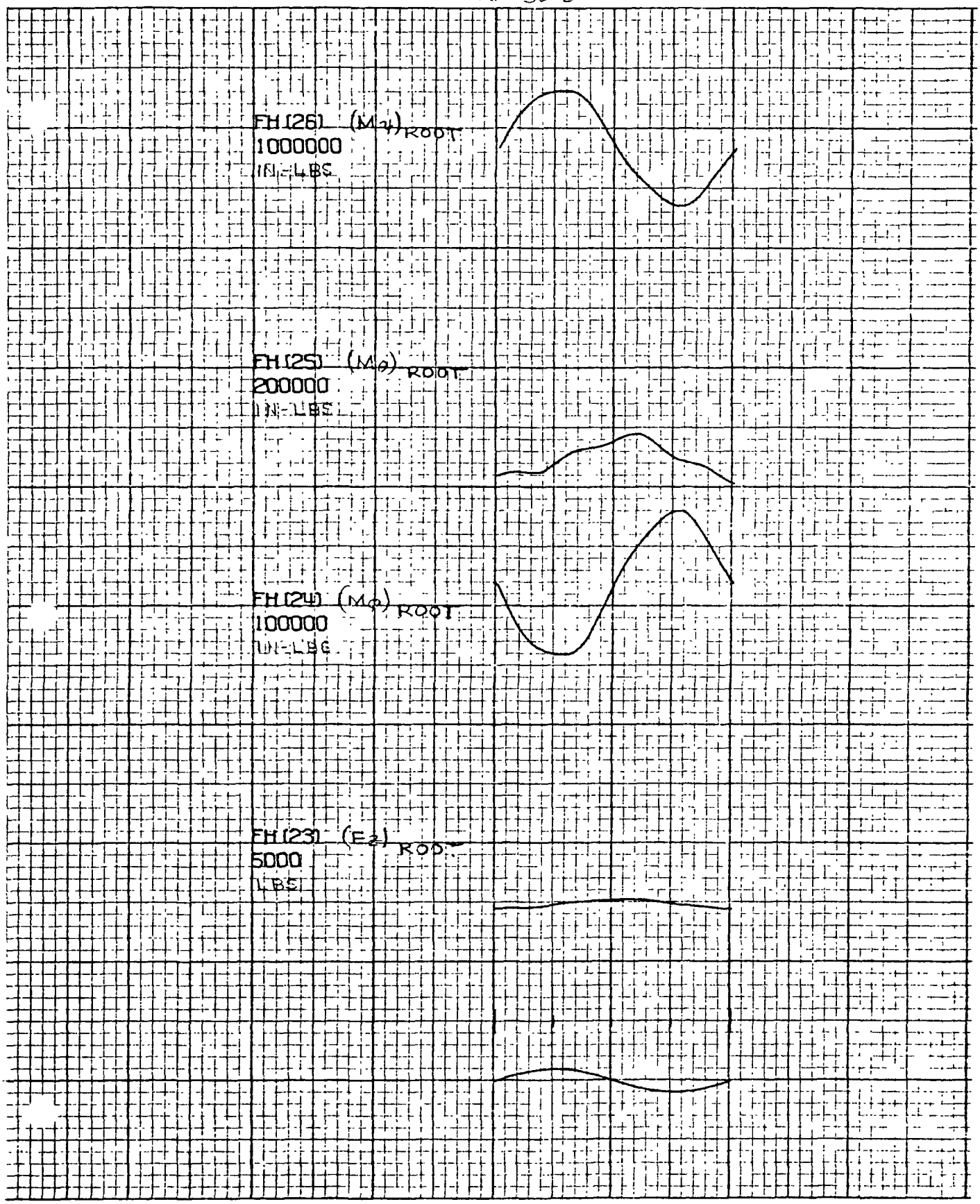

CASE 1
1-28-75

FIG. 30 C

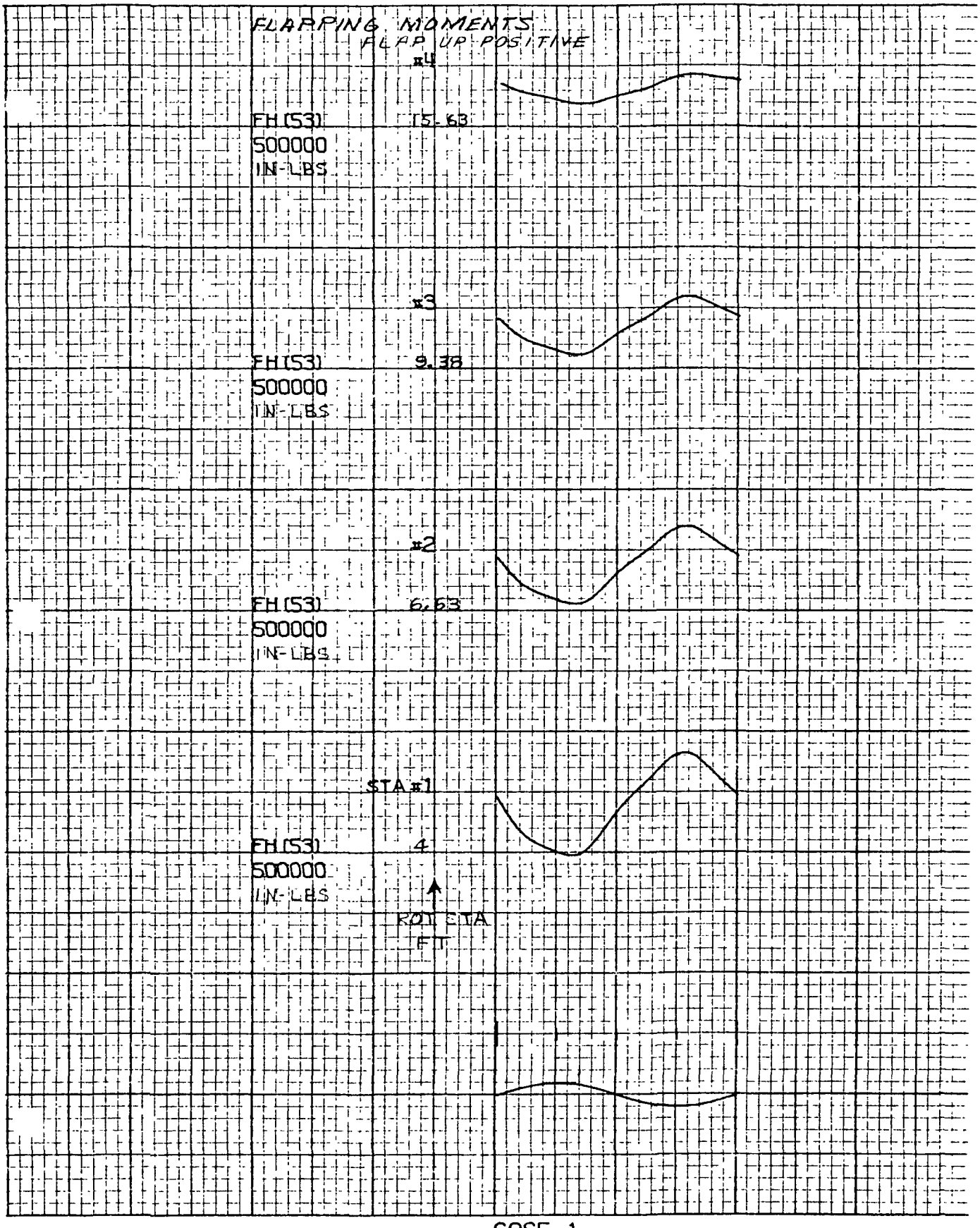

CASE 1
1-28-75

FIG 500

FLAPPING MOMENTS (CONT'D)

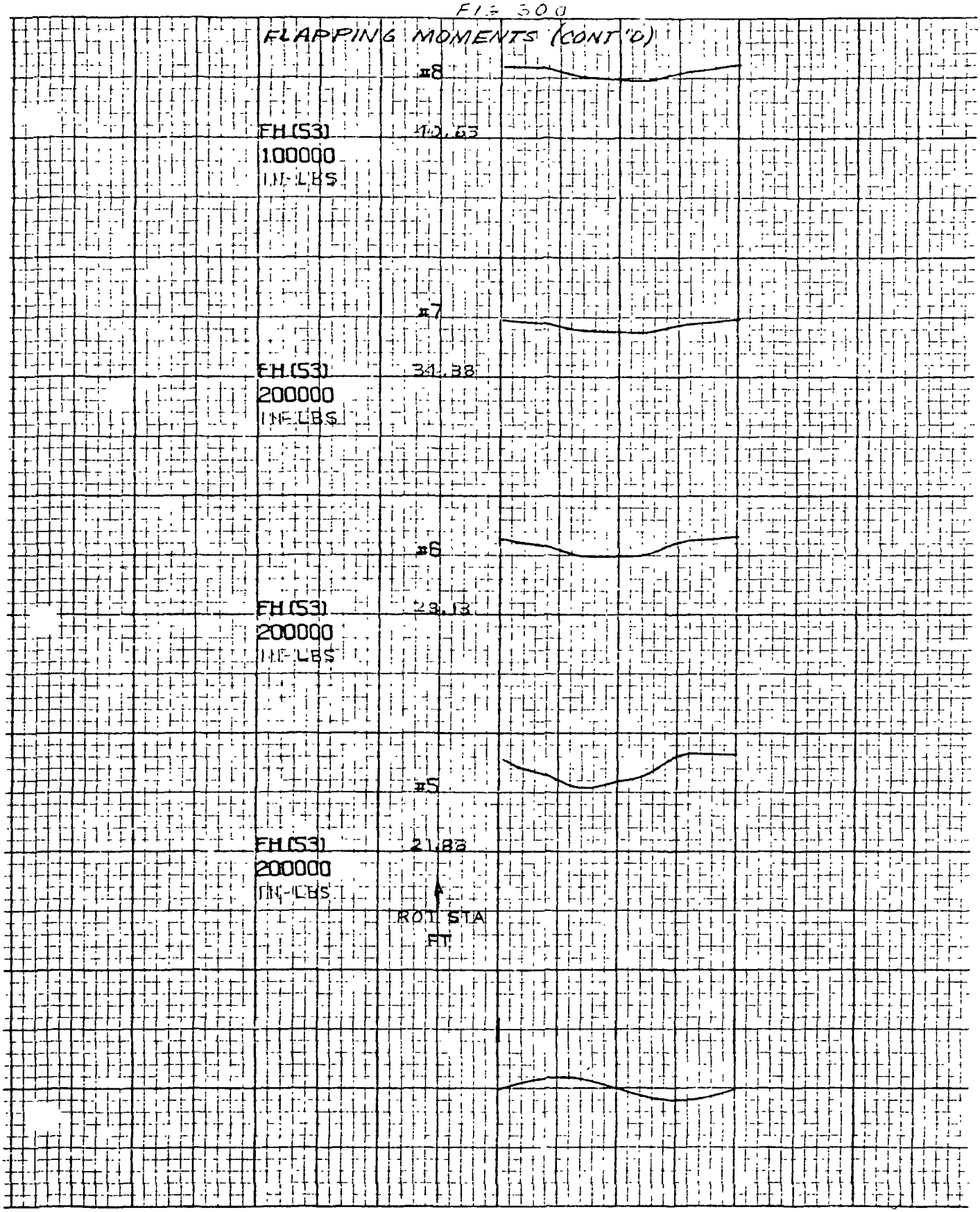

CASE 1
1-28-75

FIG 30e

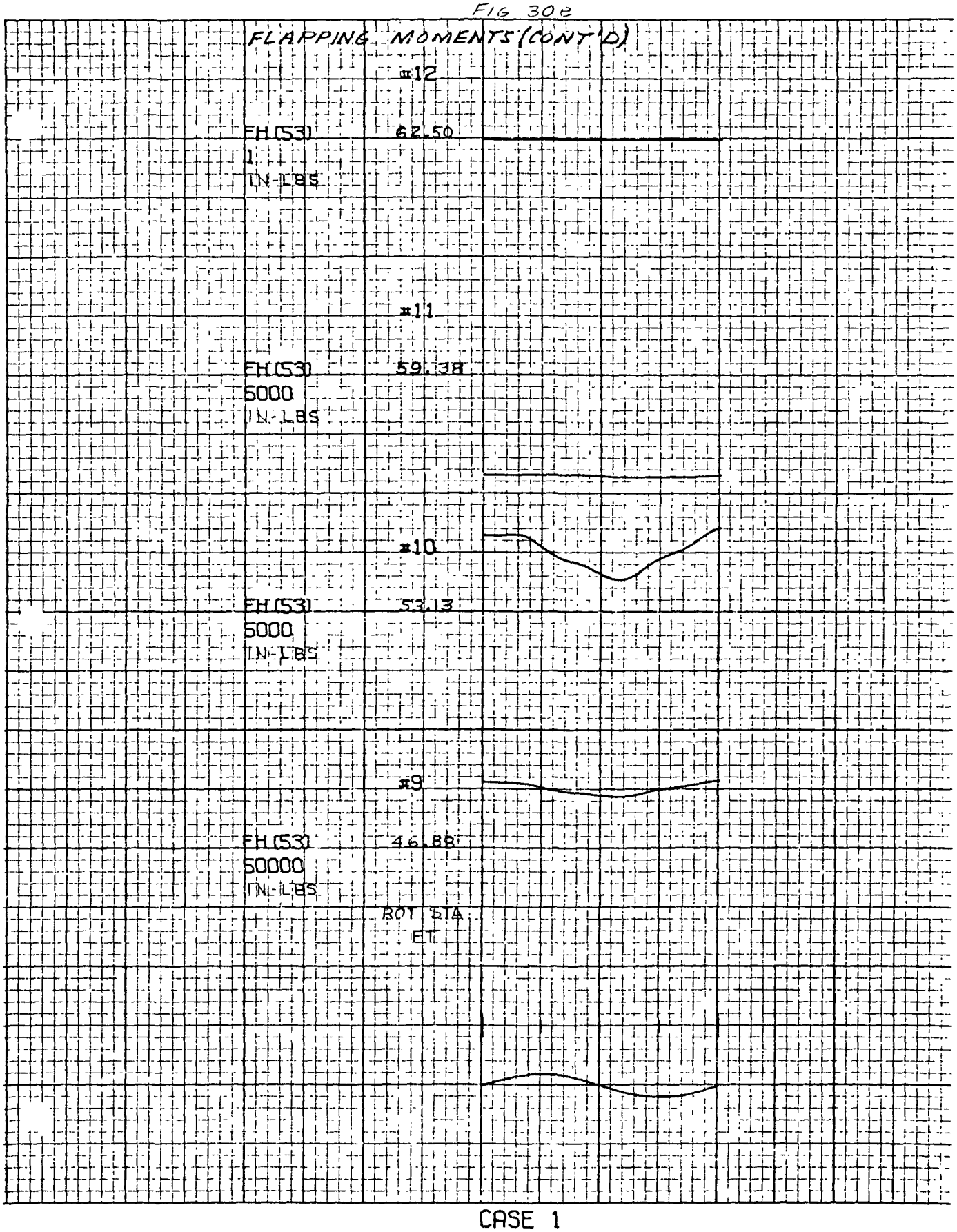

CASE 1
1-28-75

FIG 30 f

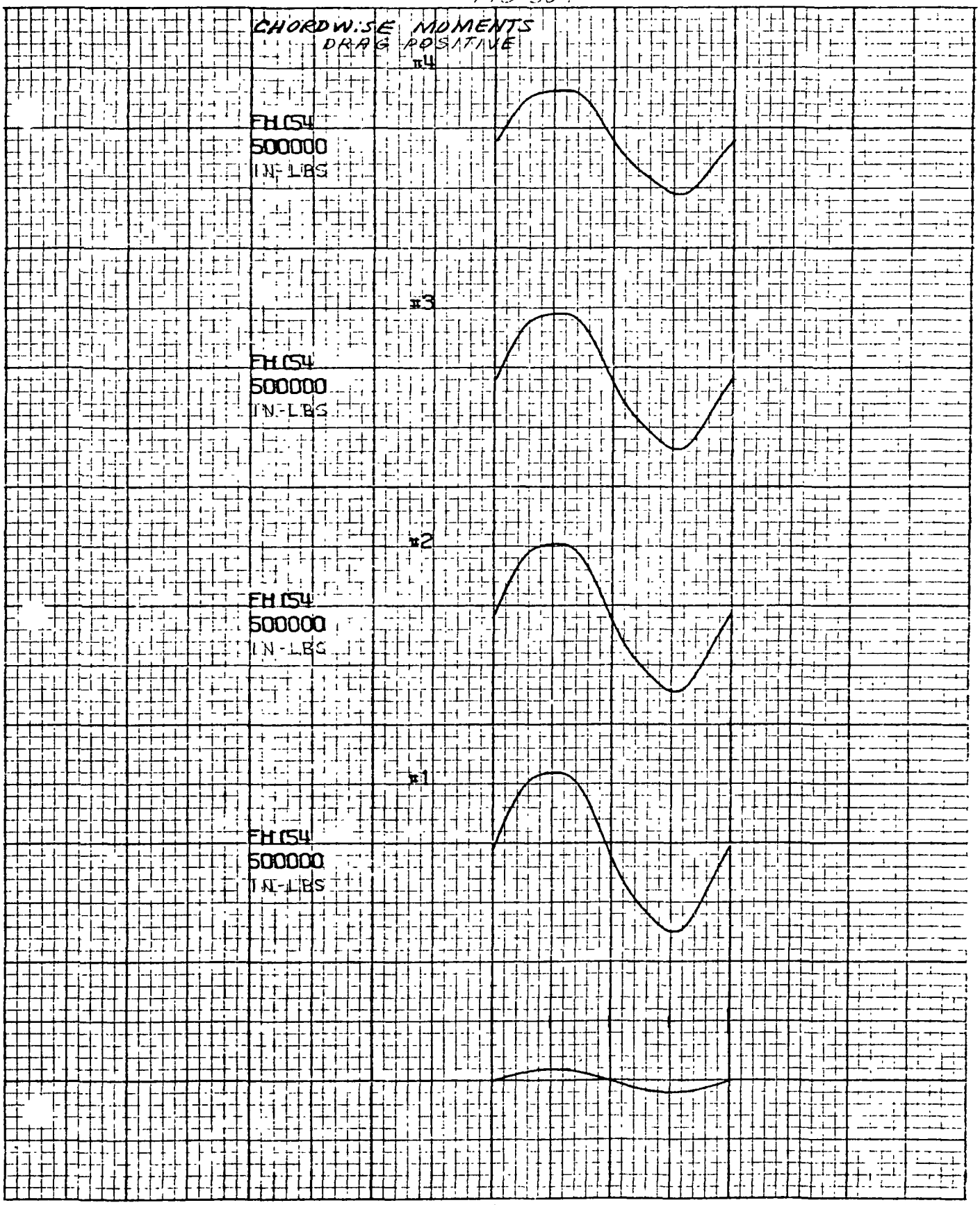

CASE 1
1-28-75

FIG 309

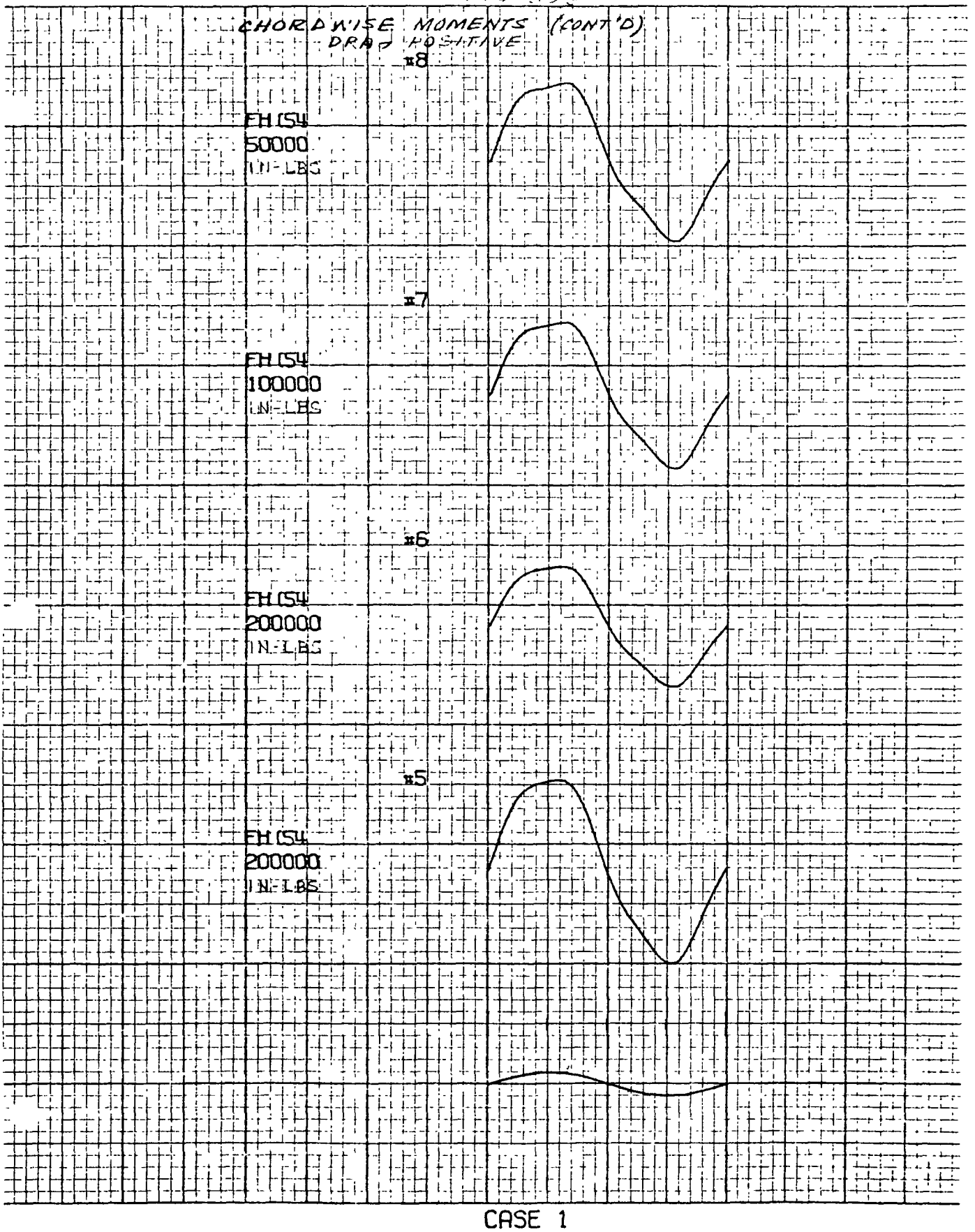

CASE 1
1-28-75

Fig 30 h

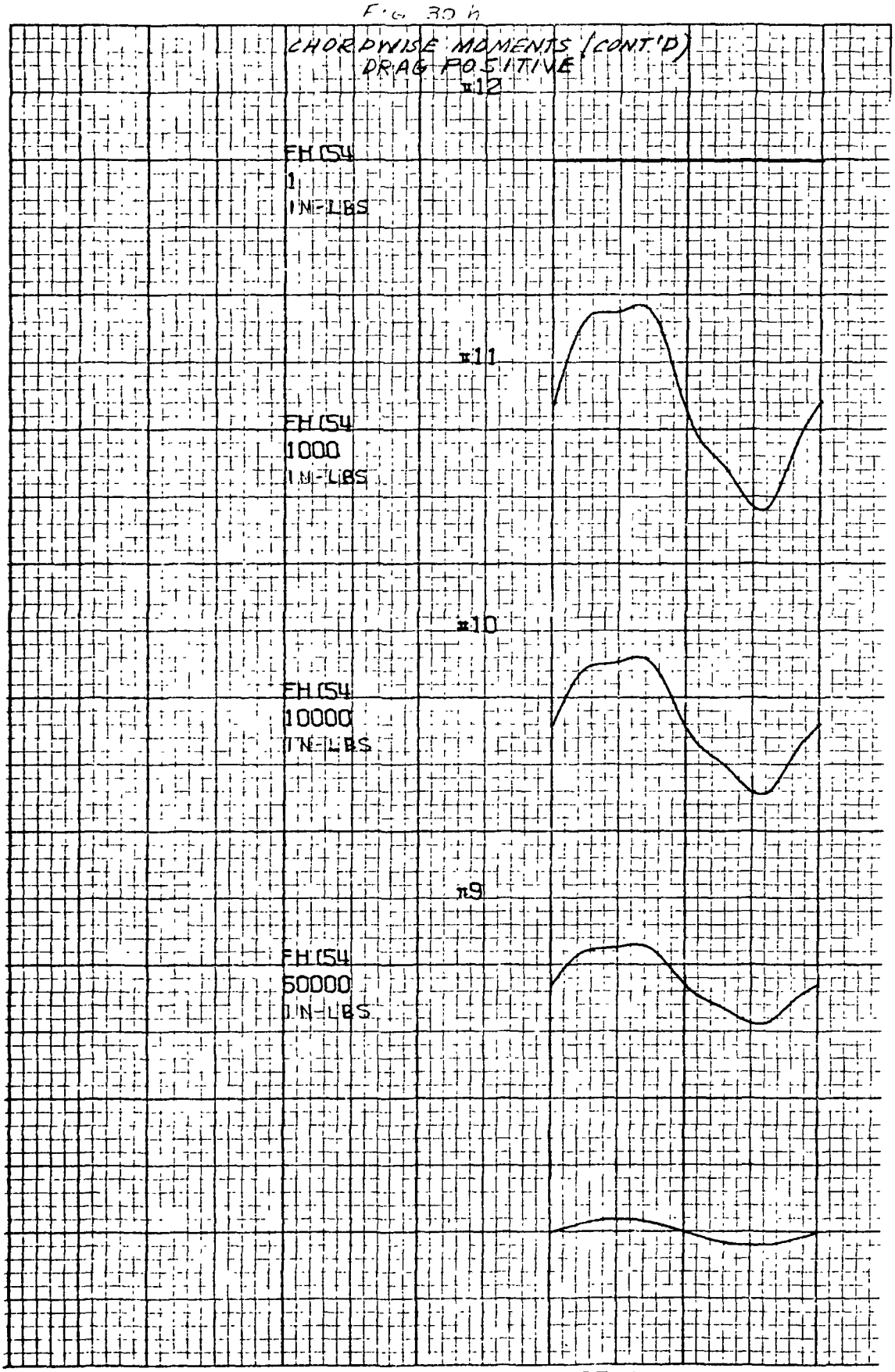

CASE 1
1-28-75

FIG 30

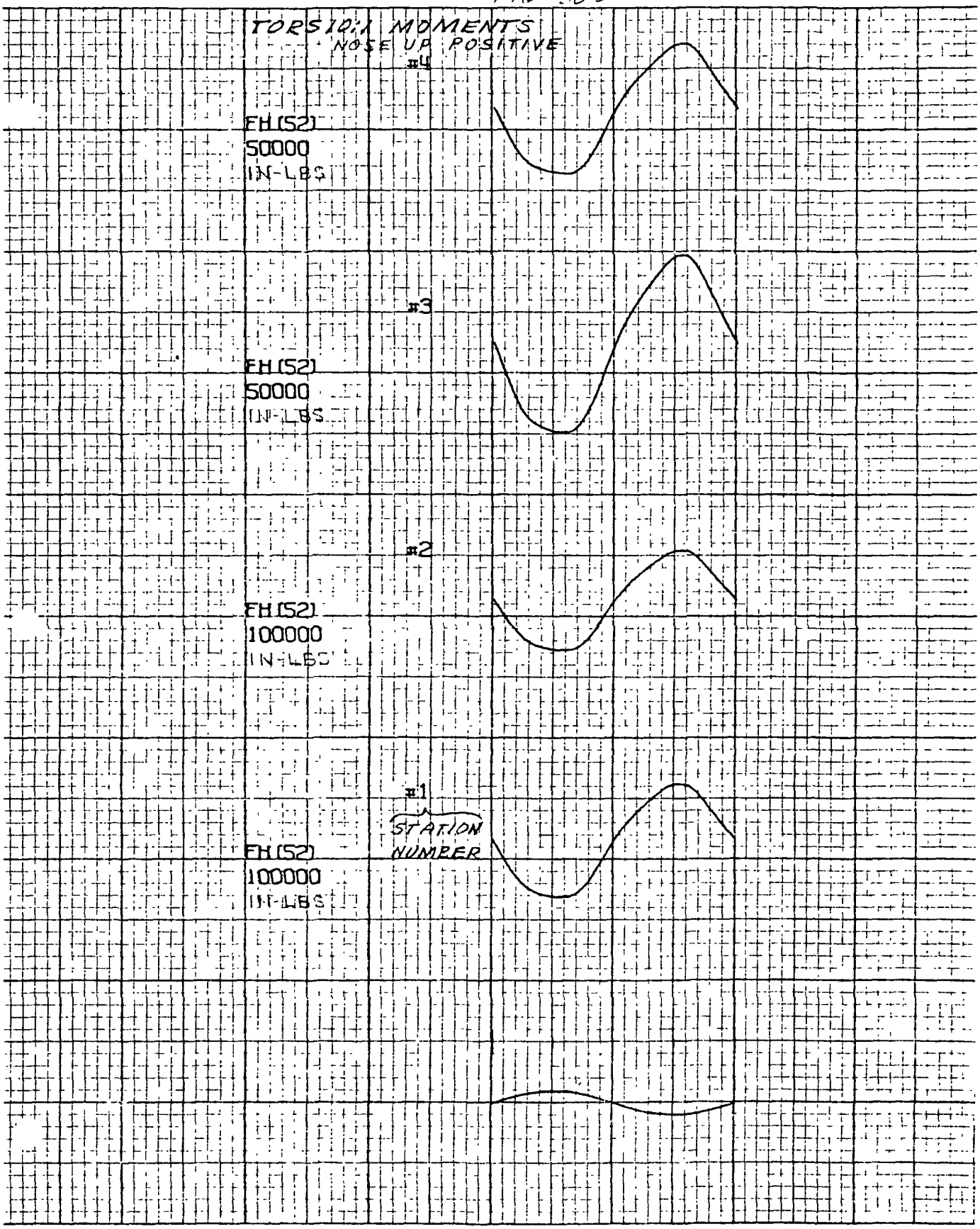

CASE 1
1-28-75

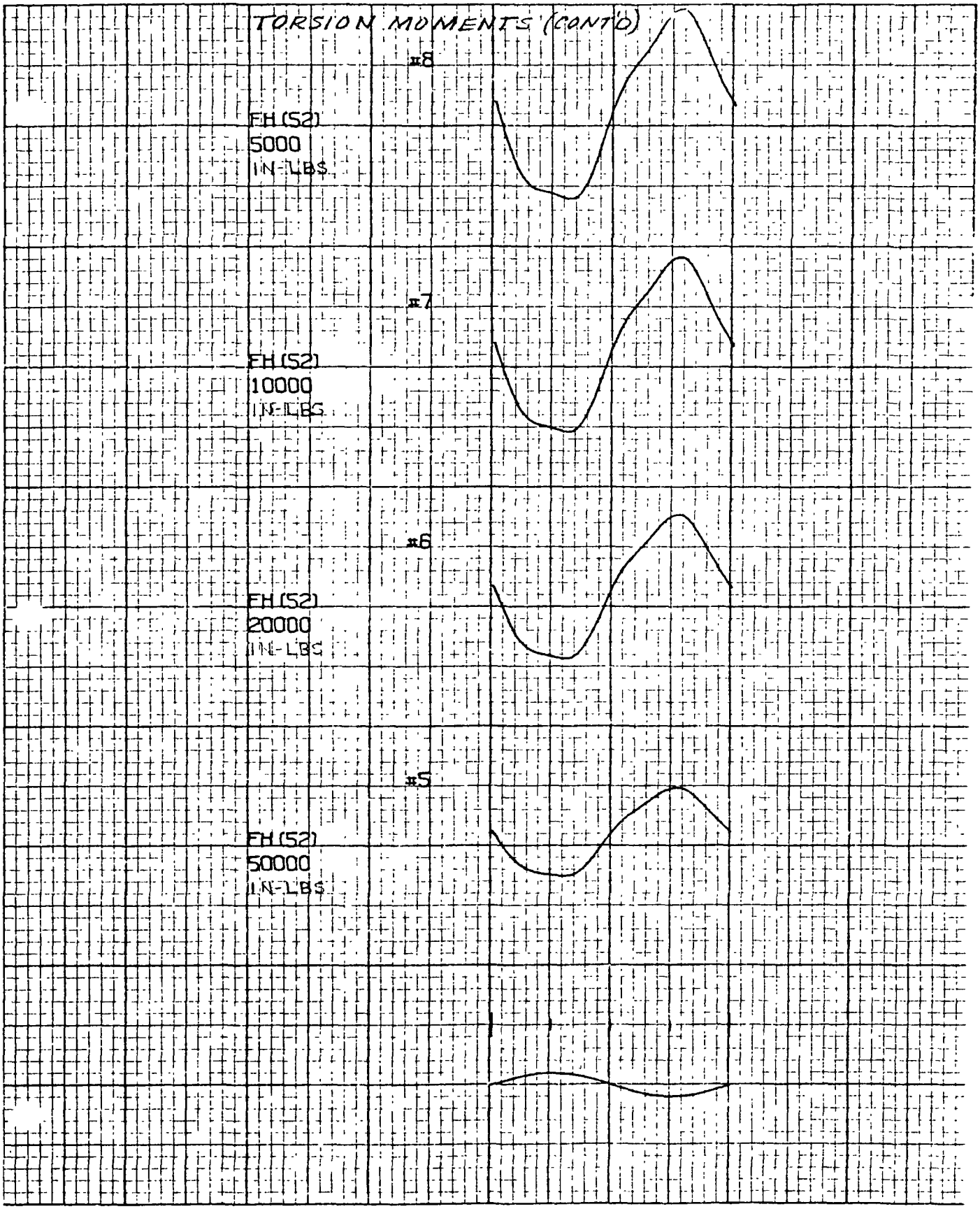
TORSION MOMENTS (CONT'D)
#8
FH(S2)
5000
IN-LBS
#7
FH(S2)
10000
IN-LBS
#6
FH(S2)
20000
IN-LBS
#5
FH(S2)
50000
IN-LBS

CASE 1
1-28-75

FIG 30k

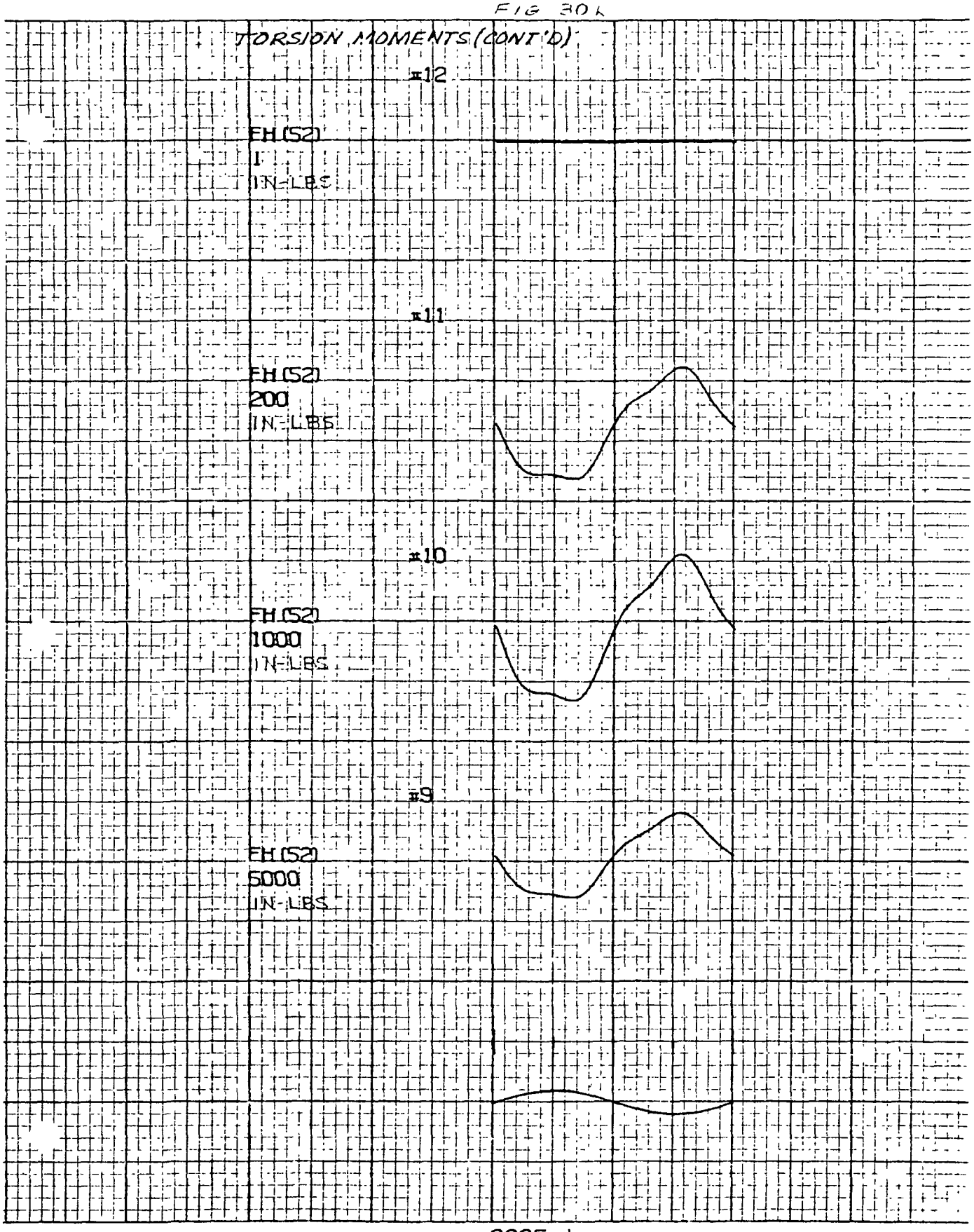

CASE 1
1-28-75

FIG 31a

WINDMILL - REXOR TRANSIENT TIME HISTORY

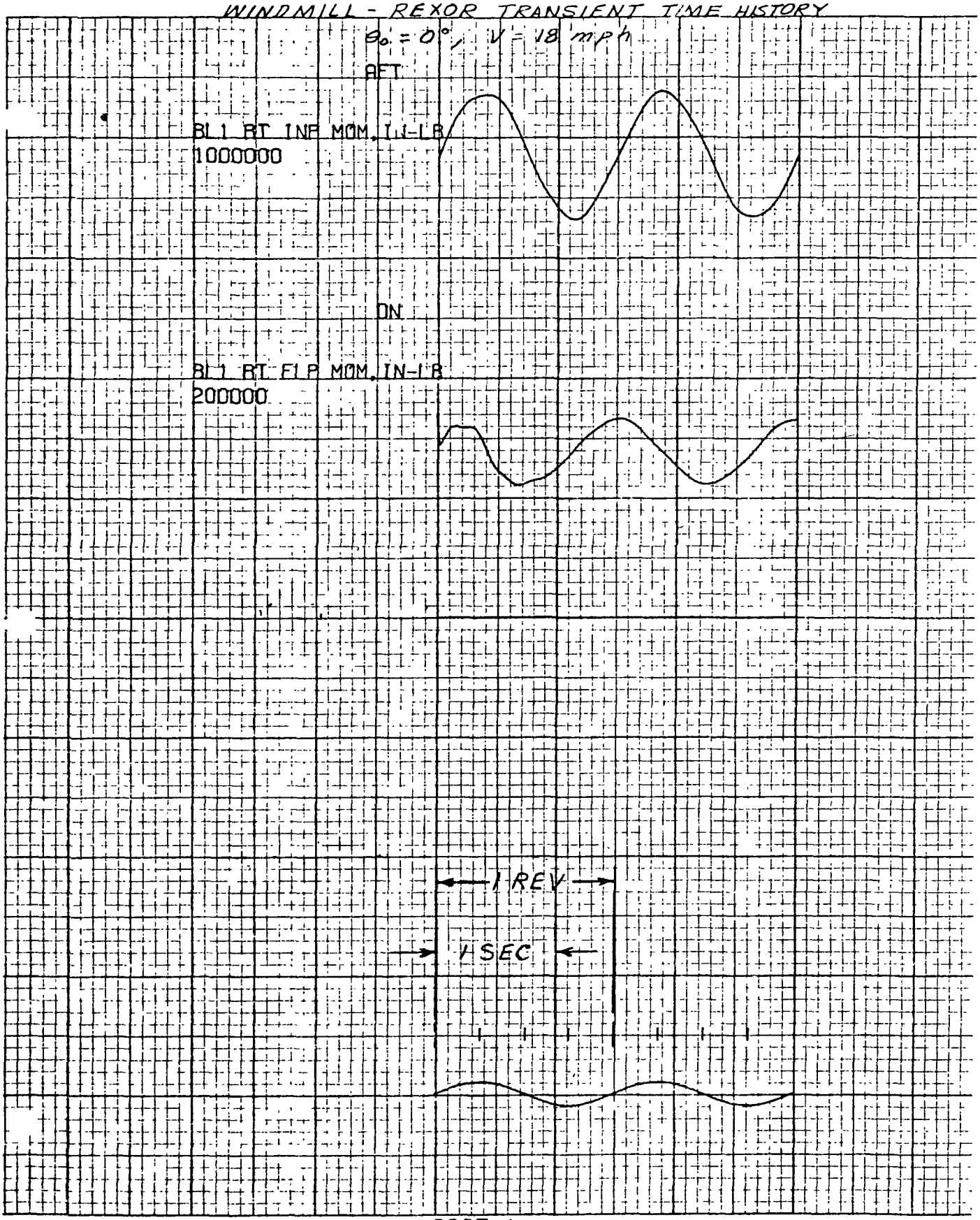

CASE 1
2- 5-75

Fig 31b

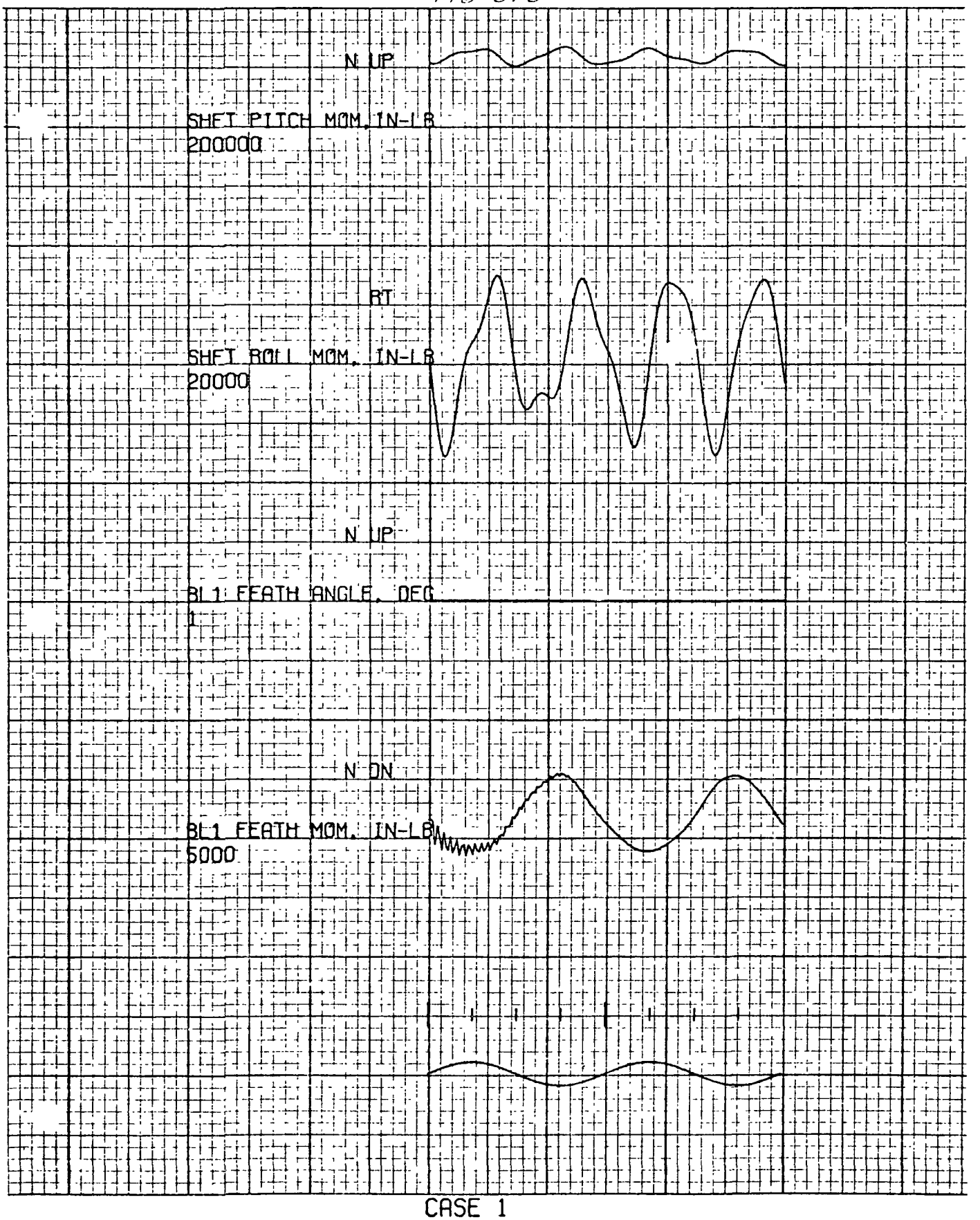

CASE 1
2- 5-75

FIG 31C

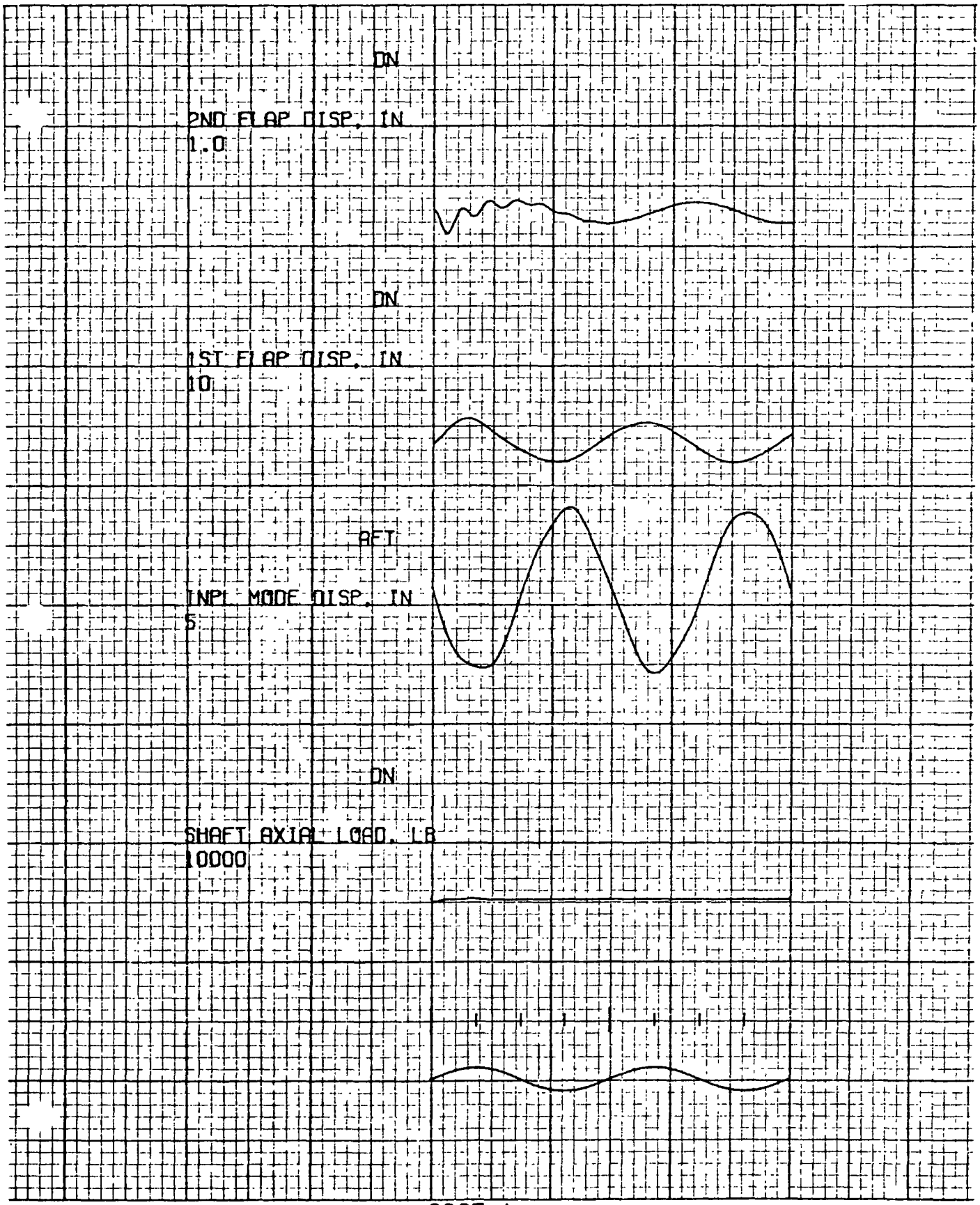

CASE 1
2- 5-75

2.3 WHIRL MODE ANALYSIS

A whirl mode stability analysis has been conducted on the windmill system using the method of propeller-nacelle whirl flutter by Houbolt and Reed, Reference 2. The rotor was assumed to be symmetric.

The unsteady aerodynamic rotor coefficients used in this analysis are plotted in Figure 32. Figure 33 shows the variation of roots with varying the pitch and yaw support spring rates symmetrically from a value of 2×10^7 ft-lb/radian to a value of 1×10^4 ft-lb/radian. Figure 34 presents the effect of the variation of the yaw stiffness while holding the pitch stiffness at 1.072×10^6 ft-lb/radian.

No pivot offset was used in either of these analyses. Zero structural damping was assumed. Also, since the rotor was treated as symmetric and no pivot offset was used, the analysis does not treat the potential mechanical instability associated with an unsymmetric rotor mounted on a flexible support.

The results due show however that as far as classical propeller whirl flutter is concerned the systems stiffness characteristics preclude the phenomenon in that the tower stiffness pylon mast stiffness at the rotor head is of the order of 1×10^7 to 2×10^7 ft-lb per radian.

2.4 STALL FLUTTER

Stall flutter is associated with operation of the rotor blade in the stall regime and it has been shown to be principally involved with the change in pitch damping characteristics in the stall region. It has been demonstrated by harmonically oscillating airfoils in forced motion that under stalled conditions the average damping in pitch over a cycle can become substantially negative and is strongly dependent on airfoil mean angle of attack, the reduced frequency of harmonic motion, the oscillation amplitude, and the airfoil configuration.

The stall flutter phenomenon is generally an amplitude-limited oscillation and exhibits itself primarily as a loads problem rather than a stability

FIG 32

NASA WINDMILL BLADE WHIRL FLUTTER, UNSTEADY AERO COEFFICIENTS

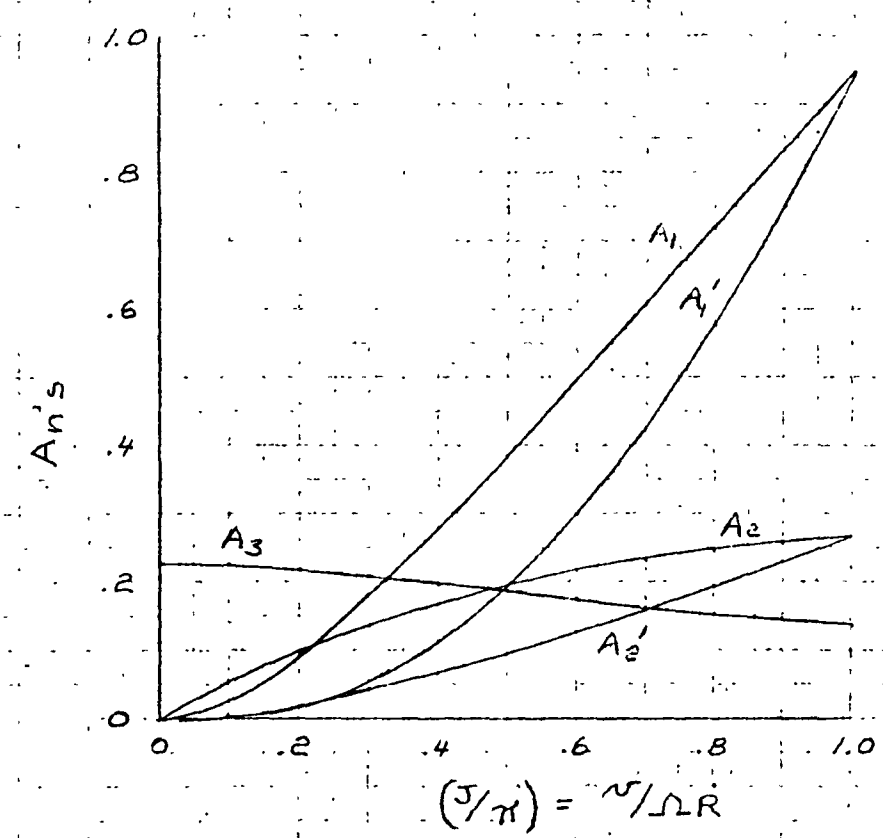

PREPARED BY JS REASER
DATE 4-7-75
CHECKED BY

LOCKHEED-CALIFORNIA COMPANY
A DIVISION OF LOCKHEED AIRCRAFT CORPORATION

FIG 33

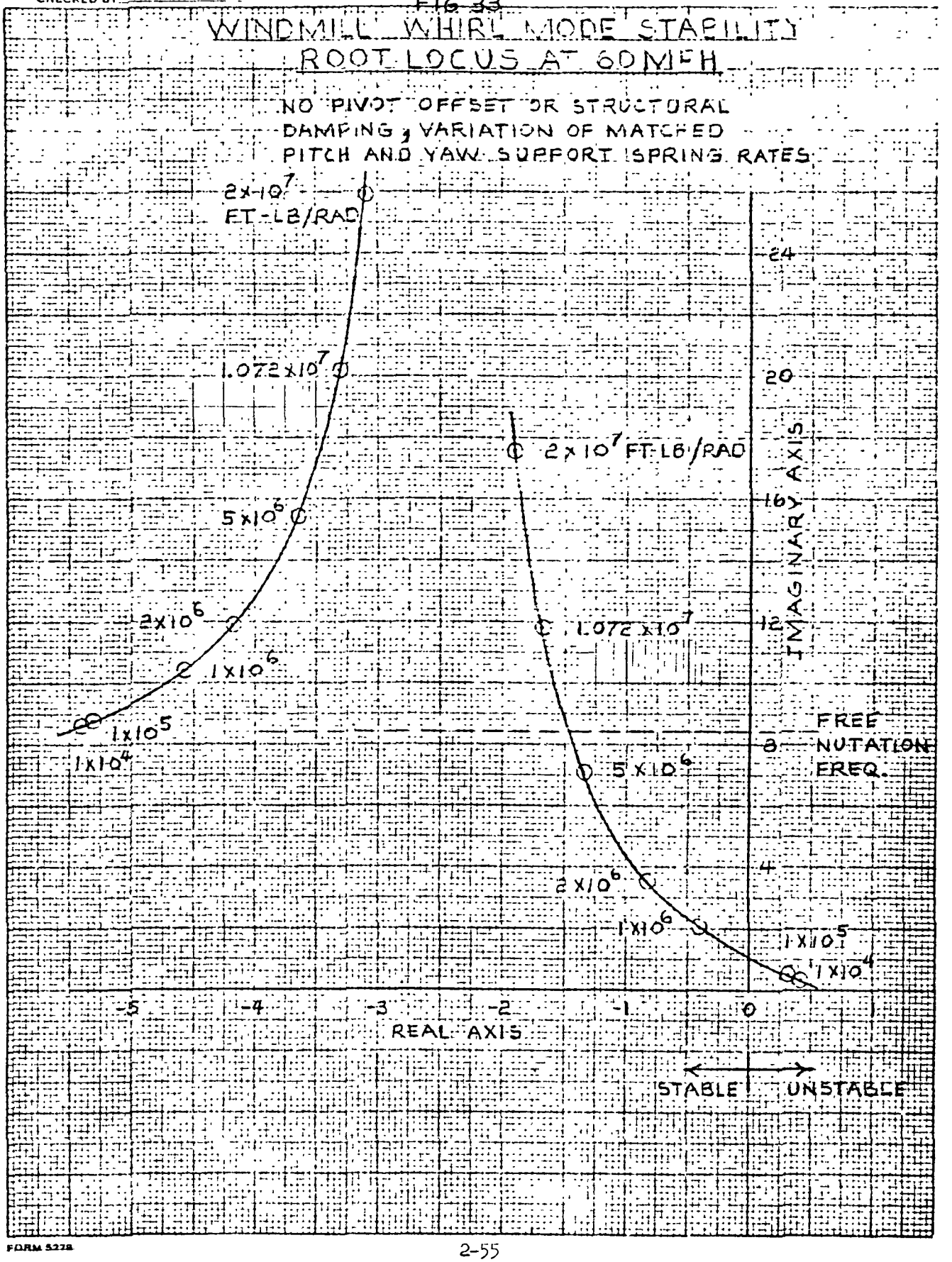

FORM 5228

PREPARED BY J.S. REASER
DATE 4-7-75
CHECKED BY

LOCKHEED-CALIFORNIA COMPANY
A DIVISION OF LOCKHEED AIRCRAFT CORPORATION

F16-34

WINDMILL WHIRL MODE STABILITY ROOT LOCUS AT 60 MPH

NO PIVOT OFFSET OR STRUCTURAL DAMPING,
VARIATION OF YAW SUPPORT SPRING RATE,
PITCH SUPPORT AT 1.072 x 10^7 FT-LB/RAD

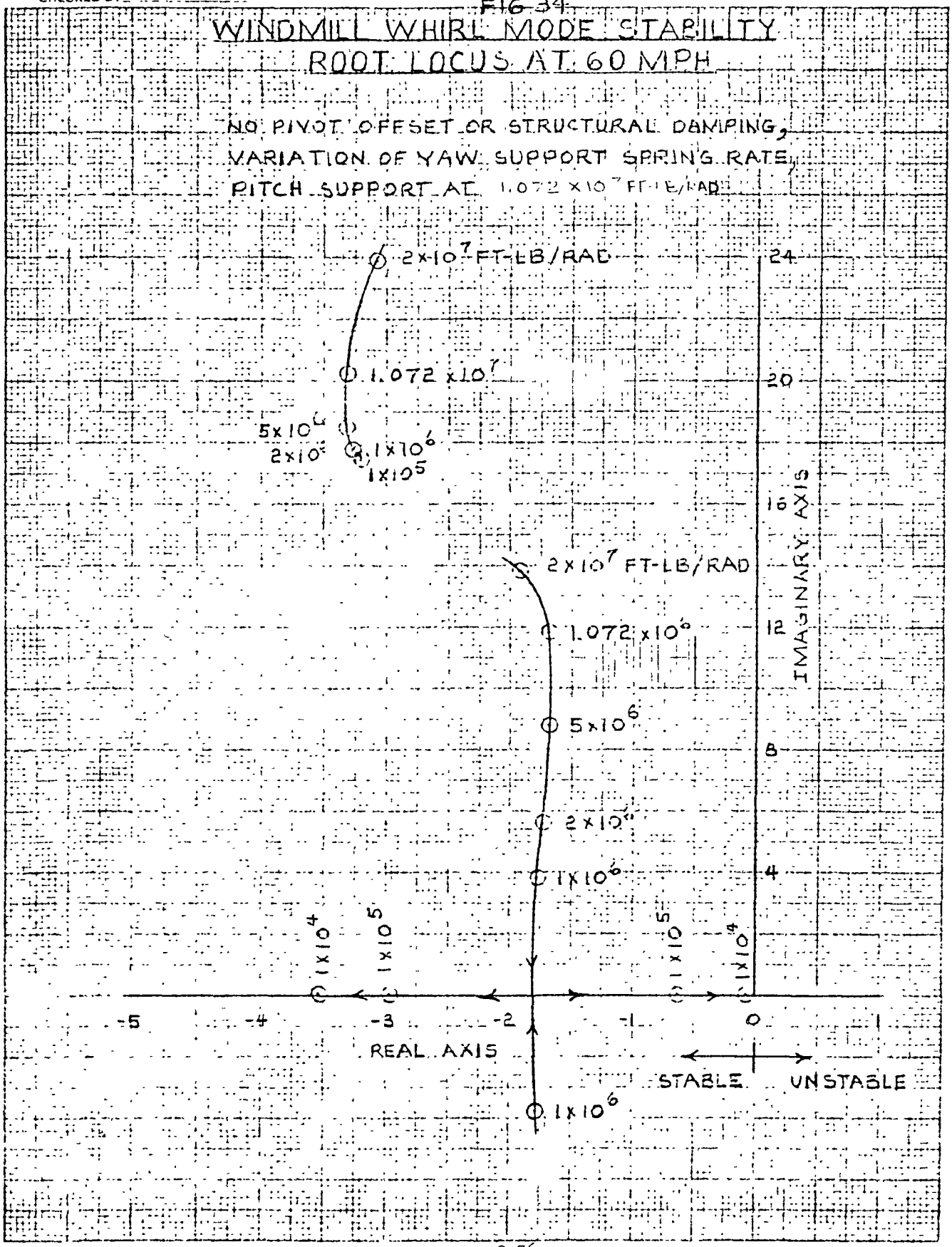

FORM 5278

problem per se. Figure 35, data extracted from Reference 3, is a plot of amplitude of limit cycle oscillation versus reduced frequency for a model tested. The minimum expected torsion mode reduced frequency for the wind turbine blade at the three-quarter radius is indicated on this figure. The data indicates the wind turbine blade should not be critical as far as stall flutter is concerned due to the placement of the blade torsional frequency.

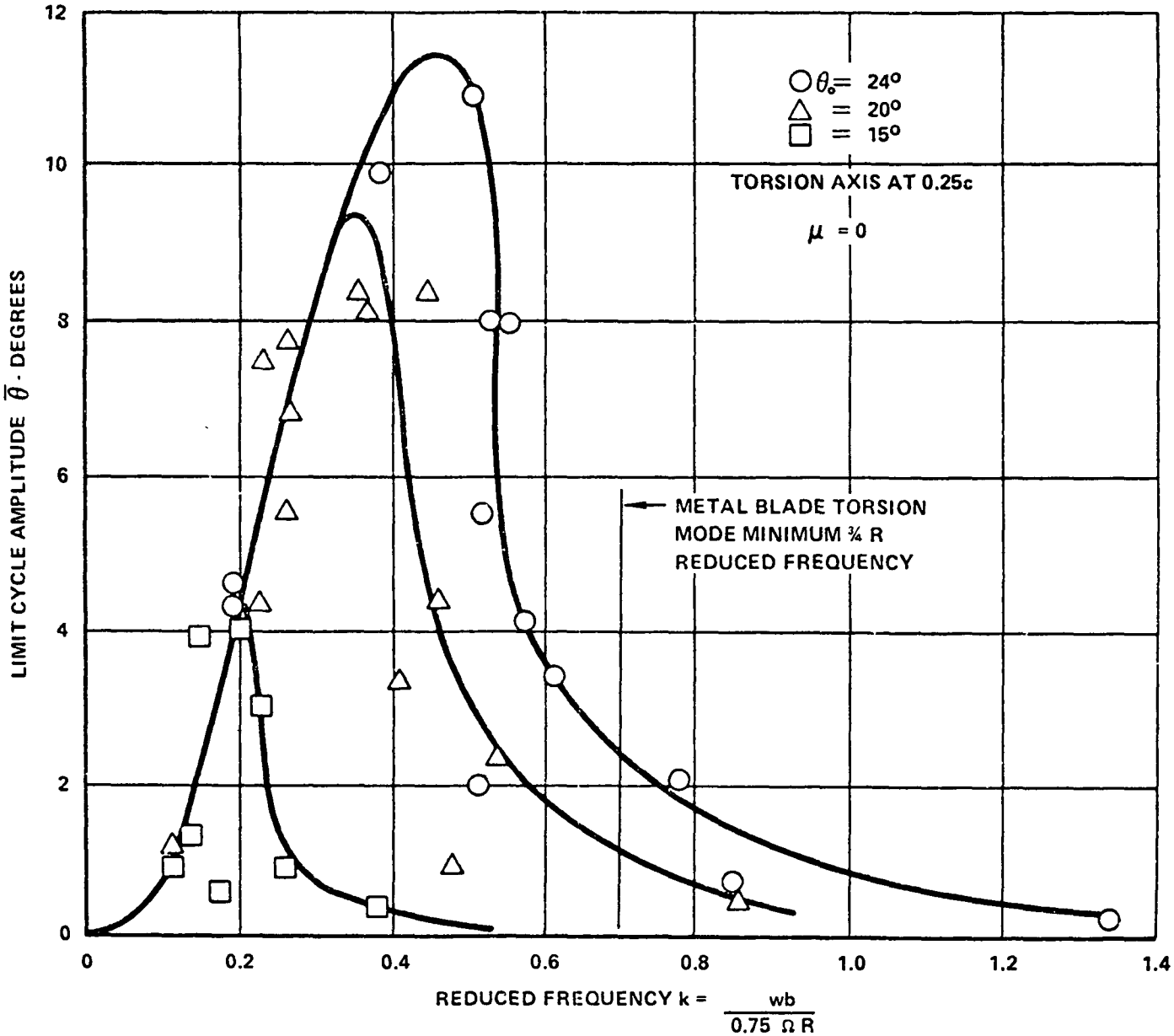

Figure 35. Limit Cycle Amplitude vs Reduced Frequency

3.0 STRUCTURAL TEST RESULTS

Static deflection and shake tests were conducted on the blades to verify their predicted stiffness and frequency characteristics. The results of these tests are presented in the following sections.

3.1 VIBRATION SHAKE TEST RESULTS

To verify blade-frequency response characteristics, a test setup that incorporated a blade mounted on a simulated rotor hub was utilized and bench shake tests were conducted. Tests were conducted with the blades at zero degree and parallel to the ground.

Electromechanical shaker(s) were used to shake the blade and conduct frequency sweeps from 1.5 to 40 Hz to identify natural frequencies. Vibration pickups were located both fixed and roving to the blade at sufficient locations and directions to identify desired modes, i.e.:

- o 1st and 2nd flatwise bending frequency
- o 1st and 2nd edgewise bending frequency
- o 1st torsional frequency.

Each of these modes were surveyed to obtain amplitude and phase versus blade radius to define the mode shape.

Tests were conducted at two pitch settings to cover the blade angle operating range, including feathered.

The results of the tests in terms of response amplitudes at different locations as a function of excitation frequency are plotted in Figures 36 through 56. These figures show response data both flap and chordwise at stations 301 and 750. Excitation forces were applied at stations 301 and 370 in flap, chord and torsion.

Blades were shaken in four configurations. These four configurations are described below with the abreviated nomenclature used on the figures to describe the configuration tested:

Nomenclature		Configuration Description
STD + TW	-	Standard Blade with full tip weight
STD	-	Standard blade with zero tip weight
Configuration A	-	Standard blade with zero tip weight and loading block at Sta 301
Configuration B	-	Configuration A plus addition 75-1/4 pounds of shot bags at mid chord at Sta 301

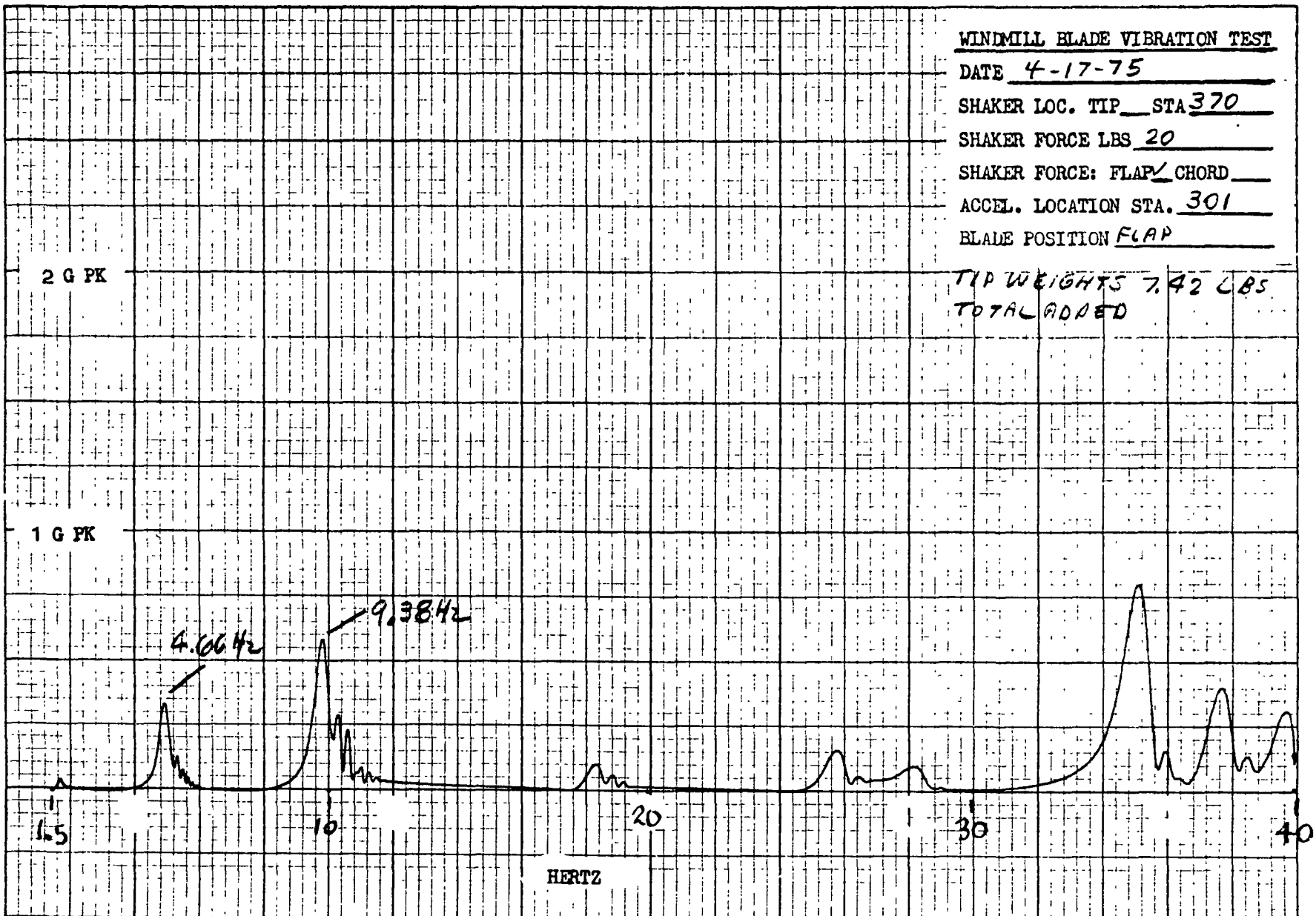

FIGURE 36. Blade Response vs Frequency, Std + TW, Flap at 301/Flap 370

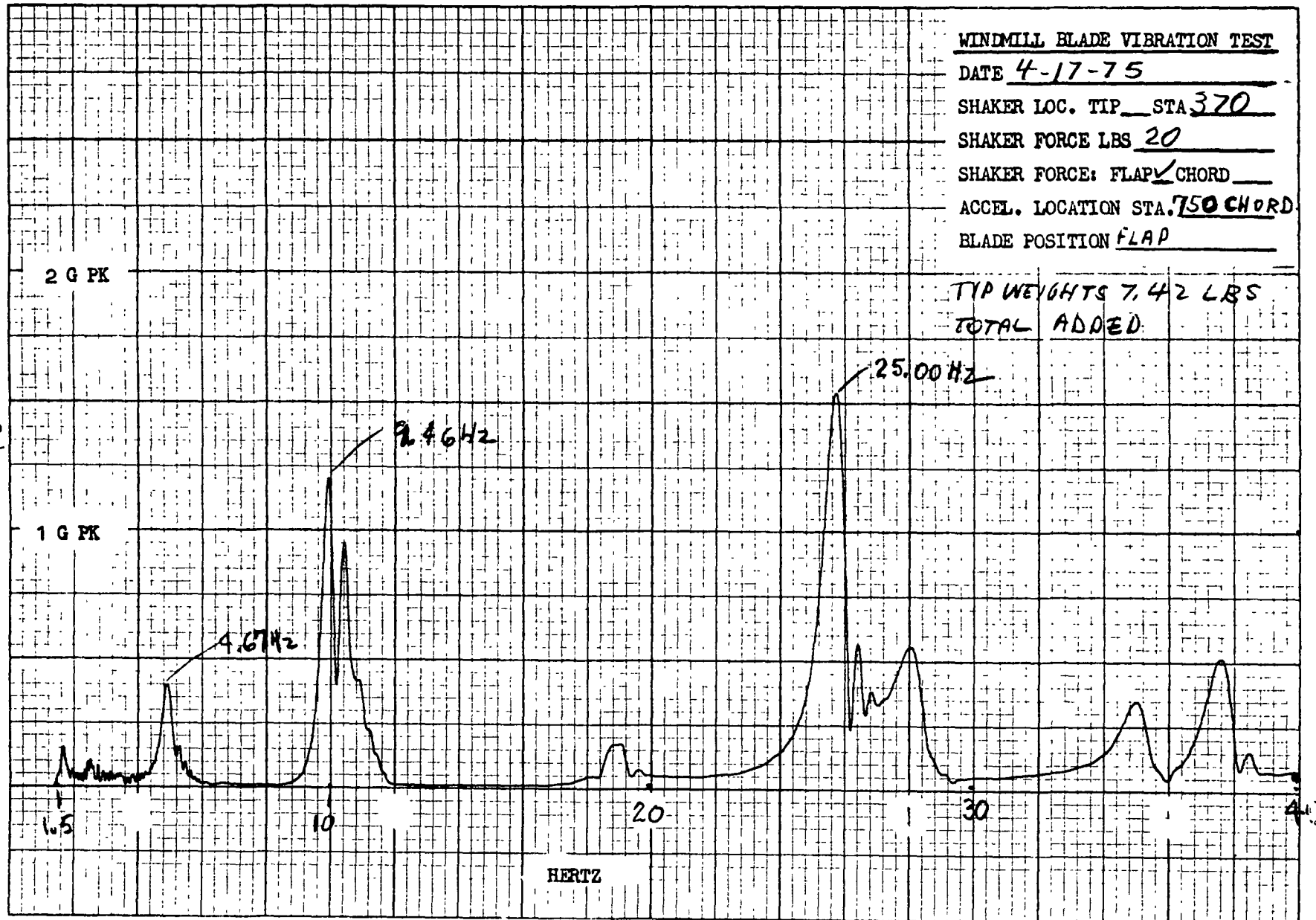

FIGURE 37. Blade Response vs Frequency, Std + TW, Chord @ 750/Flap @ 370

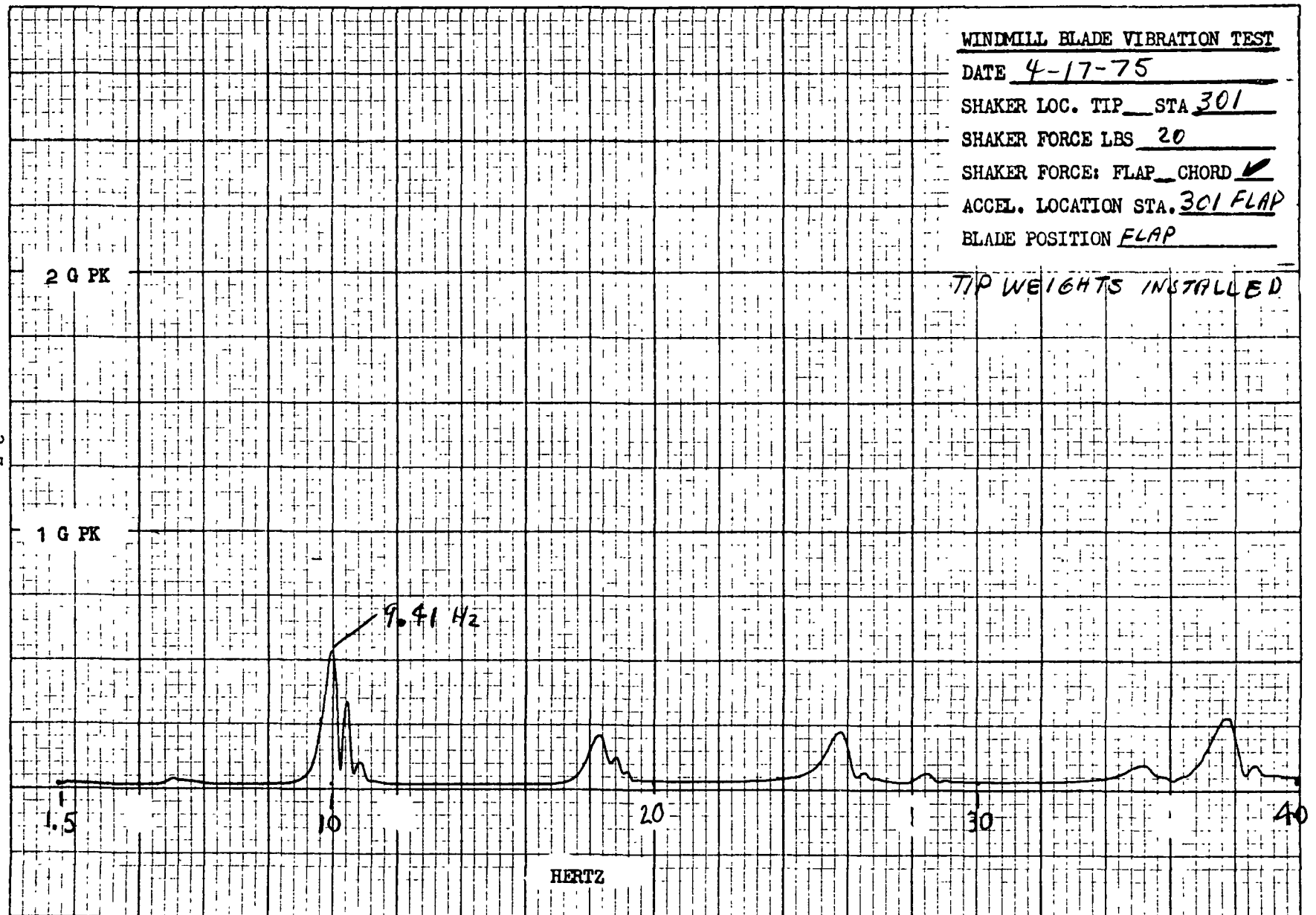

FIGURE 38. Blade Response vs Frequency, Std + TW, Flap @ 301/Chord @ 301

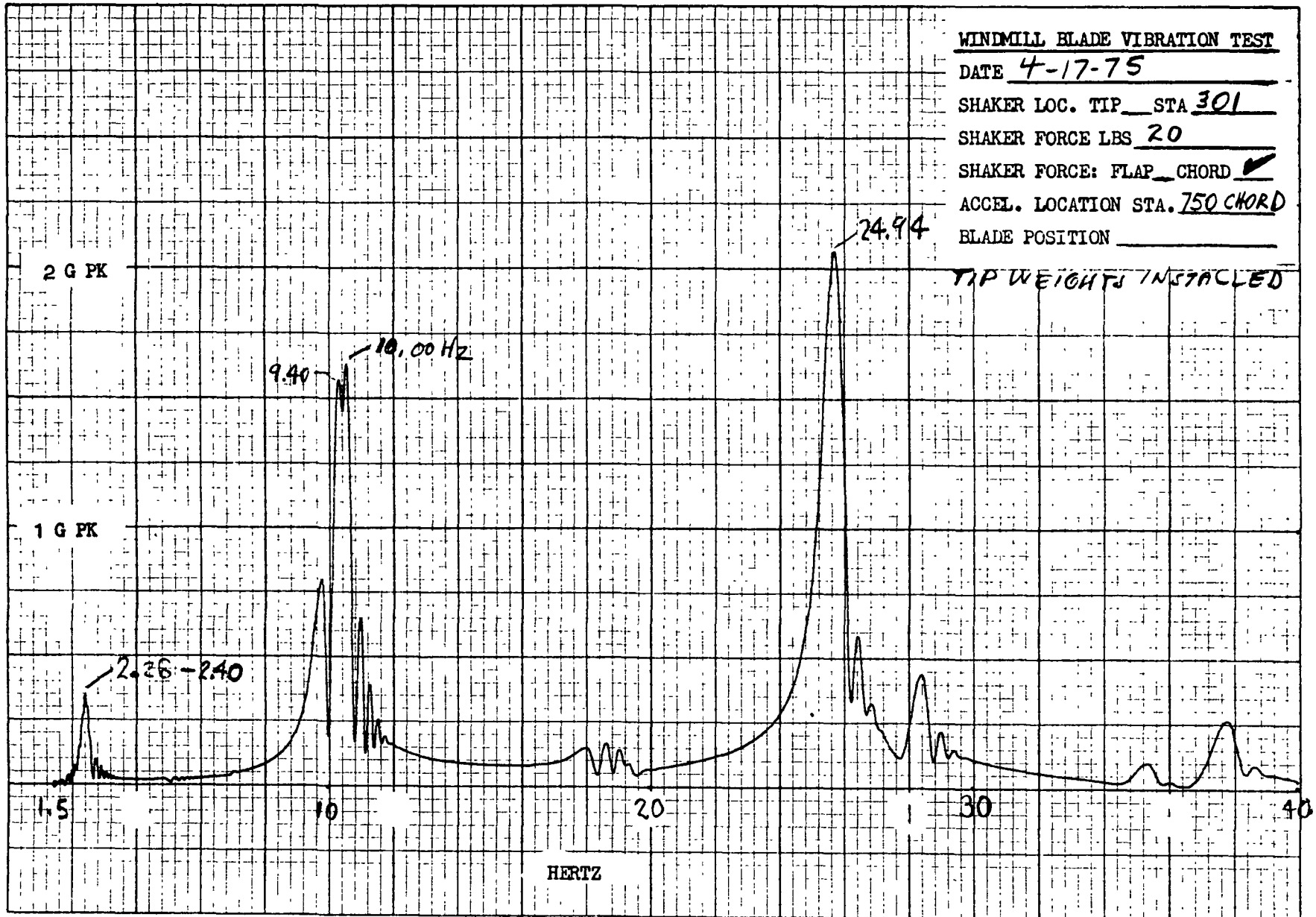

FIGURE 39. Blade Response vs Frequency, Std + TW, Chord @ 750/Chord 301

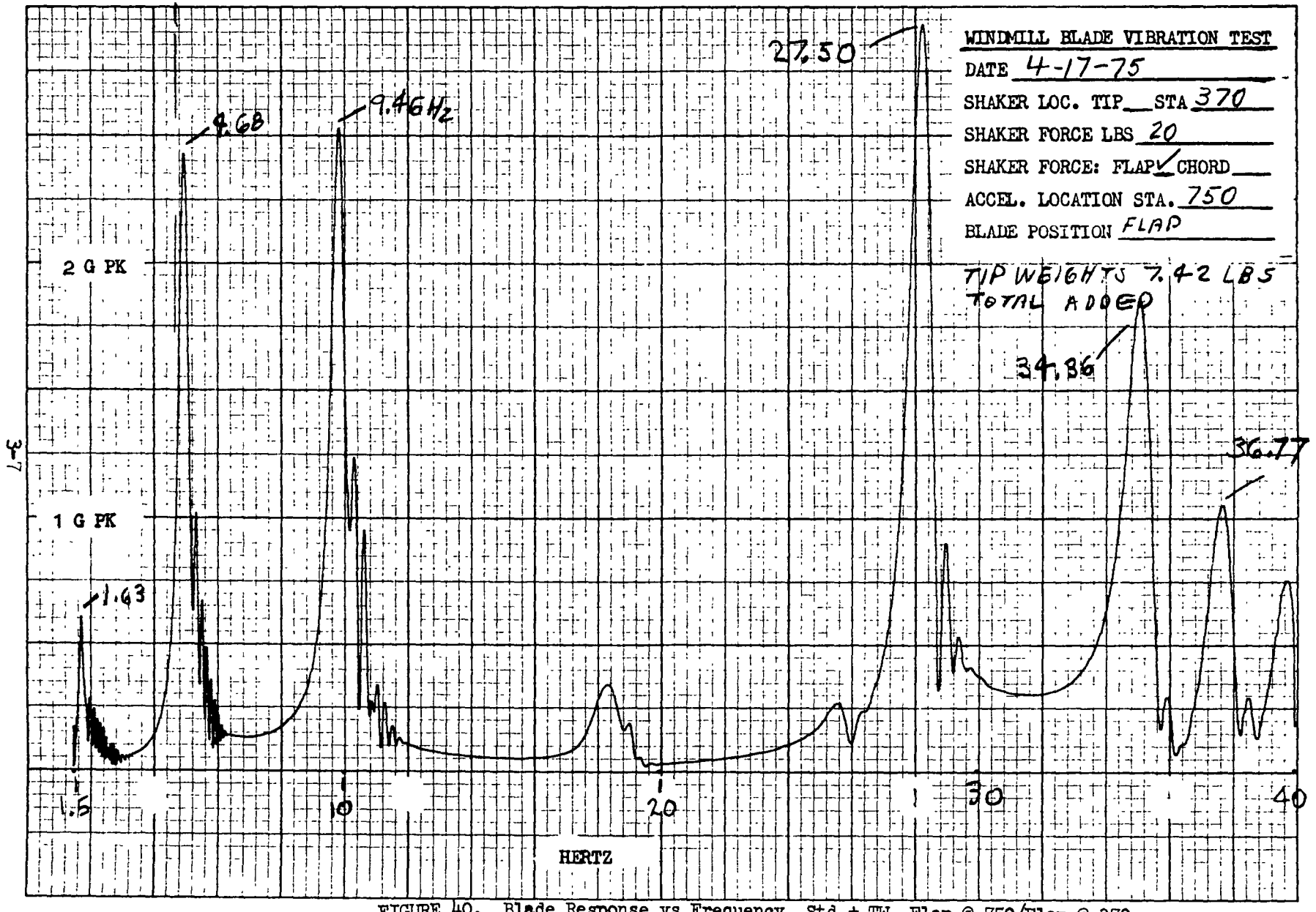

FIGURE 40. Blade Response vs Frequency, Std + TW, Flap @ 750/Flap @ 370

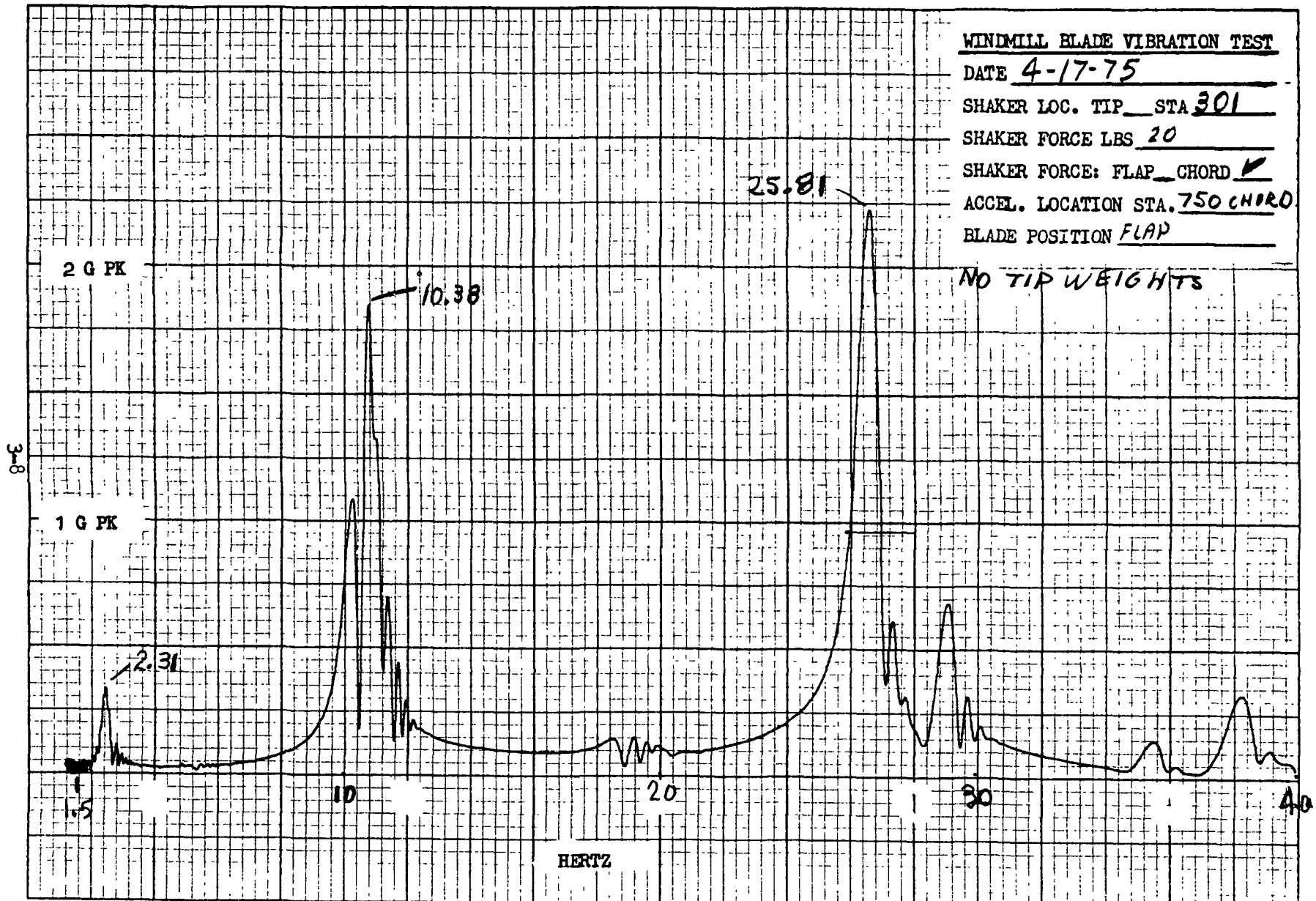

FIGURE 41. Blade Response vs Frequency, Std, Chord @ 750/Chord @ 301

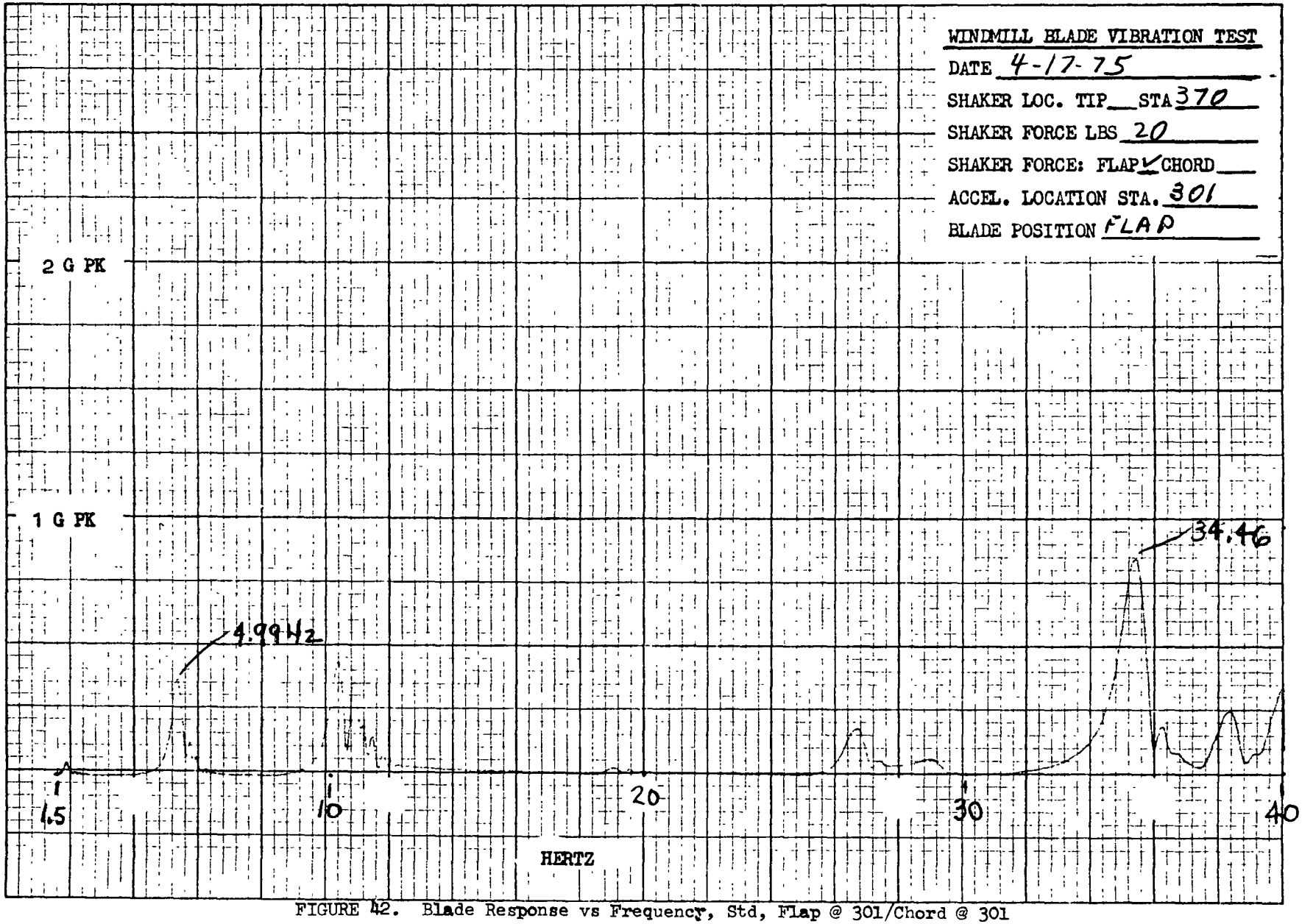

FIGURE 42. Blade Response vs Frequency, Std, Flap @ 301/Chord @ 301

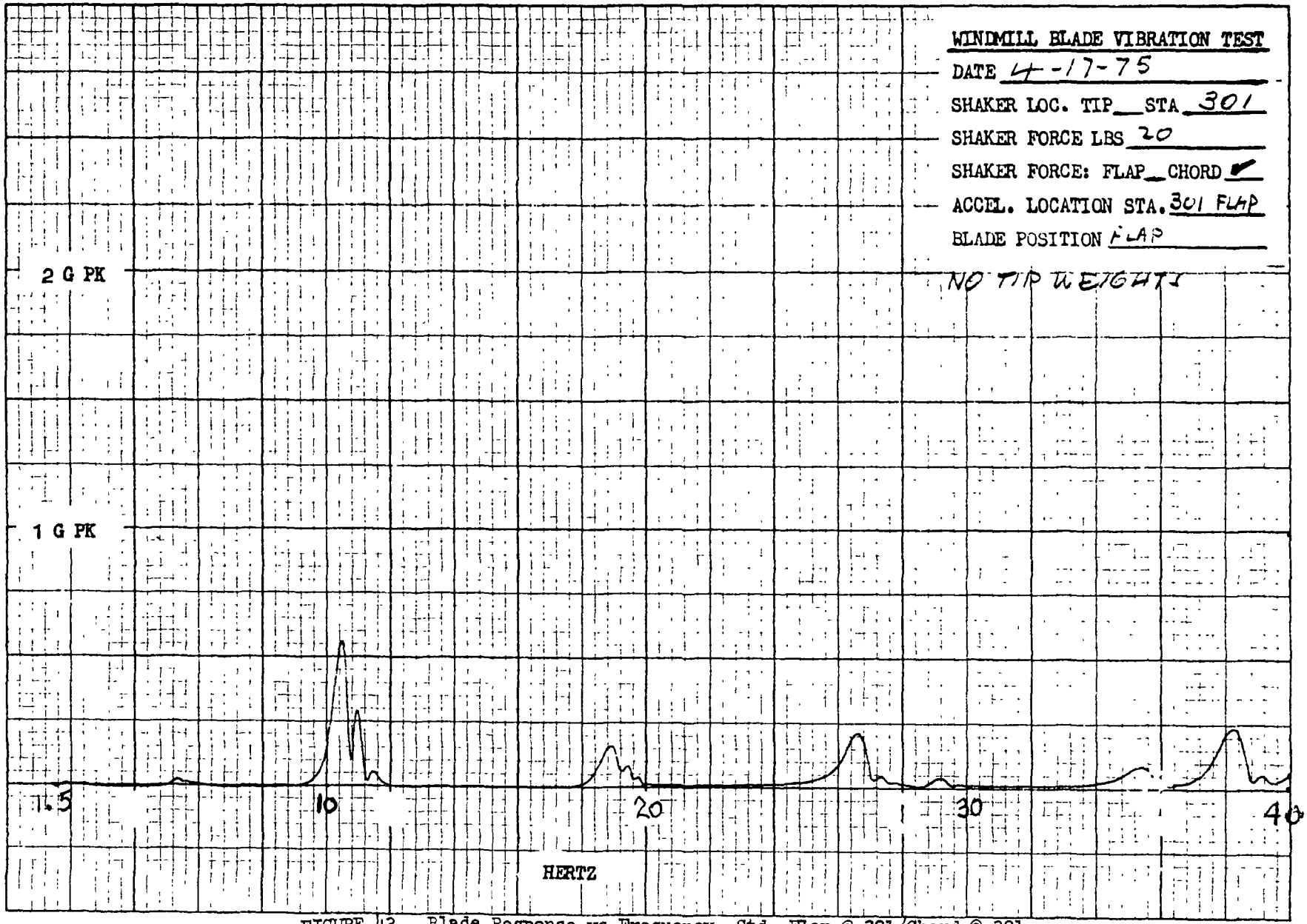

FIGURE 43. Blade Response vs Frequency, Std, Flap @ 301/Chord @ 301

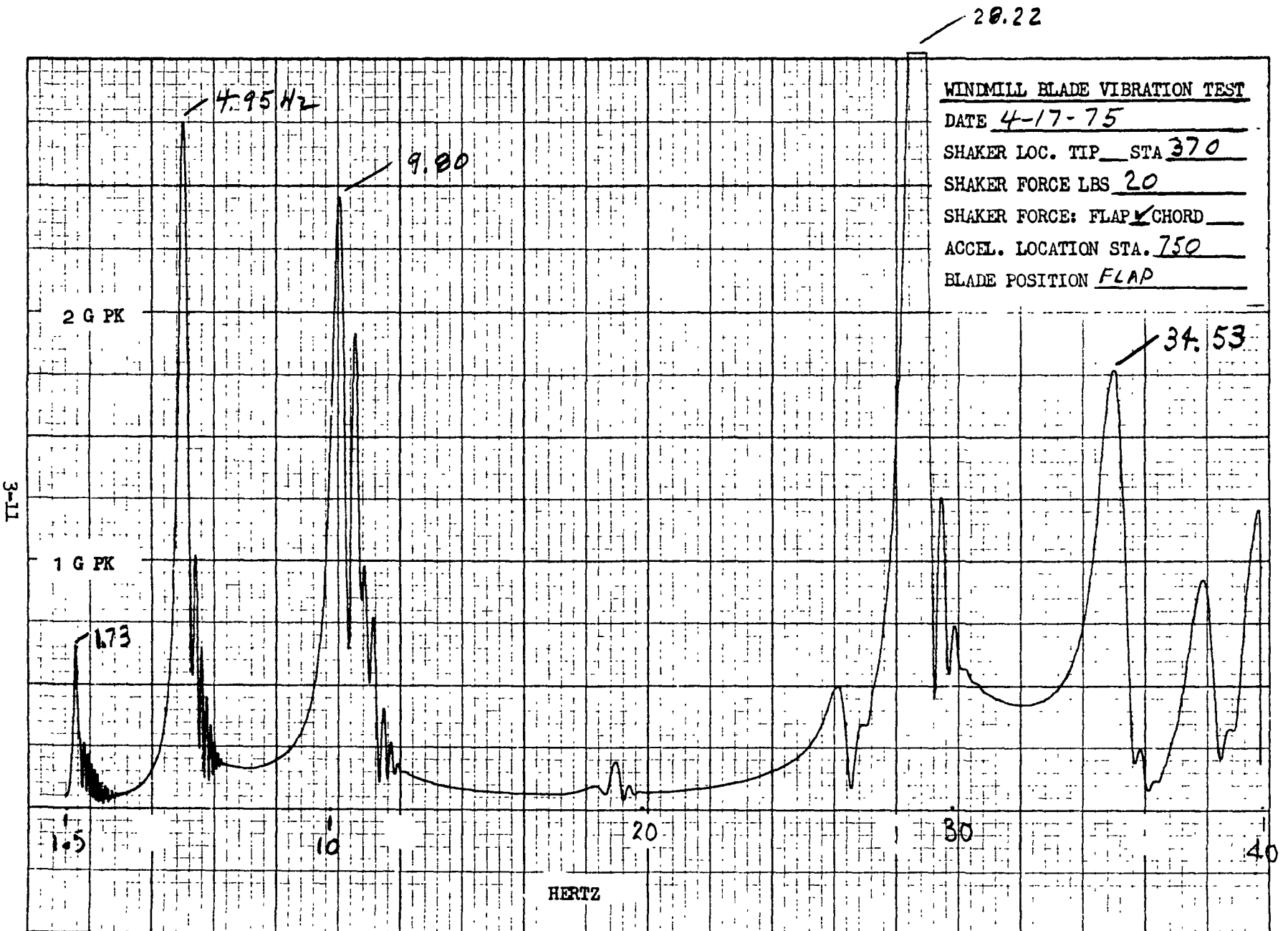

FIGURE 44. Blade Response vs Frequency, Std, Flap @ 750/Flap @ 370

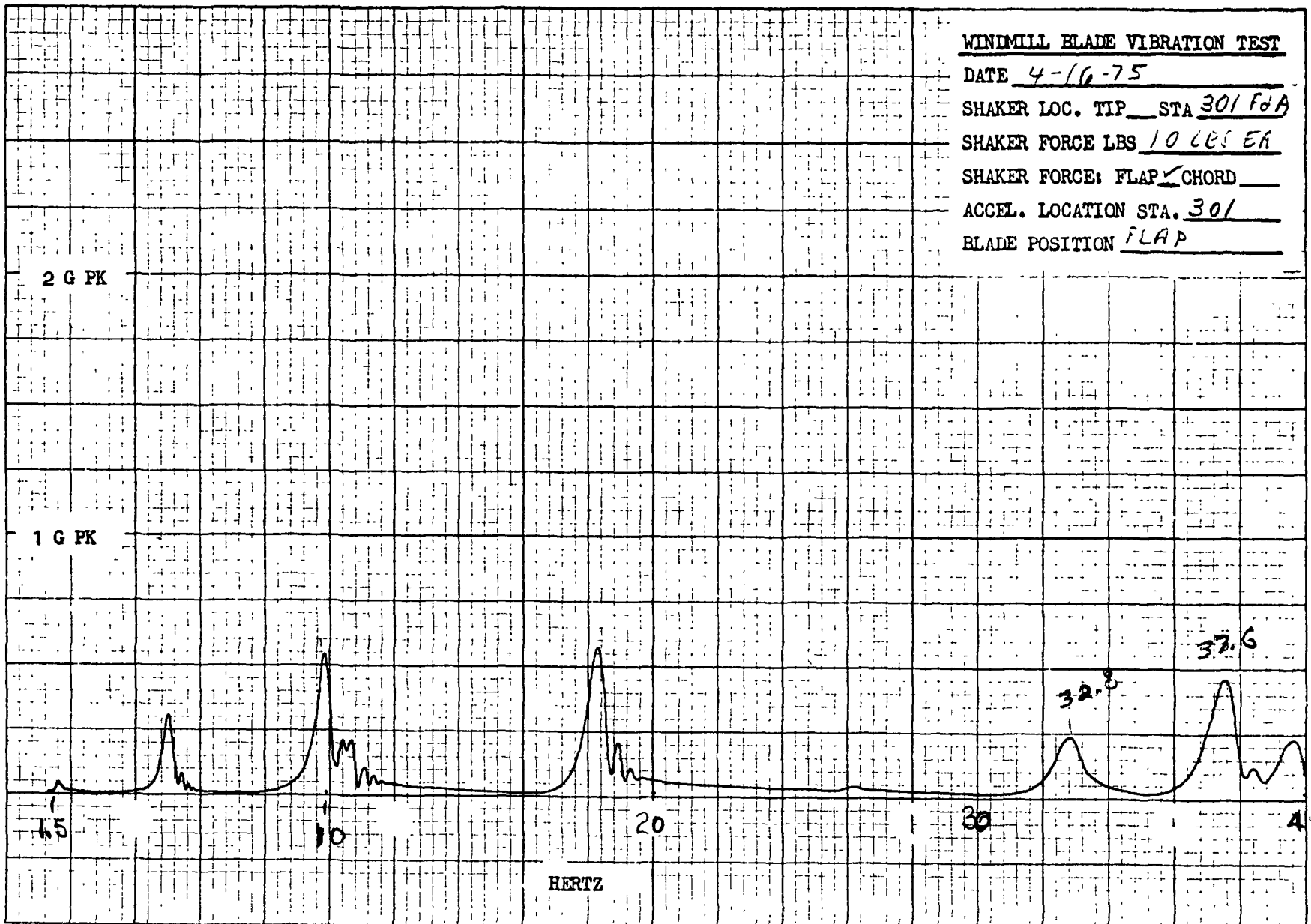

FIGURE 45. Blade Response vs Frequency, Config A, Flap @ 301/Flap @ 301

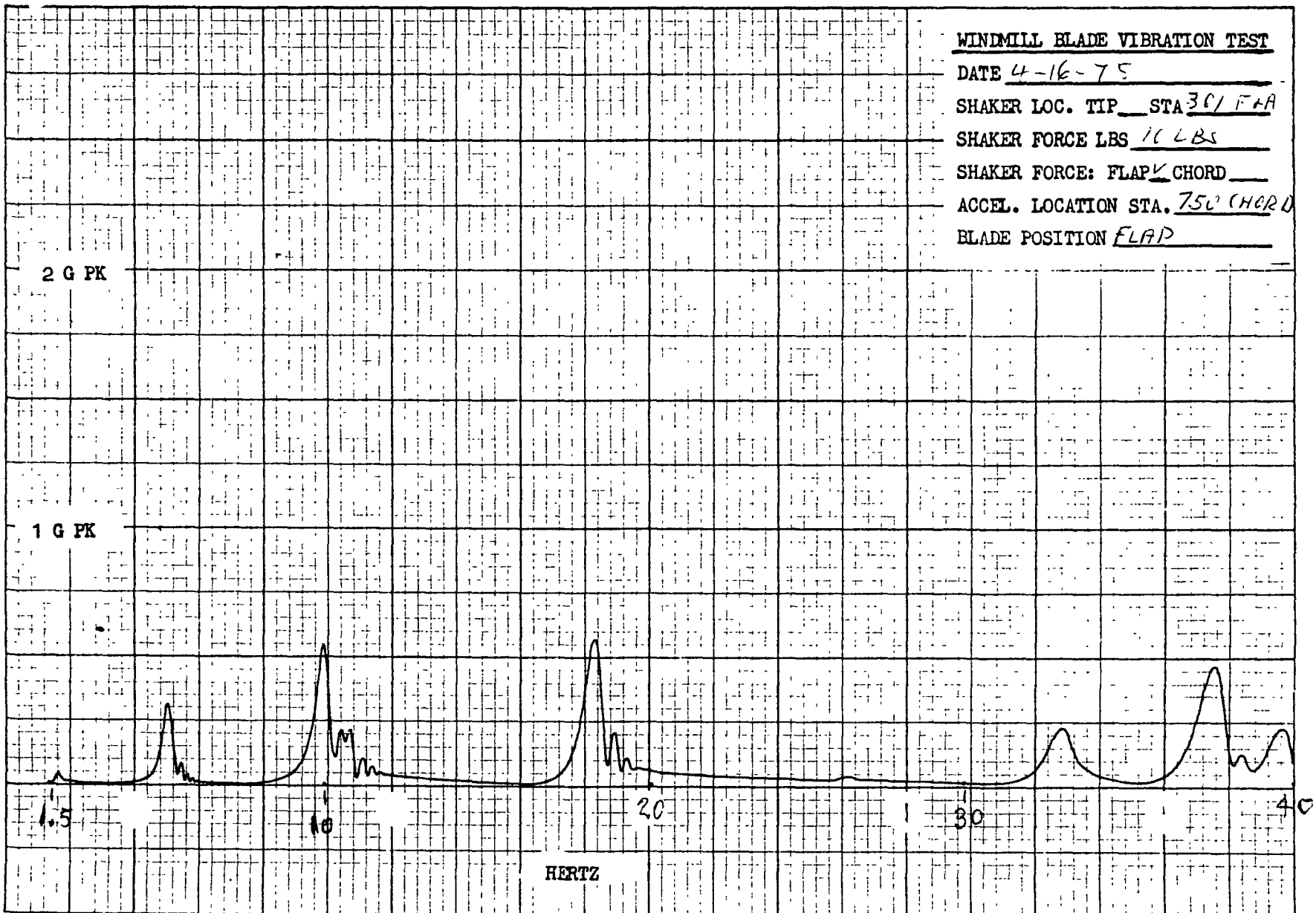

FIGURE 46. Blade Response vs Frequency, Config A, Chord @ 750/ Flap @ 750

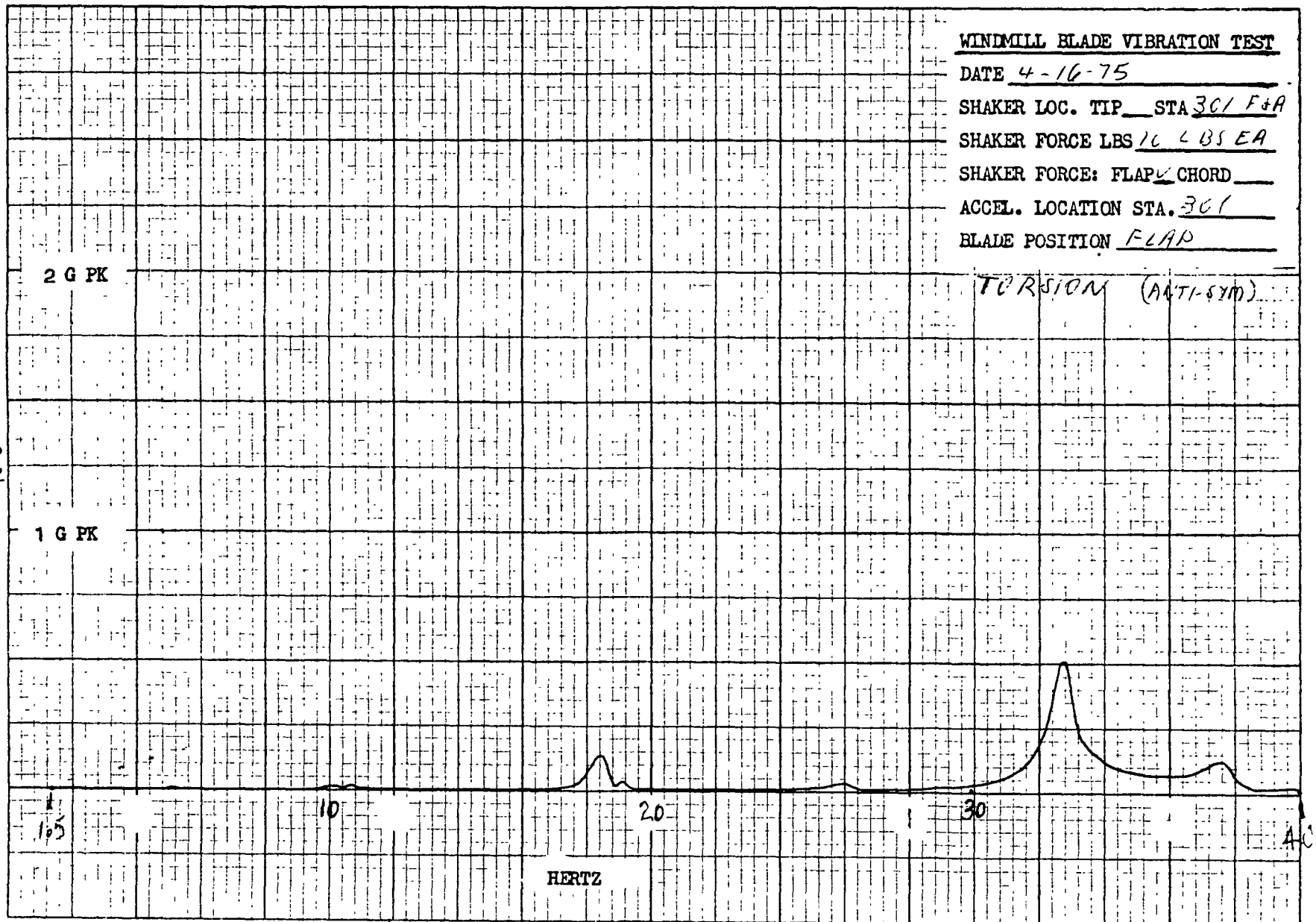

FIGURE 47. Blade Response vs Frequency, Config A, Flap @ 301/Torsion @ 301

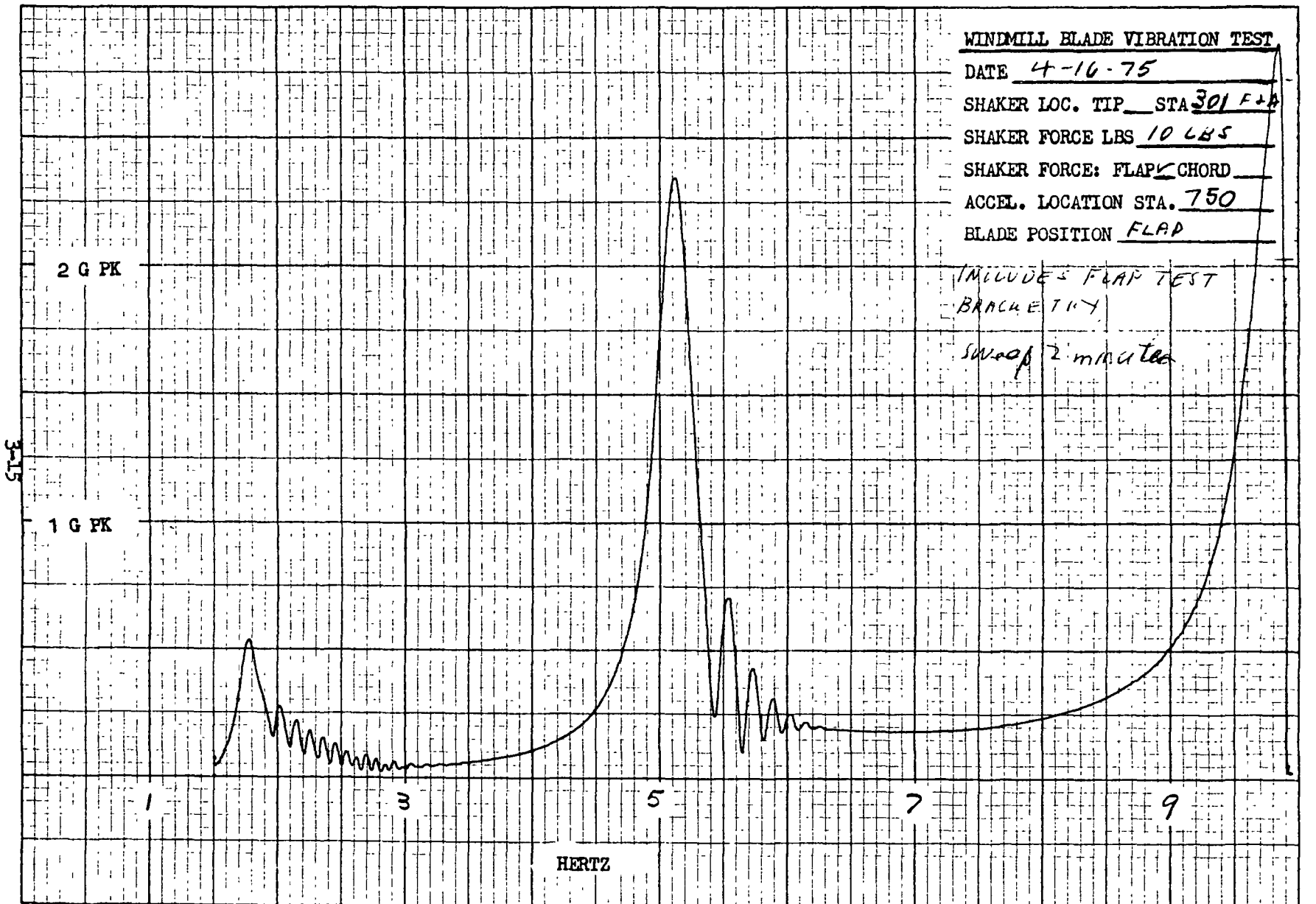

FIGURE 48. Blade Response vs Frequency, Config A, Flap @ 750/Flap @ 301

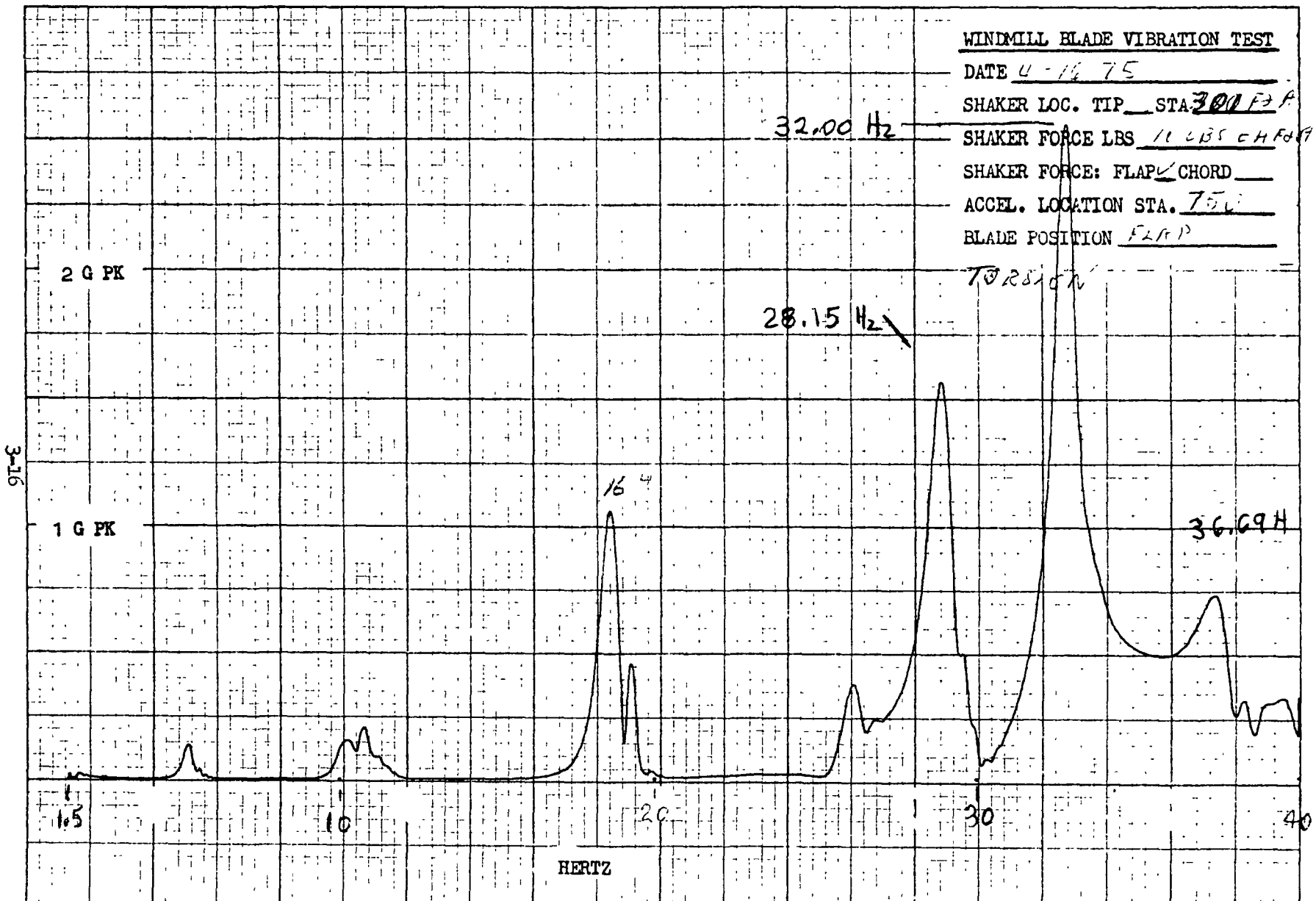

FIGURE 49. Blade Response vs Frequency, Config A, Flap @ 750/Torsion @ 301

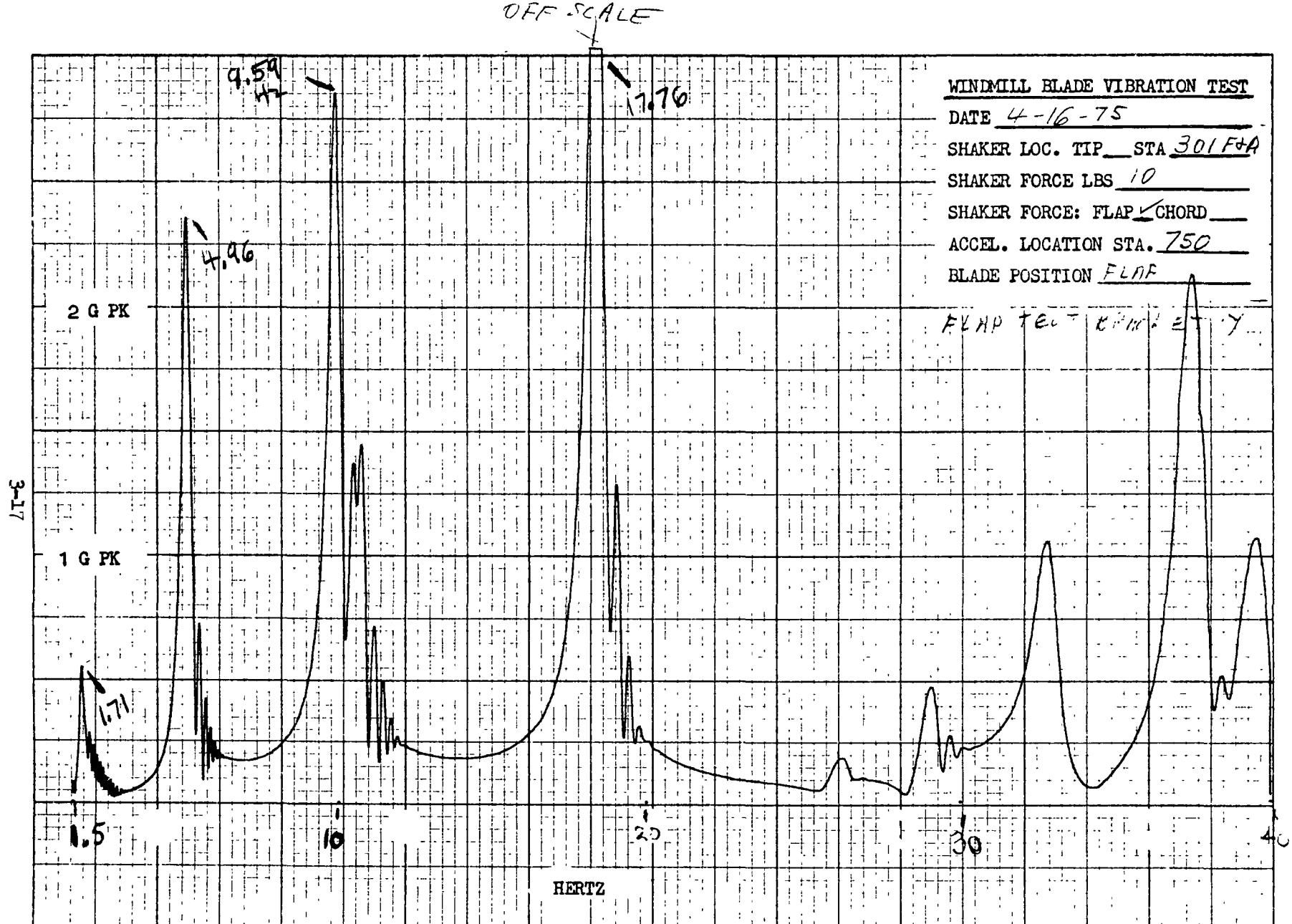

FIGURE 50. Blade Response vs Frequency, Config A, Flap @ 750/Flap @ 301

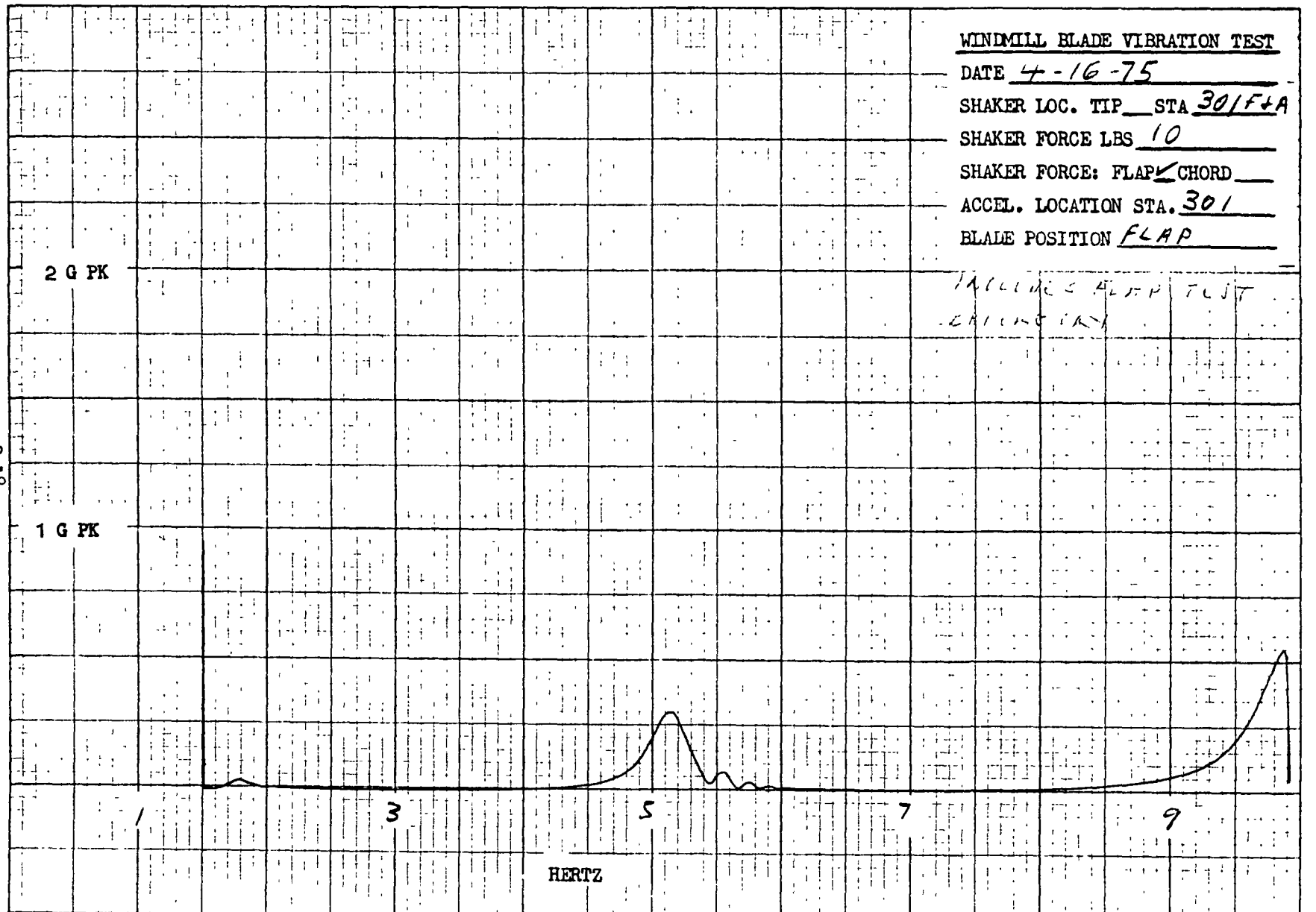

FIGURE 51. Blade Response vs Frequency, Config A, Flap @ 301/Flap @ 301

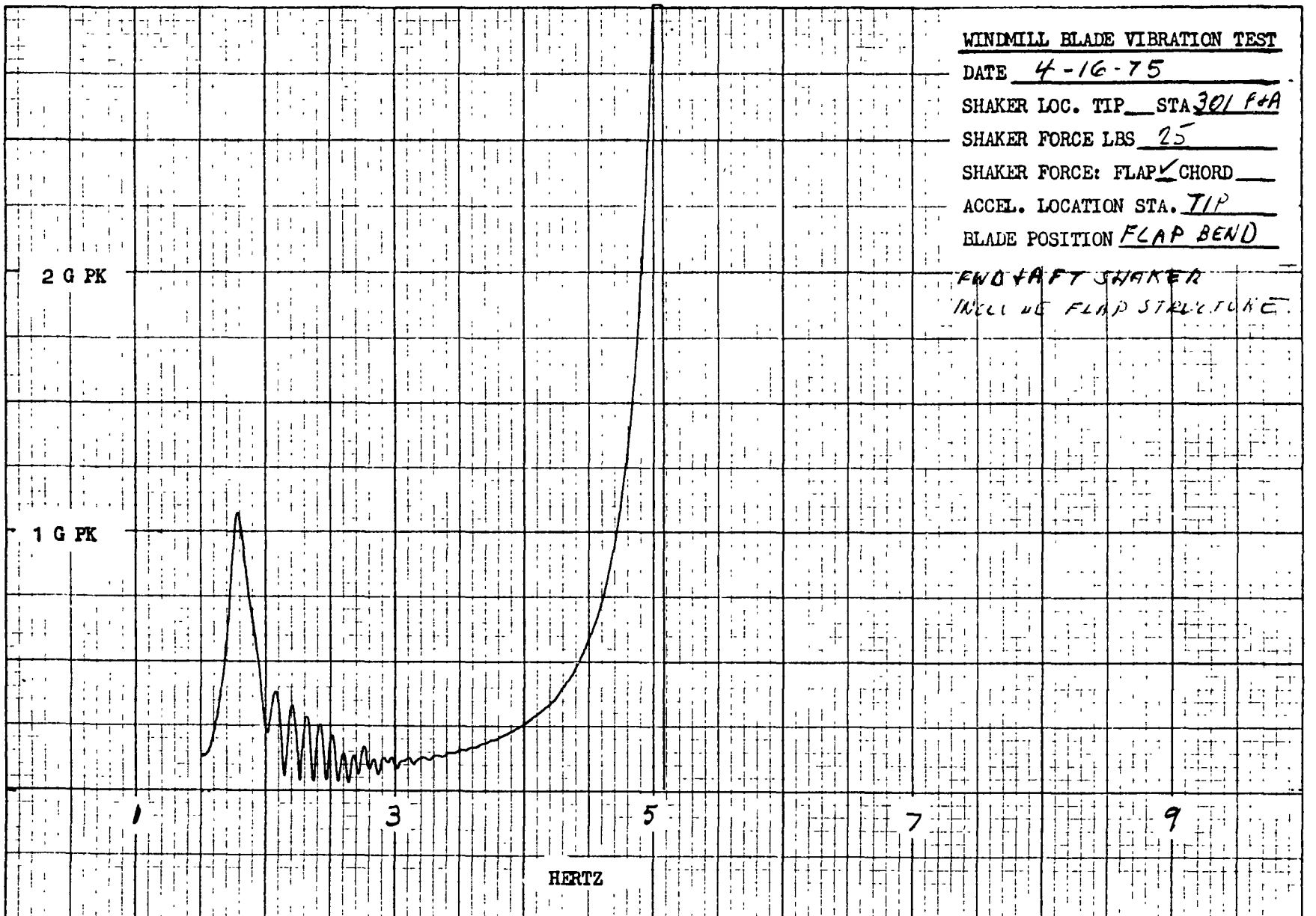

FIGURE 52. Blade Response vs Frequency, Config A, Flap @ 750/Flap @ 301

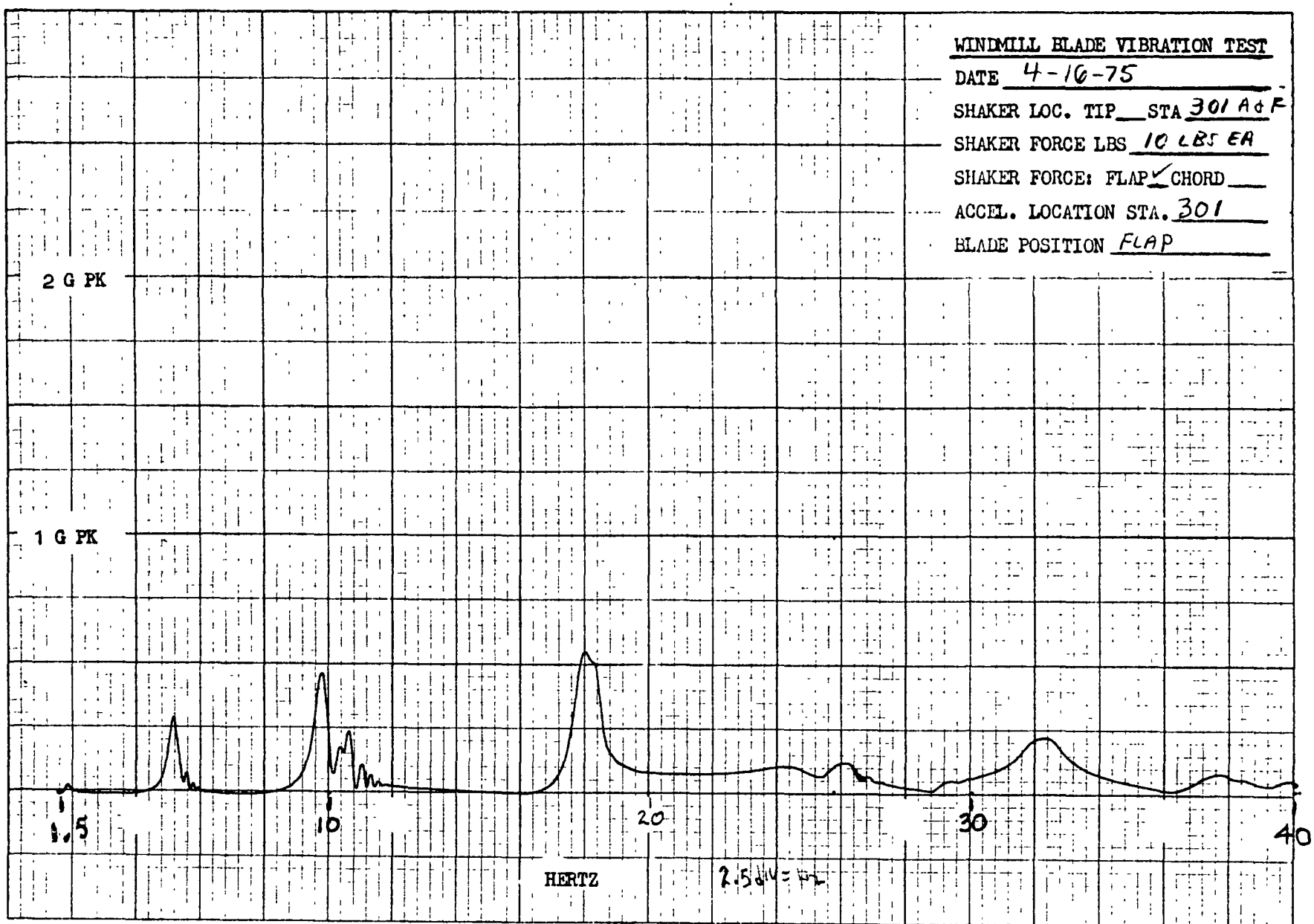

FIGURE 53. Blade Response vs Frequency, Config B, Flap @ 301/Flap @ 301

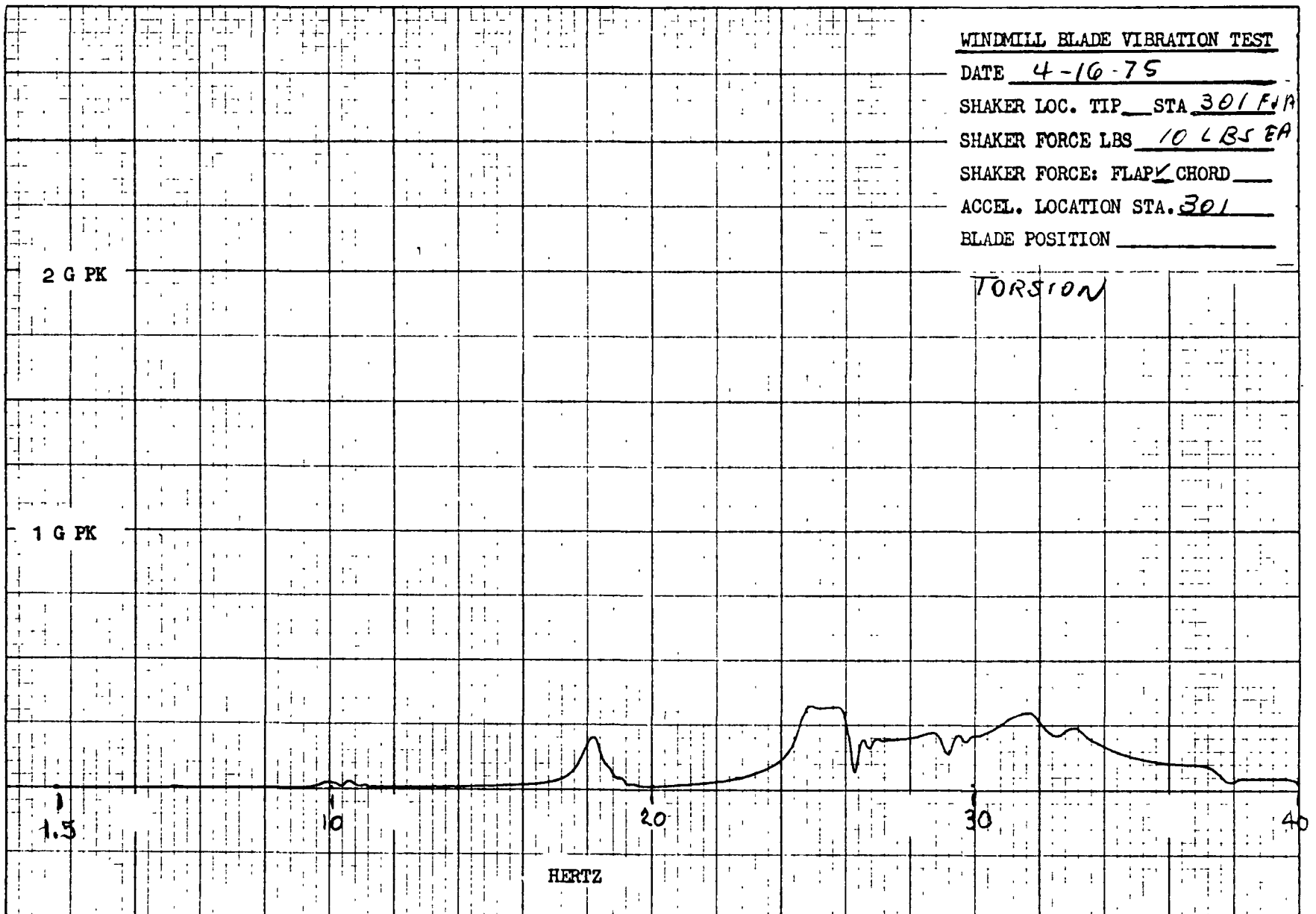

FIGURE 54. Blade Response vs Frequency, Config B, Flap @ 301/Torsion @ 301

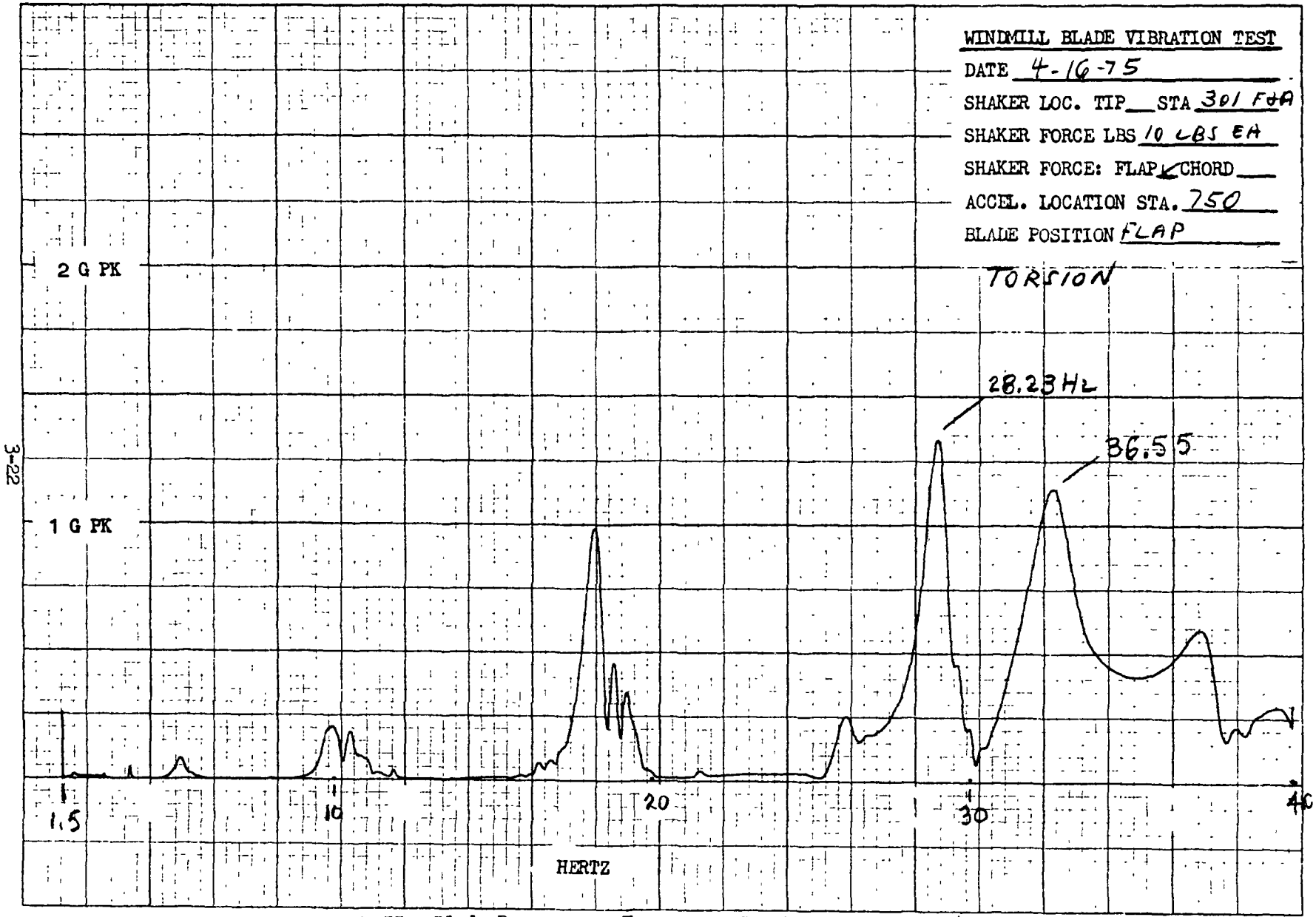

FIGURE 55. Blade Response vs Frequency, Config B, Flap @ 750/Torsion @ 301

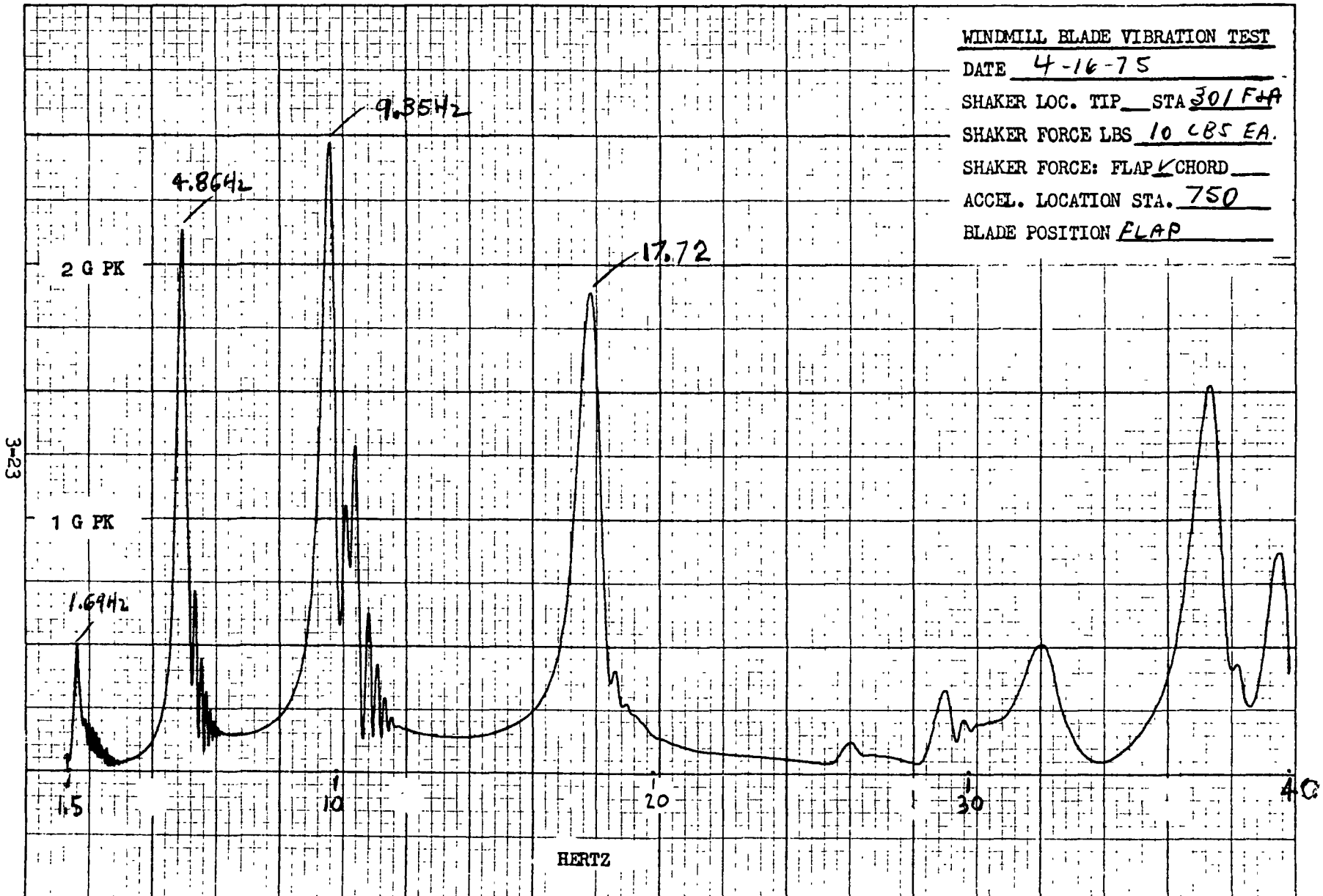

FIGURE 56. Blade Response vs Frequency, Config B, Flap @ 750/Flap @ 301

3.2 COMPARISON OF MEASURED AND STATIC INFLUENCE COEFFICIENTS

The test to measure the static deflection of the blade under load was combined with the blade loading to calibrate the bending moment strain gage bridges. The same setup as assembled for the blade frequency test was used except that a restraint will be added opposite the one being loaded to react the load.

Airfoil contour fitting blocks were fabricated from wood and clamped around each of the three spanwise stations that were loaded. The blocks were felt padded and wide enough to present a distributed load and not damage the blade skin. Loads were applied through load cells to the wooden blocks on the blade. The loads were monitored by visual load cell readout available to the operator. Gages were attached along the blade at several spanwise stations to measure the blade deflection under load.

For these tests, the three stations were loaded individually. The loading was progressively increased in approximately five increments or until sufficient data was collected to define deflection versus force and deflection versus span.

Loads were applied at stations 301, 521 and 697. Likewise deflection measurements were recorded at these same stations as well as in the blade root area. These data were reduced in terms of static influence coefficient data for the blade and a comparison of these measured data and of the predicted blade influence coefficients is given in Table 3.

TABLE 3

COMPARISON OF MEASURED AND CALCULATED
BLADE STATIC INFLUENCE COEFFICIENTS

INFLUENCE COEFFICIENTS - IN/LB.

		FLAP LOAD @ STA			INPLANE LOAD @ STA		
	STATION	301	521	697	301	521	697
FLAPPING DEFL.	301 CALC	.000545	.001276	.001793	-.000032	-.000089	-.000136
	301 MEAS	.000559	.00189	.00223	.000148	.00041	.00034
	521 CALC	.001257	.004646	.008056	-.00009	-.000344	-.000551
	521 MEAS	.001156	.00459	.008338	.000271	.000531	.000941
	697 CALC	.001727	.008014	.021592	-.000134	-.000551	-.0009
	697 MEAS	.001689	.00833	.019458	.0004	.000615	.001165
INPLANE DEFL.	301 CALC	-.000032	-.000089	-.000136	.000442	.000954	.0013262
	301 MEAS	.000094	.153E-5	-.00065	.000409	.000974	.001231
	521 CALC	-.00009	-.000344	-.000551	.000954	.002685	.004247
	521 MEAS	.000308	-.000276	-.000622	.000964	.002057	.003272
	697 CALC	-.000134	-.000551	-.0009	.001379	.004259	.008003
	697 MEAS	-.000022	-.000096	.000501	.001242	.003118	.005516

4.0 WEIGHT AND BALANCE

Each of the three windmill blades has been weighed and balance data has been determined. The measured weights and center of gravity data are summarized in Table 4 for the three blades as delivered.

TABLE 4

MEASURED WEIGHT AND CENTER OF GRAVITY DATA
OF BLADES AS DELIVERED

Blade Number	Weight lbs	Spanwise c.g.-in.	Chordwise c.g. in. aft of 1/4c
1	1981.3	270.18	1.26
2	1999.6	269.27	1.40
3	2012.5	266.67	1.56

Reasons for the manufacturing variation between blades have been studied and attributed to one or more of the following:

- Material tolerance is ±.013 for .250 stock and ±.004 for .040 stock. This could amount to ±47 pounds for the entire blade.
- Paint thickness is shown by previous experience to typically vary by 2 't' (where 't' is spec paint system thickness).
- Fit and function variation between blades is due to dimensional tolerance of individual parts and trimming on assembly.
- Scale accuracy is ±0.1%.

Balance provisions at the root rib (Sta 48) and the tip rib (Sta 750) have been provided in each blade for the required operational blade/rotor balance. Two balance pockets have been permanently installed at each of the two locations, each capable of 3.6 pounds when utilizing the steel ballast which has been provided. Since latitude exists in the way in which the blade/rotor assemblies can be ballasted, although in general it is desirable to minimize the use of ballast in the outboard pockets, the

summary given on Table 5 is but one possible method. This ballast provision is, however, entirely satisfactory and is recommended based on current static and dynamic test information.

A synoptic overview of this evaluation is briefly given in the following paragraphs.

The natural frequencies of the first two (fundamental) bending modes of the nonrotating blade have been obtained from oscillograph time histories of a freely decaying motion of the blade following hand excitation using an instrumentation accelerometer were as follows.

Natural Frequencies (No Tip Weight)
Experimentally Obtained from Oscillograph Records

	Blade Frequencies (cpm)		
Mode Shape	#1001	#1002	#1003
1st Inplane	159.6	160.0	160.0
1st Flapping	103.8	103.5	103.2

These results show excellent agreement which indicates that the dynamic properties are for practical purposes identical. Relative to the use of tip ballast for rotor assembly balance the following test results are of interest.

Experimental Measurement of Tip Weight Effect
on Blade Frequency

No Tip Weight	Full Tip Weight (7.2 lbs/blade)
103.8 cpm (2.59P)	97.8 cpm (2.45P)
159.6 cpm (3.99P)	141.0 cpm (3.53P)

Since the primary excitation of the system is at 40 cpm (1P), the modest variation of the nonrotating blade natural frequencies due to the ballast arrangement given on Table 5 is judged entirely satisfactory.

TABLE 5

WINDMILL BLADE BALANCE

ITEM	WEIGHT	SPANWISE ARM	SPANWISE MOMENT	CHORDWISE ARM	CHORDWISE MOMENT
BLADES 1 AND 2					
BLADE 1 (NO TRIM WEIGHT)	1,981.3	270.18	535,316	1.26	2,496
INBD FWD POCKET (FULL)	3.6	57.00	205	-12.00	- 43
INBD AFT POCKET (FULL)	3.6	57.00	205	+17.00	+ 61
OUTBD FWD POCKET	1.2	741.00	889	- 2.70	- 3
OUTBD AFT POCKET	1.2	741.00	889	+ 2.70	+ 3
WEIGHT ON STA 48 RIB	5.0	48.00	240	+25.00	+ 125
BLADE 1 (BALANCED)	1,995.9	269.42	537,744	1.32	2,639
BLADE 2 (NO TRIM WEIGHT)	1,999.6	269.27	538,440	1.40	2,799
DIFFERENCE	3.7	0.15	696	0.08	160
BLADES 1 AND 3					
BLADE 1 (NO TRIM WEIGHT)	1,981.3	270.18	535,316	1.26	2,496
INBD FWD POCKET (FULL)	3.6	57.00	205	-12.00	- 43
INBD AFT POCKET (FULL)	3.6	57.00	205	+17.00	+ 61
WEIGHT ON STA 48 RIB	23.2	48.00	1,114	+25.00	+ 580
BLADE 1 (BALANCED)	2,011.7	266.86	536,840	1.54	3,094
BLADE 3 (NO TRIM WEIGHT)	2,012.5	266.67	536,669	1.56	3,140
DIFFERENCE	0.8	0.19	171	0.02	46
BLADES 2 AND 3					
BLADE 2 (NO TRIM WEIGHT)	1,999.6	269.27	538,440	1.40	2,799
INBD FWD POCKET (FULL)	3.6	57.00	205	-12.00	- 43
INBD AFT POCKET (FULL)	3.6	57.00	205	+17.00	+ 61
WEIGHT ON STA 48 RIB	8.7	48.00	418	+25.00	+ 218
BLADE 2 (BALANCED)	2,015.5	267.56	539,268	1.51	3,035
BLADE 3 (NO TRIM WEIGHT)	2,012.5	266.67	536,669	1.56	3,140
OUTBD FWD POCKET	1.5	741.00	1,112	- 2.70	- 4
OUTBD AFT POCKET	1.5	741.00	1,112	+ 2.70	+ 4
BLADE 3 (BALANCED)	2,015.0	267.37	538,893	1.56	3,140
DIFFERENCE	0.0	0.19	375	0.05	105

SPECIFICATION REQUIREMENT IS THAT THE BLADES BE MATCHED IN WEIGHT WITHIN 5 POUNDS AND THE CENTER OF GRAVITY LOCATIONS SHALL BE WITHIN 0.2 INCH.

5.0 STRUCTURAL TEST RESULTS SUMMARY

Nonrotating structural tests have been conducted on the first metal wind turbine blade mounted on a test fixture. This support fixture simulated the hub/spindle stiffness of the 100-kW experimental wind turbine generator. The test/analysis frequency summary comparison presented in Table 6 shows that excellent correlation was obtained. The frequencies of the flapping modes and the inplane modes are both slightly higher than calculated which is largely attributed to higher blade bending stiffness levels being obtained. The first torsion mode was slightly lower than predicted, but for a 2000 cpm mode this is good correlation. It is concluded that the mass and stiffness distribution properties calculated by computer graphics, see figure 57, are accurate descriptions of the basic properties of the blade.

During the calibration test loading of the strain gage instrumentation, deflection measurements were taken concurrent with loading applications. Structural influence coefficients determined from these measurements are compared with theoretical predication on Table 7. These results show excellent correlation with the flapping and inplane measurements. The flapping is 1.06 times stiffer than theory and the inplane is 1.10 times stiffer than theory at blade station 301. These values when compared with the nonrotating first blade mode frequencies would explain the higher frequency results obtained between test and theory on Table 6.

TABLE 6. METAL WINDMILL BLADE FREQUENCY SPECTRUM DETERMINED BY NON-ROTATING TESTS

Test/Analysis Frequency Summary

Mode Shape	Full Tip Weight* 7.4 lb/Blade (Test)	No Tip Weight* (Test)	No Tip Weight (Analysis)
1st Falpping	97.8 cpm	103.8 cpm	98.7 cpm
2nd Flapping	280.8 cpm	299.4 cpm	286 cpm
3rd Flapping	600.0 cpm	622.8 cpm	610 cpm
1st Inplane	141.0 cpm	159.6 cpm	143 cpm
2nd Inplane	567.6 cpm	588.0 cpm	558 cpm
1st Torsion	(Not Tested)	1968 cpm	2040 cpm

*Metal blade was primed but not through final paint, surface area weight would increase by 25 lb/blade.

METAL WIND-TURBINE BLADE
LUMPED PARAMETER WEIGHT DISTRIBUTION

WEIGHT	X ARM	Y ARM	Z ARM	I_{XX}	I_{YY}	I_{ZZ}	P_{XZ}
138.77	0.00	37.31	0.00	7676	9244	7676	0
188.99	3.11	54.96	0.69	15453	25732	19117	3612
257.64	3.23	79.01	0.74	33631	19668	46594	7757
130.17	1.54	124.89	0.40	29574	26988	39414	3905
135.68	1.58	171.27	0.23	28538	26697	41962	3387
117.69	2.40	213.81	0.36	23323	21834	36461	2381
114.95	1.77	257.66	0.11	21717	17184	32556	1381
55.04	1.62	290.65	0.51	3513	7180	8106	413
68.96	-0.18	312.58	-0.46	4144	9664	11084	700
131.45	-0.36	345.96	-0.12	23018	15446	34842	871
108.01	-0.10	389.04	-0.16	18656	10265	26461	328
109.09	-0.28	433.14	-0.11	18561	8864	25503	178
98.48	-0.27	477.18	-0.08	16432	6823	22070	78
84.39	-0.22	521.19	-0.08	14358	4273	17494	-21
79.11	-0.16	564.96	-0.01	13032	3132	15624	-35
56.05	-0.21	608.22	0.01	9172	2281	11195	-71
20.08	-0.26	642.34	0.00	841	673	1453	-23
15.43	-0.13	663.66	-0.07	643	706	1307	-20
28.58	-0.04	698.11	-0.04	5512	1007	6470	-36
17.28	-0.29	736.45	-0.04	1057	398	1444	-19
1955.54	1.13	269.97	0.63	215264289	225307	215387656	26587
ROTATION TO PRINCIPAL AXES 11.66 DEGREES							
1955.54	1.13	269.97	0.63	215258803	225307	215393142	0
ABOUT CENTROID							
1955.54	1.13	269.97	1.63	72734079	222029	72866694	0

UNITS: LBS, INCHES, LB-IN^2

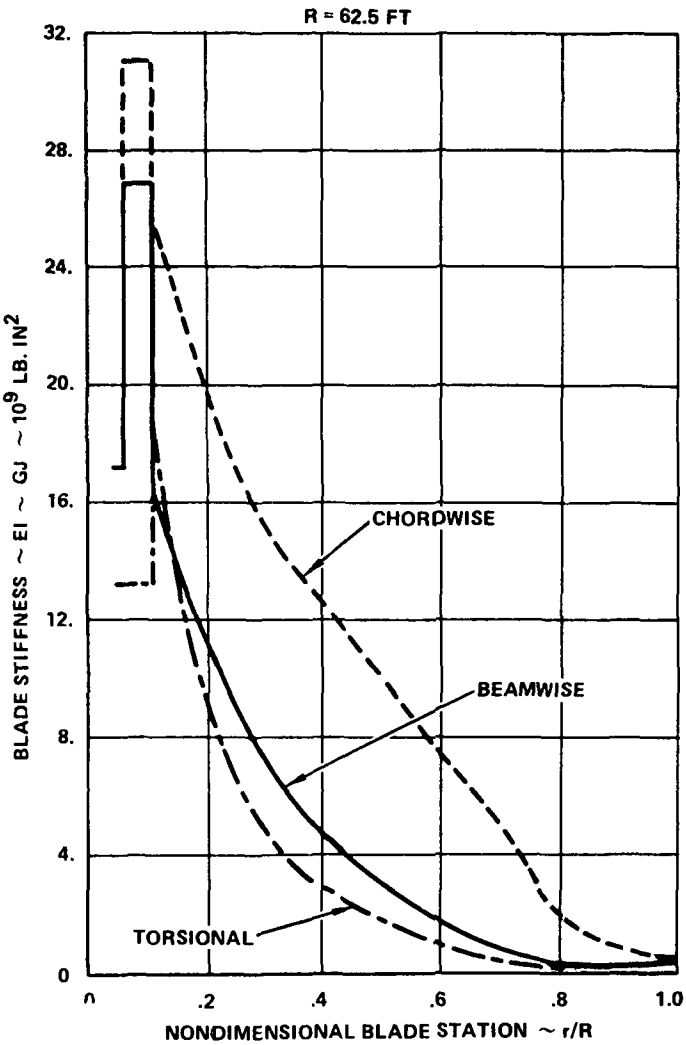

Wind-Turbine Blade Stiffness Distribution

Figure 57. Weight and Stiffness Distribution of 100-KW Metal Wind Turbine Blade

TABLE 7. MEASURED METAL WINDMILL BLADE STRUCTURAL TEST INFLUENCE COEFFICIENTS COMPARED WITH THEORY

Units – Pounds and Inches

Flapping Defl/Flap Loading

Calculated	.000595	.001256	.001727
Measured	.000559	.001156	.001689
Calculated	.001256	.004646	.008056
Measured	.001156	.004591	.008338
Calculated	.001727	.008056	.021592
Measured	.001689	.008338	.019458

$$\begin{Bmatrix} F_{301} \\ F_{521} \\ F_{697} \end{Bmatrix} = \begin{Bmatrix} Z_{301} \\ Z_{521} \\ Z_{697} \end{Bmatrix}$$

Inplane Defl/Inplane Loading

Calculated	.000442	.000954	.001362
Measured	.000409	.000964	.001242
Calculated	.000954	.002685	.004259
Measured	.000964	.002057	.003118
Calculated	.001362	.004259	.008003
Measured	.001242	.003118	.005516

$$\begin{Bmatrix} I_{301} \\ I_{521} \\ I_{697} \end{Bmatrix} = \begin{Bmatrix} X_{301} \\ X_{521} \\ X_{697} \end{Bmatrix}$$

Note: Subscripts indicate blade station locations of individual load applications and deflections.

LIST OF REFERENCES

1. Cherritt, A.W. and Gaidelis, J.A., "100 KW METAL WIND TURBINE BLADE-CL 1708 BASIC DATA, LOADS AND STRESS ANALYSIS," Lockheed Report LR 26215, June 1975

2. Houbolt, J.C. and Reed, W.H., "PROPELLER-NACELLE WHIRL FLUTTER," Proceedings of IAS 29th Annual Meeting, New York, January 1961

3. Ham, N.D. and Young, M.I., "TORSIONAL OSCILLATION OF HELICOPTER BLADES DUE TO STALL," Journal of Aircraft, Vol. 3, No. 3, May-June 1966

4. Cherritt, A.W. and Gaidelis, J.A., 100-KW METAL WIND TURBINE BLADE CL 1708 BASIC DATA, LOADS AND STRESS ANALYSIS," Lockheed Report LR 27153, June 1975.

☆U.S. GOVERNMENT PRINTING OFFICE: 1978-740-094/1391

6 SEP 78 J. W. Anderson 242/32²/279/23361 13 MAY 78

UNITED STATES ENERGY RESEARCH
AND DEVELOPMENT ADMINISTRATION
P. O. BOX 62
OAK RIDGE, TENNESSEE 37830

OFFICIAL BUSINESS
PENALTY FOR PRIVATE USE $300

POSTAGE AND FEES PAID
U. S. ENERGY RESEARCH
AND DEVELOPMENT ADMINISTRATION

U.S.MAIL

FS- 1

MCDONNELL DOUGLAS AIRCRAFT COMPANY
ATTN ENGINEERING LIB
DEPARTMENT 022
BOX 516
ST. LOUIS, MO 63166